AN IMPROVED APPROACH FOR SMALL SATELLITES ATTITUDE DETERMINATION AND CONTROL

by

Mohamed Temam Nasri

A Thesis submitted to the Faculty of Graduate Studies of
The University of Manitoba
in partial fulfilment of the requirements of the degree of

Master of Science

Department of Electrical and Computer Engineering
University of Manitoba
Winnipeg, Manitoba

To My Beloved Parents

Ahmed and Zineb

To My Dear Siblings

Fatma-Zohra, Kais Abdel-Rahmane, Aniss, and Sabra

To My Adorable Nephews and Nieces

Oussama, Asma, Imene, Abdel-Moumene, Wael, Lotfi, Al-Kaima,

and Ibrahim-Khelil

Abstract

The *attitude determination and control subsystem* (ADCS) is a critical part of any satellite conducting scientific experiments that require accurate positioning (such as Earth observation and solar spectroscopy). The engineering design process of this subsystem has a long heritage; yet, it is surrounded by several limitations due to the stringent physical constraints imposed on small satellites. These limitations (*e.g.*, limited computational capabilities, power, and volume) require an improved approach for the purpose of *attitude determination* (AD) and control. Previous space missions relied mostly on the *extended Kalman filter* (EKF) to estimate the relative orientation of the spacecraft because it yields an optimal estimator under the assumption that the measurement and process models are white Gaussian processes. However, this filter suffers from several limitations such as a high computational cost.

This thesis addresses all the limitations found in small satellites by introducing a computationally efficient algorithm for AD based on a fuzzy inference system with a gradient decent optimization technique to calculate and optimize the bounds of the membership functions. Also, an optimal controller based on a fractional proportional-integral-derivative controller has been implemented to provide an energy-efficient control scheme.

The AD algorithm presented in this thesis relies on the residual information of the Earth magnetic field. In contrast to current approaches, the new algorithm is immune to several limitations such as sensitivity to initial conditions and divergence problems. Additionally, its computational cost has been reduced. Simulation results illustrate a higher pointing stability, while maintaining satisfying levels of pointing accuracy and increasing reliability. Moreover, the optimal controller designed provides a shorter time delay, settling time, and steady-state error. This demonstrates that accurate attitude determination and control can be conducted in small spacecraft.

Visual Abstract

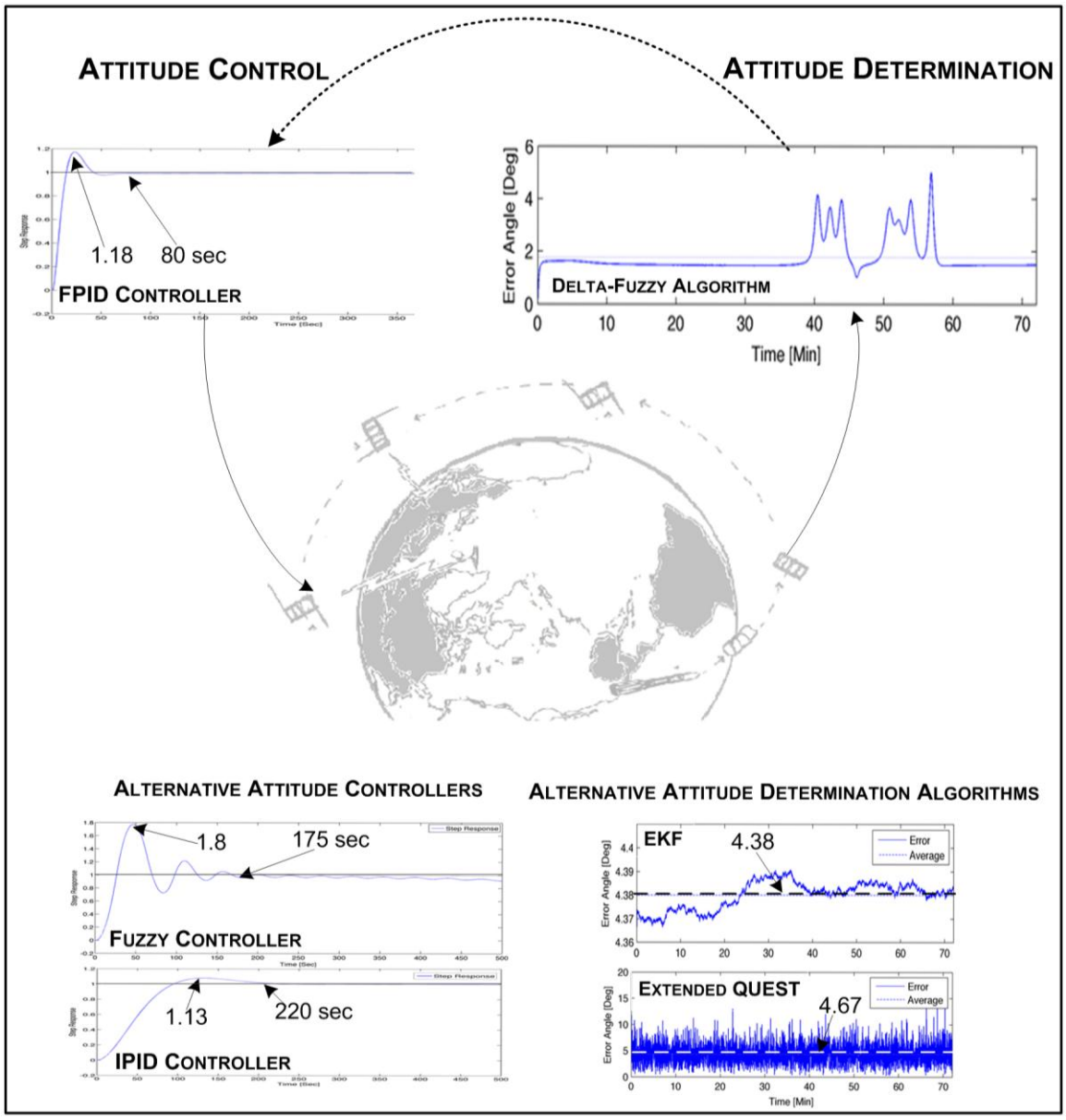

Acknowledgments

There were many people who supported and encouraged me throughout my life in order to strive to achieve my dreams and goals successfully.

I would like to express my sincere gratitude to Professor Witold Kinsner, my thesis advisor, for being a mentor, a teacher, and an educator throughout this degree. Verily, he provided me with many new dimensions that did not exist in my life. Additionally, I would like to thank Mrs. Kinsner who did not hesitate to accompany us to a conference in Regina to ensure our safety and comfort.

I take this opportunity to record my gratitude to all the faculty members of the Department of Electrical and Computer Engineering for their help. In particular, I would like to single out Amy Dario and Allan McKay who were very supportive from day one.

I am extremely grateful to current and previous members of the Delta Research Group for their help and encouragement. In particular, I would like to thank Tong Duan, Rafi Mahabbat Bin Belal, and Dario Schor who were my strongest pillars abroad. I am also grateful to my friends for their motivation and words of encouragement. In particular, special thanks to Kaouther-Saber Cherif, Ahmad Byagowi, and Aditya Kedia for helping me in times of need.

I bring my deepest respect to my father Ahmed and mother Zineb without whom I would ever have been the man I am today. Also, I would like to thank my brothers (Kais

Abderahman and Aniss) and my sisters (Fatma-Zohra and Sabra) who encouraged and helped me at each stage of my life.

Finally, but certainly not last, I am thankful to all my previous teachers and professors from the primary to the graduate level. My success with this current endeavour is a result of their teaching and effort.

I also place on record my sense of gratitude to one and all who, directly or indirectly, have lent their helping hand in this venture.

Contents

List of Tables

List of Figures

List of Acronyms

AD	***A**ttitude **d**etermination*
ADC	***A**ttitude **d**etermination and **c**ontrol process*
ADCS	***A**ttitude **d**etermination and **c**ontrol **s**ubsystem*
AEM	***A**tmospheric **e**xplorer **m**ission*
BN	***B**ayesian **n**etwork*
CDH	***C**ommand and **d**ata **h**andling subsystem*
CMOS	***C**omplementary **m**etal **o**xide **s**emi-conductor*
COM	***Com**munications subsystems*
COTS	***C**ommercial **o**ff-**t**he-**s**helf*
CSDC	***C**anadian **s**atellite **d**esign **c**hallenge*
CW	***C**omputing with **w**ords*
DCM	***D**irection **c**osine **m**atrix*
ECEF	***E**arth-**c**entered **E**arth **f**ixed*
ECI	***E**arth-**c**entered **i**nertial **f**rame*
EKF	***E**xtended **K**alman **f**ilter*
FA	***F**uzzy **a**lgorithm*
FC	***F**uzzy **c**ontrol*
FIS	***F**uzzy **i**nference **s**ystem*
FPID	***F**ractional-order **p**roportional **i**ntegral **d**erivative controller*
GrC	***G**ranular **c**omputing*
GRV	***G**aussian **r**andom **v**ariable*
IAGA	***I**nternational **a**ssociation of **g**eomagnetism and **a**stronomy*
IDS	***I**nitial **d**ata **s**et*

IPID	***I**nteger-order **PID***
KBMC	***K**nowledge **b**ased **m**odel **c**onstruction*
KF	***K**alman **f**ilter*
LEO	***L**ow **E**arth **o**rbit*
LEOP	***L**aunch and **e**arly **op**erations*
LS	***L**east **s**quares*
MF	***M**embership **f**unction*
MIMO	***M**ultiple-**i**nput **m**ultiple **o**utput*
MRP	***M**odified **R**odrigues **p**arameters*
PDF	***P**robability **d**ensity **f**unction*
PF	***P**article **f**ilter*
PID	***P**roportional **i**ntegral **d**erivative*
PLD	***P**ay**l**oa**d** subsystem*
P-POD	***P**oly-**p**icosatellite **o**rbital **d**eployer*
PWR	***P**o**w**e**r** subsystem*
QUEST	***Qu**aternion **est**imator algorithm*
RAAN	***R**ight **a**scension of the **a**scending **n**ode*
REQUEST	***Re**cursive **qu**aternion **est**imator*
SAS	***S**mall **a**stronomy **s**atellite*
SGP4	***S**implified **g**eneral **p**erturbation model version* 4
TAM	***T**hree-**a**xis **m**agnetometer*
TDS	***T**erminal **d**ata **s**et*
TLE	***T**wo-**l**ine **e**lement data set*
TRIAD	***Tri**-axis **a**ttitude **d**etermination algorithm*
TS	***T**akagi **S**ugeno*
TSat1	***T**riple pico-**sat**ellite*
UKF	***U**nscented **K**alman **f**ilter*
UMSATS	***U**niversity of **M**anitoba **s**pace **a**pplications and **t**echnology **s**ociety*
WGN	***W**hite **G**aussian **n**oise*

List of Symbols

Notation: Scalars are denoted by plain text, italics. Vectors are denoted by bold text.

Constants:

G	Universal gravitational constant ($G=6.6738\times10^{-11}$ $N(m/kg)^2$)
M_e	The mass of the Earth ($M_e= 5.972\times10^{24}$ kg)
μ_e	Earth's gravitational constant

Cartesian Coordinate Frames:

Body frame

Earth centered inertial (ECI)

Earth-centered Earth-fixed (ECEF)

Orbital frame

Scarlars:

a_i	*Tuning parameters for the QUEST algorithm*
b_1, b_2, b_3	*A dipole approximation of the Earth magnetic field*
c_{ij}	*Center of the membership function*
i	*Orbital inclination*
K	*Number of inputs for the FA*
k_p, k_i, k_d	*PID tuning parameters*

m_k	*Number of measurements for the QUEST and extended QUEST algorithms*
N	*Number of MFs in an interval* [*pi, qi*]
n	*Size of the state-vector*
q_4	*Scalar part of the quaternion*
r	*Learning rate in the fuzzy algorithm*
R_a	*Satellite's orbital radius*
R_e	*Earth orbital radius*
s	*Laplace variable*
w	*Crisp output of the fuzzy algorithm*
α	*Semi-major axis of the orbit*
β	*Semi-minor axis of the orbit*
Δt	*Integration time step*
ε	*Eccentricity*
ε_s	*Elevation of the Sun*
ζ	*Fractional-order of the derivative operator*
θ	*Rotation angle about the y-axis*
ϑ	*Rotation angle for the quaternion parameterization technique*
$\bar{\lambda}, \bar{a}, \bar{k}$	*Tuning parameters for the UKF algorithm*
λ_{max}	*Greatest eigenvalue of the* **K** *matrix for the QUEST algorithm*
λ_s	*Sun orbital parameter*
μ	*Fading memory factor in the QUEST algorithm*
ξ	*Fractional-order of the integral operator*
σ^2	*Variance of a Gaussian process*
σ_v	*Gyro measurement noise*
σ_w	*Gyro measurement drift*
Υ	*Argument of perigee*
ϕ	*Rotation angle about the x-axis*

ψ	*Rotation angle around the z-axis*
$\overline{\omega}$	*Mean motion*
ω_0	*Absolute angular velocity*
ς	*Right ascension of the ascending node*

Vectors:

$\mathbf{0}_{n\times n}$	*Null matrix of size n×n*
$\mathbf{1}_{n\times n}$	*Identity matrix of size n×n*
$\mathbf{A}$	*Attitude matrix*
$\mathbf{B}$	*Attitude profile matrix for the QUEST algorithm*
$\mathbf{b}_{body}^{mag}$, $\mathbf{b}_{body}^{sun}$	*Uncorrupted Earth magnetic field and sun vector measured in the body frame*
$\mathbf{b}_{ref}^{mag}$, $\mathbf{b}_{ref}^{sun}$	*Earth-magnetic field and sun vector in the reference frame*
$\tilde{\mathbf{b}}_{body}^{mag}$, $\tilde{\mathbf{b}}_{body}^{sun}$	*Earth magnetic field and sun vector measured in the body frame*
$\mathbf{e}$	*State-error for KFs*
$\hat{\mathbf{e}}$	*Rotation axis for the quaternion representation*
$\mathbf{f}(\mathbf{x})$, $\mathbf{h}(\mathbf{x})$	*Nonlinear functions describing the process and measurement models*
$\mathbf{H}$	*Linearized measurement matrix*
$\mathbf{I}$	*Spacecraft moment of inertia matrix*
$\mathbf{K}$	*Attitude profile matrix for the QUEST and extended QUEST*
$\mathbf{k}$	*Kalman gain matrix for KFs*
$\mathbf{m}_{\text{ctrl}}$	*Torquers' magnetic moment*
$\mathbf{n}$	*Vector representing measurement and process noises*
$\mathbf{n}_{\text{d}}$	*External disturbances encountered in LEO for a linearized dynamics model*

$\mathbf{N}_{\text{ctrl}}$	*Magnetic control torque*
$\mathbf{N}_{\text{dist}}$	*Vector representing all the disturbances encountered in LEO*
$\mathbf{N}_{\text{gg}}$	*Gravity gradient torque*
$\mathbf{P}$	*Covariance matrix for KFs*
$\mathbf{P}_k^{yy}$	*Innovation matrix for the UKF*
$\mathbf{P}_k^{xy}$	*Cross-correlation for the UKF*
$\mathbf{P}_k^{yy}$	*Output covariance for the UKF*
$\mathbf{q}$	*Quaternion*
$\hat{\mathbf{q}}$	*Estimated quaternion*
$\mathbf{Q}$, $\mathbf{R}$	*Process and measurement noise covariance matrices*
$\mathbf{q}_{\text{opt}}$	*Optimal quaternion*
$\mathbf{r}$	*Unit-norm reference vector*
$\tilde{\mathbf{R}}_{\mathbf{qq}}$, $\tilde{\mathbf{R}}_{\mathbf{xq}}$, $\tilde{\mathbf{R}}_{\mathbf{xx}}$	*Linearized weighting matrix for the extended QUEST*
$\mathbf{R}_{\mathbf{ww}}$, $\mathbf{R}_{\mathbf{qq}}$, $\mathbf{R}_{\mathbf{xq}}$, $\mathbf{R}_{\mathbf{xx}}$	*Weighting matrices for the extended QUEST*
$\mathbf{R}_x(\phi)$	*Rotation around the x-axis*
$\mathbf{R}_y(\theta)$	*Rotation around the y-axis*
$\mathbf{R}_z(\psi)$	*Rotation around the z-axis*
$\boldsymbol{R}_b^a$	*Rotation matrix from a to b*
$\mathbf{S}$	*Innovation covariance matrix*
$\mathbf{s}$	*Sun vector position*
$\mathbf{T}_{\text{b}i}$	*TRIAD component in the body frame*
$\mathbf{T}_{\text{r}i}$	*TRIAD component in the reference frame*
$\mathbf{v}$	*Measurement noise vector*
$\mathbf{w}$	*Process noise covariance*
$\mathbf{W}^{(\text{c})}$, $\mathbf{W}^{(\text{m})}$	*Weights coefficients in UKF*
$\mathbf{x}$	*State-vector*
$\hat{\mathbf{x}}$	*Estimated state-vector*
$\mathbf{y}_k$	*Observables uncorrupted with noise in EKF and UKF*
$\hat{\mathbf{y}}_k$	*Predicted mean of the observation vector for the UKF*

$\tilde{\mathbf{y}}_k$	*Measurement residual for the UKF*
$\boldsymbol{\beta}$	*The drift*
$\boldsymbol{\delta q}$	*Error in the estimated quaternion*
$\boldsymbol{\Delta q}$	*Correction term for the quaternion*
$\boldsymbol{\Delta \hat{x}}$	*Correction term for KFs state-vector*
$\boldsymbol{\Delta \beta}$	*Error in the drift*
$\boldsymbol{\Delta \hat{\beta}}$	*Correction term for the drift*
$\boldsymbol{\eta}_w, \boldsymbol{\eta}_v$	*Zero-mean gyro noise vectors*
$\boldsymbol{\delta\theta}$	*The error angle*
$\boldsymbol{\Lambda}$	*Vector representing all parameters that can be optimized for the delta-fuzzy algorithm*
$\boldsymbol{\varphi}$	*Vector part* (3×1) *of the quaternion*
$\boldsymbol{\chi}_k$	*Sigma points*
$\boldsymbol{\Psi, \Phi, \Theta}$	*State transition matrices*
$\boldsymbol{\omega}$	*Actual angular rate vector*
$\hat{\boldsymbol{\omega}}$	*expected angular rate vector*
$\boldsymbol{\Upsilon}$	*The predicted observation matrix for the UKF*

Operators and Other Symbols:

$(\hat{\bullet})_{k\|k}$	*A posteriori estimate of the variable* (•) *at time k with k measurements*
$(\hat{\bullet})_{k\|k-1}$	*A priori estimate of the variable* (•) *at time k given k*-1 *measurements*
$P(\bullet\|\bullet)$	*Conditional probability*
$C(s)$	*Controller transfer function*
$[\bullet\times]$	*Cross-product matrix operator*
$E[\bullet]$	*Expectation*
D	*Fractional derivative operator*
I	*Fractional integral operator*

$\Gamma(\bullet)$	*Gamma operator for fractional calculus*
$\int(\bullet)$	*Integral operator*
$[p, q]$	*Interval for fuzzy MFs*
$(\bullet)^{-1}$	*Inverse operator*
F, C, G	*Linear functions for the EKF*
$\mu(\bullet)$	*Membership function for the fuzzy algorithm*
$T_1(s)$	*Pitch angle transfer function*
$\otimes$	*Quaternion multiplication (not related to exclusive nor)*
$T_2(s)$	*Roll/yaw angles transfer function*
$\Pi(\bullet)$	*Skew-symmetric matrix operator*
$\dot{(\bullet)}$	*The derivative of* $(\bullet)$
$\hat{(\bullet)}$	*The expected value of* $(\bullet)$
$(\bullet)^T$	*Transpose operator*

List of Algorithms

- Tri-Axis Attitude Determination
- Quaternion Estimator
- Extended Quaternion Estimator
- Discrete Kalman Filter
- Extended Kalman Filter
- Unscented Kalman Filter
- Delta-Fuzzy Algorithm

List of Controllers

- Fuzzy Controller
- Integer-Order Proportional Integral Derivative
- Fractional-Order Proportional Integral Derivative

Chapter 1

INTRODUCTION

"*Small satellites represent robots of the future*"

Witold Kinsner, 2009

Conducting a space mission relying on a large satellite can be very costly; yet, if the satellite fails, the entire mission collapses. Relying on small satellites in a swarm and cluster configurations provide an alternative that mitigates the risk of failure and reduces the mission cost. A specific example was addressed in [Yash98], in which a study of distributed satellites systems, determination of propulsion system requirements for satellites clusters, and an analysis of a micro-propulsion system for use in swarms of micro-satellites was carried out. The study indicated clearly the reduction in the mission costs and an increase in the reliability as compared to a single large satellite configuration. Additionally, small satellites have gained tremendous attention from the academic community due to their educational impact on students. The introduction of these satellites into university programs provides unique opportunities for collaboration on design, implementation, and testing of complex systems. Such collaboration allows students of different backgrounds to complement their theoretical knowledge with hands-on experience.

The reduced cost of launching and *commercial off-the-shelf* (COTS) low-power electronics has played a major role in encouraging the design and implementation of such spacecraft under the umbrella of competitions (*e.g.*, the *Canadian satellite design challenge* (CSDC) run by the Geocentrix Inc.) [Geoc09]. In order to undertake these projects successfully, an appropriate space mission engineering process has to be followed. Space mission engineering is the definition of mission parameters and refinement of requirements so as to meet the broad and often poorly defined objectives of a space mission in a timely manner at a minimum cost and risk [WeLa99]. This process becomes extremely complicated to manage when a spacecraft is subjected to stringent limitations in mass, volume, and power, which is the case for small spacecraft. Furthermore, the interdependency between the different subsystems makes the idea of a codesign process critical for optimal use of the available resources [Kins07]. This thesis addresses the challenges related to the design and implementation of one of the most difficult subsystems in a satellite; that is, the *attitude determination and control subsystem* (ADCS).

1.1 Problem Statement

The ADCS for large satellites has a deep heritage with several approaches proposed for the purpose of attitude determination [CrMC07]. These approaches include deterministic and probabilistic algorithms that have been implemented with relatively good performances in satellites whose masses exceed 100 kg and power generation capabilities in the range of hundreds of watts. These spacecraft have sufficient computational resources to rely on standard algorithms and run functions associated with the rest of the entire satellite (such as the *command and data handling subsystem*, CDH). Furthermore, large sat-

ellites have enough room and power to host different types of actuators for an accurate control of the attitude.

Unlike large satellites, small satellites face severe physical limitations that limit the computational resources and power available for all subsystems, including the ADCS. This section provides specifications about the targeted spacecraft with their respective limitations.

1.1.1 Motivation

The ADCS is a critical subsystem for any satellite that requires accurate positioning to conduct science experiments (such as solar spectroscopy and Earth observation) or to conduct orbit manoeuvring (such as one-tangent burn and Hohmann transfer) [WeLa99]. The *attitude determination and control* (ADC) process is responsible for calculating the orientation of the spacecraft relative to either an inertial reference frame, or some specific object of interest (*e.g.,* the Sun) and the application of corrective measures based on the mission needs. This process requires one or more sensory measurements that can be obtained from onboard sensors (such as the *three-axis magnetometer*, TAM, Sun sensor, Earth-horizon sensor) and reference models (*e.g.,* the *international geomagnetic reference field model*, IGRF).

Today's challenges (*e.g.*, mitigating the risks of a space mission failure and its respective costs) and modern miniaturization techniques allow for the realization of small satellites such as pico- and nano-satellites. Pico-satellites are defined as satellites whose physical dimensions are $10\times10\times10$ cm^3 with a mass less than 1 kg. Nano-satellites are satellites whose physical dimensions are $10\times10\times30$ cm^3 with a mass less than 10 kg

[KSFC12][CPKM03]. These spacecraft suffer from stringent limitations for onboard hardware (sensors and actuators), computational capabilities, and maximum power generated. Furthermore, all the resources ought to be shared with other subsystems (*e.g.*, *payload*, PLD, CDH, and *communications*, COM) in order to perform scientific experiments in orbit, process the data, and send it to the ground station for post-analysis. Some of these tasks have to be executed with no tolerance for missed deadlines (i.e., hard real-time), while others can be performed within a certain tolerance (i.e., soft real-time). Considering high density computing engines has to account for the effect of radiation and its impact on digital errors in space. The errors are caused by single event effects that occur due to the impact of high energy particles with *complementary metal oxide semiconductor* (CMOS) circuitry. The excess of charge causes the memory cell to lose its current value and changes the storage cell. Thus, considering the density of the transistors used in the chips is of paramount importance. The higher the transistors' density, the more sensitive would be the computing engine to single event effects [Wats01]. Consequently, ADCS has to share available resources with the other subsystems, while satisfying their own requirements to accomplish its mission successfully.

One way to achieve this goal is to evaluate and minimize the computational load of the algorithms selected for the *attitude determination* (AD). Moreover, the limitations on mass and volume, as well as the competition requirements (the spacecraft should carry no fuel) render certain type of actuators unusable (*e.g.*, thrusters). Consequently, current options are restrained to magnetic torquers only. A magnetic torque rod, which consists of coils fed with an electric current to generate a magnetic moment that will interact with the Earth magnetic field creating the desired torque, might be extremely costly in terms

of power consumption. Therefore, an optimal controller has to be designed to minimize the overshoot, settling time, and steady-state error. A poorly tuned controller would result in unnecessary power consumption.

The *extended Kalman filter* (EKF) has been used extensively for the attitude estimation since its development as a practical method for real-time onboard navigation in the Apollo mission [GrAn10][Aure12]. A *Kalman filter* (KF) has several limitations that include a low convergence rate and high computational load due to the intensive mathematical operations required for a single recursion. These impediments raise questions related to the applicability of this specific algorithm in pico- and nano-satellites.

Today, an improved approach for the purpose of attitude determination ought to be considered for such tiny spacecraft compared to standard large satellites. This approach must reduce the computational loads imposed on the onboard computer. Moreover, optimal controllers have to be implemented for the satellite to be more energy efficient to keep the mission alive.

1.1.2 Problem Definition

Starting from October 2010, the *University of Manitoba Space Applications and Technology Society* (UMSATS) participated in the first satellite design competition. In this competition, the students had to design, implement, and test a triple pico-satellite (TSat1) whose dimensions are $10\times10\times34$ cm^3 with a mass that does not exceed 4 kg. The project included over 100 students who developed the satellite and over 50 advisors from academia, industry, military, and other groups who assisted in the development [KSFC12]. The objective of TSat1 was to perform two scientific experiments (the tardi-

grade and solar spectroscopy experiments) once deployed in a Sun-synchronous orbit with an altitude from 600 km to 800 km [SAFG12]. Unlike the tardigrade experiment, the solar spectroscopy experiment requires pointing the spectrometer towards the Sun with an accuracy of ±7.5 deg. [RCHB13]. The satellite had a single computing unit onboard for running, monitoring all subsystems (such as CDH, PWR, and COM), and transmitting the collected data to the University of Manitoba ground station.

TSat1 illustrates a practical example of the limitations found in small satellites. For example, the computational capabilities of the spacecraft put stringent constraints on the algorithms selected for the AD. The estimation process requires reference models for the Sun data and the Earth magnetic field models (*e.g.*, IGRF) to be calculated to feed the algorithms. Also, orbit propagators are extremely important with the updated *two-line elements* (TLE) data set (*e.g.*, *simplified general perturbation model version* 4, SGP4) [NaNa11][HoRo80]. They are required to predict the position and velocity of the spacecraft after being ejected from the *poly-picosatellite orbital deployer* (P-POD). The P-POD represents the mechanism used to launch and deploy nano-satellites. All these computations will increase the computational load of the ADCS. Moreover, the error, accuracy, and stability of the different computational environments have to be taken into consideration. Computers store numbers with a finite precision that can be packed into a fixed number of bits (the precision of a computer is much larger than a microcontroller unit). Consequently, round off and truncation errors may result. Sometimes, these errors get mixed into the calculations at an early stage causing successive magnifications of the errors; thus, an unstable behavior [PTVF07].

The maximum power generated per orbit was estimated to be about 5W for the entire spacecraft (an average light bulb used in a house requires 60 W). The power distribution for each subsystem was as follows. The ADCS, COM, CDH, and PLD were allocated a maximum of 2W, 1,75W, 0.5W, and 0.7W, respectively [DDTA12]. This shortcoming impacts directly the concept of operation of the different subsystems. For instance, due to the power required to transmit the data to the ground station and the power consumption of the actuators, COM and ADCS subsystems will never operate at the same time. Adding more batteries cannot solve this problem, since it is related directly to the power generation and not to the power storage capabilities.

Early satellites relied mostly on probabilistic approaches (*e.g.*, the EKF and the *unscented Kalman filter*, UKF) since it yields an optimal estimator under the assumption that measurement and process models are white Gaussian processes. The AD process requires one or more reference vectors and sensory information that can be obtained using numerous sensors. For example, typical *low Earth orbit* (LEO) missions rely on TAM to measure the Earth magnetic field. Multifractal analysis has shown that the evolution of the Earth magnetic field is chaotic in nature approximated using a power law relationship [HSAD98]. Chaos, which is a class of signals originating from nonlinear dynamical systems, has unique properties (*e.g.*, slightly different initial conditions would result in a signal trajectory that diverges exponentially, as well as a short horizon of predictability) [Kins09]. Thus, relying on approaches, based on the assumption that the process and measurement models follow a Gaussian distribution, will not constitute an optimal choice. Consequently, alternative approaches have to be considered for the identification and estimation of uncertainties in a dynamical environment [Kins09]. Furthermore, these

approaches are extremely costly in terms of space and time due to the intensive calculations required for a single recursion of the filter [NaKi13]. Other deterministic algorithms (*e.g.*, *tri-axis attitude determination*, TRIAD, *quaternion estimator*, QUEST, and extended QUEST) have been considered also; however, they deal poorly with uncertainty in the process and measurement models as shown in Chapter 4.

The *attitude control* plays a role of paramount importance as well. Current controllers are based on nonlinear formulations [OrZF06][BeMF07], evolutionary algorithms, [NVTK03], or optimization techniques [ZeKS03]. Thus, an optimal tuning requires an accurate modeling of the targeted environment. A poorly tuned controller will result in large overshoots, long time delays, and slow convergence rates (under some conditions oscillatory behaviours); thus, power losses. Since the operating conditions (specifically during *launch and early operations*, LEOP) are unknown and the environment is poorly defined, it is important to develop a robust controller that preserves its performance in a nonlinear dynamical environment.

1.1.3 Proposed Solution

Many challenges surround the engineering design process of a small satellite. This thesis addresses the challenges related to the control and optimal positioning of pico- and nano-satellites in LEO at an altitude between 600 and 800 km.

Starting from the moment the satellite is released in space, most of the operating conditions are unknown and cannot be predicted accurately. Consequently, uncertainty arises due to the lack of information and knowledge resulting in situations in which actions have to be taken based on premises for which reliability has not been defined clearly

[LeBS06]. This type of uncertainty is referred to as epistemic uncertainty (also known as reducible uncertainty, type B, or knowledge uncertainty) that can be reduced through an increased understanding, more relevant data, and robust filtering and estimating approaches. Several approaches have been suggested for the analysis of uncertainty. They include probability theory, rough sets, and fuzzy theory. Current attitude determination approaches are either deterministic or probabilistic.

The proposed solution is based on an alternative approach; fuzzy theory (introduced by Lotfi Zadeh [Zade65]). Unlike probability theory that relies on a single measure to provide the likelihood of a certain event occurring, possibility theory relies on two measures (possibility and necessity set of measures) for a better reasoning under uncertainty. This provides a more expressive power when dealing with epistemic uncertainty as compared to probability theory. As a result, a custom attitude determination algorithm based on a fuzzy inference system is implemented. Furthermore, in order to select an optimal structure and configuration of the *membership functions* (MFs), the approximation capabilities of the different type of MFs are considered. Also, to estimate the upper and lower bounds of the MFs, a gradient decent optimization technique is utilized.

In order to solve problems related to the controllability and power consumption of the spacecraft, three different types of controllers have been studied and evaluated. These controllers are: (i) integer-order *proportional integral derivative* (PID) controller, (ii) fractional-order PID controller, and (iii) Mamdani fuzzy controller. All these controllers have been implemented and evaluated in both the time and frequency domains.

1.1.4 Validation of the Proposed Solution

The challenges addressed in this thesis relate to the computational complexity and limitations of current stochastic and deterministic attitude determination algorithms. Additionally, this thesis suggests an energy-efficient controller to correct for the error in the attitude. In order to validate the proposed solution different test cases are considered for the attitude determination algorithm and the controller implemented.

1.1.4.1 Attitude Determination

The proposed attitude determination algorithm must satisfy the following performance measures: (i) short transient response, (ii) minimum steady-state error, and (iii) resilience to errors in the initial conditions and noisy measurements. To evaluate the algorithm for these performance measures the following experiments are conducted:

1. Large initial error. This experiment considers introducing a large initial error during the estimation process. The error is determined based on the performance of current approaches when subjected to similar cases; that is, the error at which current approaches exhibit a diverging behavior constitutes the lower threshold in the experiments. The rationale behind selecting this approach to determine the lowest threshold is driven by the applicability of current approaches in real-life space missions;
2. Sensitivity to noisy measurements. To evaluate the sensitivity to noisy measurements, an additive white Gaussian noise is added to the measurements. Similarly, the level of noise added is determined from the response of current approaches based on the same rationale; and
3. Transient response and steady-state error. These performance measures are obtained from the previous cases considered.

These experiments are enough to evaluate the proposed algorithm based on the aforementioned performance measures and limitations of current approaches.

1.1.4.2 Attitude Control

The control scheme selected must be energy-efficient and robust. To evaluate for such characteristics, the following experiments are considered:

1. Step response. The selected controller is subjected to a step function with a plant representing the linearized dynamics model of a satellite in space. This test allows for the evaluation of the overshoot, transient response, and steady-state error. Minimizing these performance measures will result in an energy-efficient scheme; and
2. Frequency analysis. This analysis is conducted using bode plots to determine the sensitivity to high frequency noise and distortion of the phase.

These experiments constitute a sufficient set of test cases to determine about the performance of the selected control scheme.

1.2 Thesis Formulation

1.2.1 Thesis Statement

This thesis aims to develop a computationally efficient algorithm for the purpose of pico- and nano-satellites attitude determination based on a fuzzy inference systems and a gradient decent optimization technique for the estimation of the upper and lower bounds of the membership functions. Moreover, an optimal controller is implemented to minimize the power consumption of the actuators during the positioning of the satellite.

1.2.2 Thesis Objectives

The primary objectives of this thesis are twofold: (i) developing a computationally efficient algorithm for the purpose of attitude determination, and (ii) implementing an optimal controller for small satellites.

1.2.3 Research Questions

The attitude determination and control is one of the most challenging problems to solve for reliable navigation of a spacecraft. The ADC is surrounded by hard limitations, including limited computational capabilities and power. Additionally, it is subjected to a certain level of epistemic uncertainty. This section highlights the major questions addressed in subsections 1.2.3.1 and 1.2.3.2.

1.2.3.1 Attitude Determination

Since its application in the Apollo project in 1960 [GrAn10], which required estimates of the trajectories of manned spacecraft going to the moon and back, the EKF has been used extensively in numerous space missions. Consequently,

1. Why is the EKF so attractive for orbital guidance and navigation?

Multifractal analysis of the Earth magnetic field has proven its chaotic nature. Chaos belongs to a class of signals approximated using a power-law relationship, and not a Gaussian *probability density function* (PDF) [Kins09]. Therfore,

2. Can KFs filters deal with uncertainty in a dynamical non-stationary process optimally?

KFs are probabilistic approaches that rely on a single measure that provides the likelihood of certain events to occur with the assumption that the PDF is Gaussian. Further-

more, it approximates any type of nonlinearity using a first-order linearization relying on the first and second moment (mean and variance) only. Consequently,

3. What are the limitations of probabilistic approaches when dealing with epistemic uncertainty in a dynamical environment?

The positioning of a satellite has to be conducted as fast as possible with minimum computational resources used. Therefore,

4. What are the time and space computational complexities of current approaches?
5. Can these approaches be implemented in a single low power-computing unit?
6. What are the attributes of fuzzy theory in dealing with epistemic uncertainty?
7. How is uncertainty represented and characterized using fuzzy theory?
8. Can a computationally efficient algorithm based on a fuzzy inference system be developed to estimate the attitude of small satellites optimally?
9. How is the granulation of data accomplished?
10. How is the optimality of the structures and configuration of data granules defined?

Though some of these questions will not be fully answered since they require a more extensive work that lies beyond the scope of the topics related to this thesis, they will be addressed partially.

1.2.3.2 Attitude Control

Energy generation and consumption represent one of the most important issues small satellites face. Consequently, the control scheme selected has to be conducted in an optimal way maximizing its performance to lengthen the battery life. Therefore,

11. What constitutes an optimal and robust control scheme for the attitude control?

12. What are the relative merits of a fractional-order proportional-integral-derivative and fuzzy controllers when dealing with this nonlinear navigation problem?

1.3 Organization of the Thesis

This thesis presents a computationally efficient algorithm based on a fuzzy inference system and a gradient decent optimization technique for the estimation of the upper and lower bounds of the membership functions for the purpose of attitude determination in pico- and nano-satellites. Furthermore, the design of an optimal fractional-order PID controller to minimize the power consumption associated with the activation of the actuators is described.

This thesis is divided into seven chapters. It is structured as follows: (i) three chapters for the theoretical knowledge describing the important components related to the attitude determination (such as the orbital elements and parameterization techniques), as well as the evaluation of current approaches; and (ii) two chapters for the introduction of the improved AD algorithm and the design of an optimal control scheme.

Chapter 2 introduces a background on attitude determination. This chapter discusses the different orbital elements and reference frames required to define the attitude. Additionally, several attitude parameterization techniques (*e.g.*, Euler Angles, Quaternions, and Modified Rodrigues Parameters) are compared.

Chapter 3 introduces current deterministic and probabilistic approaches for the purpose of AD. In this chapter, three different deterministic algorithms (TRIAD, QUEST, and extended QUEST) and two probabilistic ones (Kalman filters) are discussed extensively.

Their respective computational complexity, advantages, and disadvantages are studied as well.

Chapter 4 evaluates all approaches introduced in Chapter 3 to establish conclusions regarding their limitations. This is based on test cases mimicking the different conditions that might be encountered in space. Among these cases, large initial errors in the attitude and noisy measurements are considered.

Chapter 5 provides the background knowledge needed to develop an algorithm based on fuzzy theory. Additionally, the improved attitude determination algorithm is introduced, as well as its simulation results. The improved attitude algorithm is evaluated using the experiments described in subsection 1.2.3.1.

Chapter 6 addresses challenges related to the controllability and power consumption of small satellites. This chapter introduces three different controllers (integer-order PID, fractional-order PID, and fuzzy) and evaluates them based on the test cases discussed in subsection 1.2.3.2 for the purpose of selecting an optimal control.

Chapter 7 provides answers to the research questions addressed in Section 1.2.3, as well as acknowledge the limitations of the current work. Additionally, recommendations and suggestions for future work are mentioned.

Chapter 2

BACKGROUND ON ATTITUDE DETERMINATION

The *attitude determination* is the process responsible for estimating the orientation of the spacecraft relative to either an inertial reference frame or some specific object of interest such as the Sun. This process requires one or more measurements that can be obtained from attitude sensors such as TAM, Sun sensors, and Earth-horizon sensor. This process requires the selection of key components such as the attitude representation and parameterization techniques. This chapter discusses the orbital elements, reference frames, and rotation matrices required for the attitude representation, as well as the attitude parameterization techniques.

2.1 Attitude Representation

The orbit or trajectory is the path of a spacecraft or a natural body through space. Typically, the trajectory is specified by a state-vector (such as the position and velocity of the spacecraft) at some specified time or epoch. This is accomplished through the mathematical analysis of the orbits and their properties, referred to as *astrodynamics*. The state-vector at any point in time allows for the prediction of the position and the velocity of the spacecraft at all future times based on the assumptions made in the models used [ThSh10]. Astrodynamics provides a list of successive positions called *ephemeris.*

A Keplerian (after Johann Kepler [1571-1630]) orbit is one orbit, in which the gravity is the only force; the central body is spherically symmetric; the central body's mass is much greater than that of the satellite; and the central body and the satellite are the only two objects in the system [WeLa99]. Based on these definitions, the orbital elements and the reference frames are introduced.

2.1.1 Orbital Elements

In order to define an orbit, Keplerian elements are used for this purpose. Figure 2.1 shows a graphical representation of the orbital elements, including: (i) the orbital inclination, (ii) the right ascension of the ascending node, (iii) the eccentricity, (iv) the argument of perigee, (v) the mean motion, (vi) the mean anomaly, and (vii) the epoch.

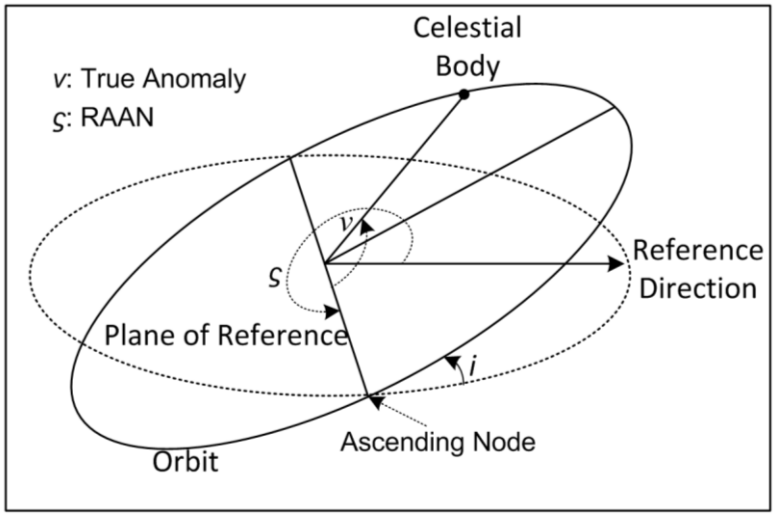

Fig. 2.1. Three-dimensional elements defining an orbit.

The first four orbital elements specify the orientation of the orbital ellipse and its shape, while the last three elements describe the motion and the position of the satellite in its orbit.

2.1.1.1 Orbital Inclination

The orbital ellipse lies in a plane called the orbital plane. This plane goes through the center of the Earth and might be tilted with an angle relative to the equator, which is known as the orbital inclination. The orbital inclination (denoted *i*) is a number between 0 deg. and 180 deg. Orbits with an inclination near zero or ninety degrees are referred to as equatorial or polar orbits, respectively. The line of nodes is the line resulting from the intersection of the equatorial and the orbital plane that passes through the center of mass. The orbital inclination is shown in Figure 2.1.

2.1.1.2 Right Ascension of the Ascending Node

The *right ascension of the ascending node* (RAAN), denoted ς, is defined by the angle in the equatorial plane measured eastward from the vernal equinox to the ascending node of the orbit. The ascending node is a result of the intersection of the line of nodes with the equatorial plane going from south to north [WeLa99].

2.1.1.3 Argument of Perigee

The perigee defines the point in the ellipse closest to the focus point in the Earth, while the apogee defines the farthest point in the ellipse from the Earth. The argument of perigee (denoted Υ) is the angle between the line crossing the perigee through the center of the Earth to the apogee, and the line of nodes. In other words, it is the angle from the ascending node to the perigee.

2.1.1.4 Eccentricity

The orbital eccentricity is a parameter that determines the amount by which it deviates from a perfect circle. The eccentricity is calculated using Eq. (2.1).

$$\varepsilon = \sqrt{1 - \frac{\beta^2}{\alpha^2}} \tag{2.1}$$

where α is the semi-major-axis (defined as half the distance between the apogee and the perigee) and β is the semi-minor axis (defined as half the distance between the edges perpendicular to the semi-major axis).

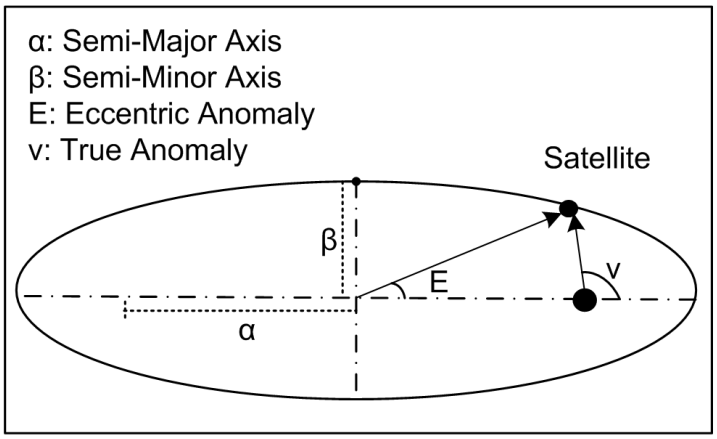

Fig. 2.2. Orbital elements**.**

2.1.1.5 Mean Motion

The mean motion is the average angular velocity in rad/sec (denoted $\bar{\omega}$). It is also defined as the number of revolutions per days. The semi-major-axis is related through Kepler's third law as shown in Eq. (2.2).

$$\bar{\omega}^2 \alpha^3 = \mu_e \tag{2.2}$$

where u_e=GM_e represents the Earth's gravitational constant with G representing the universal gravitational constant and M_e is the mass of the Earth.

2.1.1.6 Mean Anomaly

The mean anomaly is the angle that marches uniformly in time (from 0 deg. to 360 deg.) representing where the satellite is positioned during one revolution. By convention, it is 0 deg. at the perigee and 180 deg. at the apogee.

2.1.2 Reference Frames

This section describes the main reference frames required to estimate the attitude with respect to an inertial frame [Rohd07].

2.1.2.1 Earth-Centered Inertial Frame

The *Earth centered inertial* (ECI) frame is a fixed non-accelerating frame where Newton's laws of motion apply. The center of the ECI frame (denoted x_i, y_i, and z_i) coincides with the Earth's center and the z-axis is directed towards the North Pole. Also, the x-axis is directed towards the vernal equinox and the y-axis completes the Cartesian coordinate based on the right-hand rule system.

2.1.2.2 Earth-Centered Earth-Fixed Frame

The *Earth-centered Earth-fixed* (ECEF) frame has its origins (x_e, y_e, and z_e) fixed with the center of the Earth, while rotating relatively to the ECI frame with a frequency of rotation approximated to 7.29×10^{-5}. The z-axis points towards the North Pole and the x-axis is directed towards the intersection between the Greenwich meridian and the equator.

2.1.2.3 Orbital Frame

The orbital-frame is centered in the satellite's center of mass. The origin rotates relative to the ECI frame with an angular velocity ω_0. The z-axis points towards the center of the Earth, the x-axis is the normal direction of the orbital plane and the y-axis completes the Cartesian based on a right-hand rule system.

2.1.2.4 Body Frame

The body frame is a moving Cartesian coordinate frame fixed to the satellite with its origin fixed on the center of mass. The x-axis points forward towards the direction of travel, while the z-axis points towards the nadir-side of the satellite, and the y-axis completes the Cartesian based on a right-hand rule system.

2.2 Attitude Parameterization

The representation of the satellite's orientation in space is not a trivial task. This section describes two techniques for a three-axis attitude parameterization. These techniques are Euler's and unit quaternion parameterization techniques.

Assuming that there exists an orthogonal, right-handed tri-axis system $\hat{\mathbf{u}}$, $\hat{\mathbf{v}}$, and $\hat{\mathbf{w}}$ of unit vectors fixed in the body such that

$$\hat{\mathbf{u}} \times \hat{\mathbf{v}} = \hat{\mathbf{w}} \tag{2.3}$$

The main objective is to specify the orientation of the system with respect to a reference coordinate frame, as illustrated in Fig 2.3.

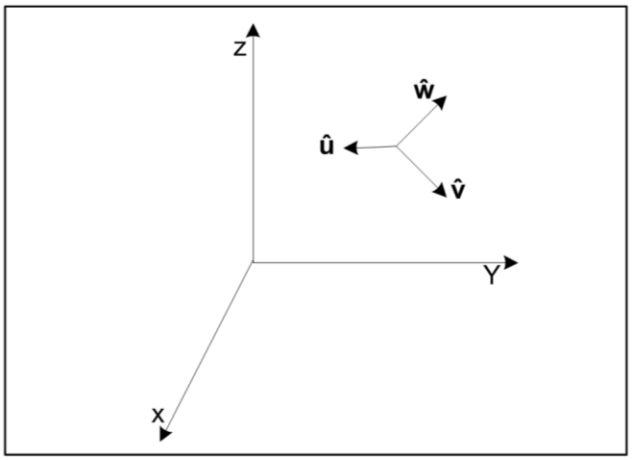

Fig. 2.3. Attitude representation using right-handed tri-axis systems.

Specifying the components of $\hat{\mathbf{u}}$, $\hat{\mathbf{v}}$, and $\hat{\mathbf{w}}$ along the three axes of the reference coordinate frame will fix the orientation completely. This requires the definition of the ***attitude matrix*** (denoted **A**). This matrix provides the rotation that brings the axis of the reference frame onto the axis of the body frame. It is a 3×3 matrix having the following form

$$\mathbf{A} \equiv \begin{bmatrix} u_1 & u_2 & u_3 \\ v_1 & v_2 & v_3 \\ w_1 & w_2 & w_3 \end{bmatrix} \tag{2.4}$$

where $\hat{\mathbf{u}} = (u_1, u_2, u_3)^T$, $\hat{\mathbf{v}} = (v_1, v_2, v_3)^T$, and $\hat{\mathbf{w}} = (w_1, w_2, w_3)^T$. $(\bullet)^T$ represents the transpose operator.

Each element in the **A** matrix represents the cosine of the angle between a unit vector in the body frame and a reference axis (the attitude matrix is also referred to as the *direction cosine matrix*, DCM). This technique requires 9 elements to represent the attitude of a rigid body.

2.2.1 Euler Angles

Unlike the DCM, Euler angles require three parameters to represent the rigid body in space. The typical set of parameters used for describing the motions of spacecraft is the roll-pitch-yaw angles. Based on these parameters, a rotation matrix from *a* to *b* is given as

$$\mathbf{R}_b^a = \mathbf{R}_{x,\,y,\,z}(\psi, \theta, \phi) = \mathbf{R}_z(\psi)\mathbf{R}_y(\theta)\mathbf{R}_x(\phi) \tag{2.5}$$

where $\mathbf{R}_x(\phi)$, $\mathbf{R}_y(\theta)$, and $\mathbf{R}_z(\psi)$ denote a rotation around the *x*-axis, y-axis, and z-axis with angles ϕ, θ, and ψ, respectively as defined in Eqs. (2.6), (2.7), and (2.8) [Rohd07].

$$\mathbf{R}_x(\phi) = \begin{bmatrix} 1 & 0 & 0 \\ 0 & \cos\phi & -\sin\phi \\ 0 & \sin\phi & \cos\phi \end{bmatrix} \tag{2.6}$$

$$\mathbf{R}_y(\theta) = \begin{bmatrix} \cos\theta & 0 & \sin\theta \\ 0 & 1 & 0 \\ -\sin\theta & 0 & \cos\theta \end{bmatrix} \tag{2.7}$$

$$\mathbf{R}_z(\psi) = \begin{bmatrix} \cos\psi & -\sin\psi & 0 \\ \sin\psi & \cos\psi & 0 \\ 0 & 0 & 1 \end{bmatrix} \tag{2.8}$$

The main disadvantages of Euler angles are: (i) they suffer from singularities under certain rotations (gimbal lock). The gimbal lock is the loss of one degree of freedom in a three-dimensional system; and (ii) they are less accurate when used to integrate incremental changes in the attitude over time compared to alternative techniques (such as the unit-quaternion) [Dieb06]. These disadvantages have led to the selection of the unit-quaternion as a parameterization technique.

2.2.2 Unit-Quaternion

William Rowan Hamilton (1805-1865) introduced quaternions as an extension to complex numbers. The quaternion, as shown in Fig. 2.4, is a 4×1 matrix, which consists of a vector part $\boldsymbol{\varphi}$ and a scalar part q_4. The quaternion is defined by

$$\mathbf{q} = \begin{bmatrix} \boldsymbol{\varphi} & q_4 \end{bmatrix}^T \tag{2.9}$$

where

$$\boldsymbol{\varphi} = \begin{bmatrix} q_1 & q_2 & q_3 \end{bmatrix}^T = \hat{\mathbf{e}} \sin(\vartheta/2) \tag{2.10}$$

$$q_4 = \cos(\vartheta/2) \tag{2.11}$$

with $\hat{\mathbf{e}}$ is the axis of rotation and ϑ represents the angle of rotation.

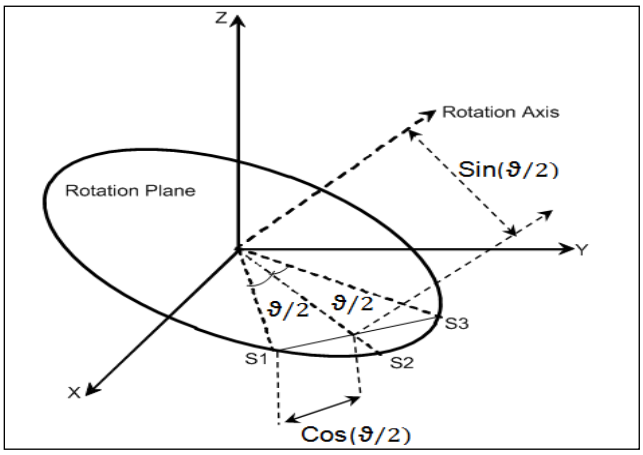

Fig. 2.4. Graphical representation of the quaternion.

The quaternion is subjected to a single constraint given by

$$\mathbf{q}^T\mathbf{q} = 1 \tag{2.12}$$

For small angles, the quaternion is approximated by

$$\mathbf{q} \approx \begin{bmatrix} \frac{\vartheta}{2}\hat{\mathbf{e}} \\ 1 \end{bmatrix} \tag{2.13}$$

The *attitude matrix* can be obtained from the quaternion according to the following relation [LeMS82]

$$\mathbf{A}(\mathbf{q}) = (q_4^2 - \boldsymbol{\varphi}^T\boldsymbol{\varphi})\mathbf{1}_{3\times3} + 2\boldsymbol{\varphi}\boldsymbol{\varphi}^T - 2q_4[\boldsymbol{\varphi}\times] \tag{2.14}$$

where $\mathbf{1}_{3\times3}$ is the 3×3 identity matrix and $[\boldsymbol{\varphi}\times]$ is the cross product matrix, which is defined by

$$[\boldsymbol{\varphi}\times] \triangleq \begin{bmatrix} 0 & -q_3 & q_2 \\ q_3 & 0 & -q_1 \\ -q_2 & q_1 & 0 \end{bmatrix} \tag{2.15}$$

The quaternion kinematics equation is given by the following differential equation

$$\dot{\mathbf{q}} = \frac{1}{2}\Pi(\boldsymbol{\omega})\mathbf{q} \tag{2.16}$$

where Π is a 4×4 skew-symmetric matrix, which is a function of the three-component angular rate vector **ω**. **ω** is the velocity of the body with respect to the reference frame projected onto the body frame [Chou03]. Finally,

$$\Pi(\boldsymbol{\omega}) \triangleq \begin{bmatrix} -[\boldsymbol{\omega}\times] & \boldsymbol{\omega} \\ -\boldsymbol{\omega}^T & 0 \end{bmatrix} \tag{2.17}$$

Though the quaternions are the preferred parameterization technique for the attitude, other parameterization techniques have been used for similar applications. For instance, the *modified Rodrigues parameters* (MRP) have been used for the implementation of an unscented Kalman filter [CrMa96]. Table 2.1 highlights the characteristics of the techniques presented [Shus93][JeVi10].

Table 2.1: Comparison between attitude parameterization techniques.

Representation	Parameters	Characteristics
Euler Angles	3	Minimal set Intuitive interpretation Relies on trigonometric functions.
DCM	9	Inherently nonsingular. Intuitive representation. Difficult to maintain orthogonality. Expensive computational cost. Six redundant parameters.
MRP	3	Minimal set. Suffer from singularities. Simple kinematic relation.
Quaternions	4	Orthogonality of rotation matrix easily preserved. Immune to singularities. Linear simple kinematic equations. One redundant parameter only.

The main advantages of using the quaternion as a parameterization scheme for the attitude are the following:

1. The rotations are expressed by the quaternion product. Composite rotations can be performed in terms of quaternion multiplications without involving trigonometric functions;
2. Quaternion unit-norm provides an easy way to preserve the orthogonality of the rotation matrix; and
3. The kinematics equation is linear in the quaternion.

2.3 Reference Models

2.3.1 International Geomagnetic Reference Field Model

The *international geomagnetic reference field* (IGRF) is a standard mathematical model that describes the main magnetic field vector from the Earth's core out into space with its secular variation (annual rate of change). The IGRF model is updated every five years by the *international association of geomagnetism and astronomy* (IAGA). Eq. (2.18) shows the modeling of the IGRF based on the Gauss coefficients which define a spherical harmonic expansion of the magnetic scalar potential.

$$V(d,\varphi,\theta) = R_{\mathrm{e}} \sum_{n_1=1}^{L} \sum_{n_2=0}^{n_1} \left(\frac{R_{\mathrm{e}}}{d} \right)^{n_1+1} \left(g_{n_1}^{n_2} \cos n_2\varphi + h_{n_1}^{n_2} \sin n_2\varphi \right) P_{n_1}^{n_2}(\cos\theta) \qquad (2.18)$$

where d is the radial distance from the Earth's center, L is the maximum degree of the expansion, φ is East longitude, θ is colatitude (the polar angle), R_e is the Earth's radius, $g_{n_1}^{n_2}$ and $h_{n_1}^{n_2}$ are Gauss coefficients, and $P_{n_1}^{n_2}(\cos\theta)$ are the Schmidt normalized associated

Legendre functions of degree n_1 and order n_2 [Ghuf09]. Other mathematical models assume coefficient varying in time at a constant rate [MaMa05]. Figure 2.5 shows the total magnetic field of the Earth in nano-Teslas.

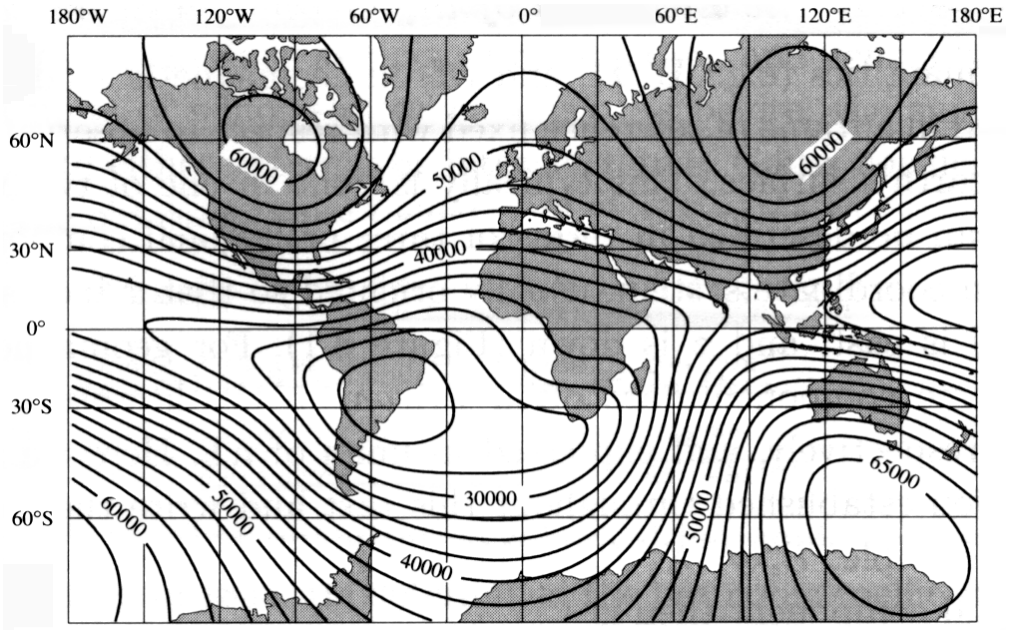

Fig. 2.5. Graphical representation of the total magnetic field in nano-Teslas [Magn13].

2.3.2 Sun Reference Model

A Sun reference model is required to estimate the reference data in the orbital frame. This estimation is based on the assumption that the Earth's orbit has duration of 365 days with the satellite positioned in the center of the Earth. The error introduced by this assumption is negligible and approximately equal to

$$error = \arctan(\frac{R_a}{R_e}) \tag{2.19}$$

where R_a is the radius of the satellite's orbit.

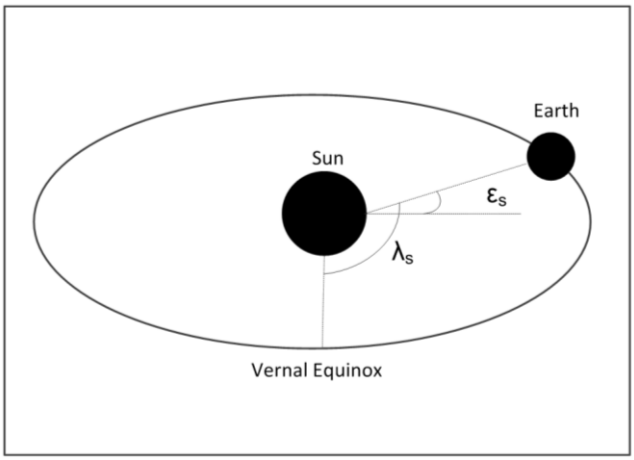

Fig. 2.6. The position of the Sun relative to the Earth.

The elevation of the Sun (denoted ε_s) varies between -23 deg. and 23 deg. depending on the time of the year [Rohd07]. The period is given by

$$\varepsilon_S = \frac{23\pi}{180}\sin(\frac{T_S}{365}2\pi) \tag{2.20}$$

$$\lambda_S = \frac{T_S}{365}2\pi \tag{2.21}$$

where λ_s is called the Sun's orbit parameter. T_s denotes the period in time. The Sun's position when the Earth passes vernal equinox is

$$\mathbf{s}_0^i = [1 \quad 0 \quad 0]^T \tag{2.22}$$

and with this vector we can express the Sun position at any given time as

$$\mathbf{s}^i = \mathbf{R}_y(\varepsilon_S)\mathbf{R}_z(\lambda_S)\mathbf{s}_0^i \tag{2.23}$$

2.4 Summary

Chapter 2 provided the background knowledge required to define and parameterize the attitude of a rigid body in space. Additionally, a comparison between several parameterization techniques was presented to justify the use of the unit-norm quaternion to represent the attitude. Finally, the Earth magnetic field and Sun reference models have been introduced. These models are critical for the estimation of the attitude since they are required to calculate the innovation in the body frame measurements using the deterministic and stochastic algorithms that are introduced in Chapter 3.

Chapter 3

ATTITUDE DETERMINATION ALGORITHMS, LITERATURE REVIEW

This chapter introduces standard and state-of-the-art deterministic and stochastic approaches to estimate the relative orientation of a spacecraft. Deterministic approaches provide point-by-point solutions, where the attitude is found based on two or more vector observations from a single point in time. These approaches suffer from a lack of probabilistic significance resulting in a poor performance when subjected to uncertainty in the estimation process and measurements collected from onboard sensors. On the other hand, stochastic approaches are recursive probabilistic estimators that statistically combine measurements from onboard sensors with dynamics and/or kinematics models to converge towards a solution. Both of these approaches belong to the realm of the linear *least squares* (LS) estimation theory, where the term "least squares" refers to the constrained least square for deterministic approaches and the minimum variance least square for stochastic approaches [Chou03].

3.1 Literature Survey

Attitude determination requires the specification of a Cartesian coordinate frame orientation fixed to the rigid-body with respect to a given reference. If the reference frame is non-moving, then it is referred to as an inertial frame. This process requires the definition of two coordinate systems with orthogonal unit-vectors. The first one is fixed to the spacecraft body and the second one is attached to the reference frame.

The attitude matrix maps the reference frame to the body frame. This can be expressed by the following linear equation

$$\tilde{\mathbf{b}}=\mathbf{A}\mathbf{r}+\mathbf{v} \tag{3.1}$$

$$\mathbf{v}^T\mathbf{A}\mathbf{r}=0 \tag{3.2}$$

where **r** represents the reference frame vector, while $\tilde{\mathbf{b}}$ denotes sensor measurements corrupted with a Gaussian noise **v** with the following properties

$$E[\mathbf{v}]=0 \tag{3.3}$$

$$\mathbf{R}\equiv E[\mathbf{v}\mathbf{v}^T]=\sigma^2[\mathbf{1}_{3\times 3}-(\mathbf{A}\mathbf{r})(\mathbf{A}\mathbf{r})^T] \tag{3.4}$$

where $E[\bullet]$ denotes the expected value, σ represents the standard deviation of the process.

3.2 Deterministic Approaches

3.2.1 The Original TRIAD Algorithm

One of the first attitude determination algorithms introduced is the *tri-axis attitude determination* (TRIAD) algorithm developed by Harold Black in 1964 [TaSh07][Blac64]. This algorithm was used in numerous space missions (such as *small astronomy satellite*, SAS, Seasat, *atmospheric explorer missions*, AEM, and Magsat) for the purpose of attitude estimation due to its simplicity and low computational cost [ShOh81]. The TRIAD algorithm knows different deterministic formulations for the estimation of the attitude matrix, which are guaranteed to be equivalent for data uncorrupted with noise only. These formulations encompass: (i) the TRIAD algorithm (TRIAD-I), (ii) the *reversed TRIAD* algorithm (TRIAD-II), (iii) the *symmetric TRIAD* algorithm (S-TRIAD), (iv) the TRAD algorithm, (v) and the *optimal* TRIAD algorithm (O-TRIAD) [TaSh07]. This section discusses the original TRIAD algorithm only.

The TRIAD algorithm relies on a pair of unit-vectors represented in both the spacecraft body frame and the reference frame

$$\tilde{\mathbf{b}}_1 = \mathbf{A}\mathbf{r}_1 + \mathbf{v} \tag{3.5}$$

$$\tilde{\mathbf{b}}_2 = \mathbf{A}\mathbf{r}_2 + \mathbf{v} \tag{3.6}$$

The algorithm estimates the attitude matrix as a product of two proper orthogonal matrices. The first matrix has its columns defined by a right-hand orthonormal triad of column vectors constructed from the two vector observations. Similarly, the second matrix has its

rows defined in the same way based on reference vectors. The original asymmetric triads $\{\mathbf{T}_{b1}, \mathbf{T}_{b2}, \mathbf{T}_{b3}\}$ and $\{\mathbf{T}_{r1}, \mathbf{T}_{r2}, \mathbf{T}_{r3}\}$ are constructed as follows [ShOh81]

$$\mathbf{T}_{b1} = \tilde{\mathbf{b}}_1, \quad \mathbf{T}_{b2} = \frac{\tilde{\mathbf{b}}_1 \times \tilde{\mathbf{b}}_2}{|\mathbf{b}_1 \times \mathbf{b}_2|}, \quad \mathbf{T}_{b3} = \mathbf{T}_{b1} \times \mathbf{T}_{b2} \tag{3.7}$$

$$\mathbf{T}_{r1} = \mathbf{r}_1, \quad \mathbf{T}_{r2} = \frac{\mathbf{r}_1 \times \mathbf{r}_2}{|\mathbf{r}_1 \times \mathbf{r}_2|}, \quad \mathbf{T}_{r3} = \mathbf{T}_{r1} \times \mathbf{T}_{r2} \tag{3.8}$$

with the attitude defined by

$$\mathbf{A} = \sum_{i=1}^{3} \mathbf{T}_{bi} \mathbf{T}_{ri}^{T} \tag{3.9}$$

The solution obtained based on this algorithm is not symmetric with respect to the indices 1 and 2. This can be seen from the way the first and second observation vectors are handled. The information contained in the second vector is discarded partially. Unlike the first vector, it contributes to the cross-product only. Moreover, this algorithm knows two important limitations: (i) the first one is related to the calculation of the covariance matrix that requires numerous partial derivatives computed as differences. Calculating the covariance matrix is more computationally complex than the estimation of the attitude; (ii) it can handle two measurements at a time only [ShOh81].

In order to deal with these limitations, alternative batch algorithms were introduced to provide an improved estimate of the attitude based on loss functions. These loss functions can take into account all or part of the available measurements at the expense of a longer processing time. An example of such loss functions is Wahba's problem.

3.2.2 Wahba's Problem

In 1965, Grace Wahba introduced a constrained least square optimization problem to estimate the attitude of a spacecraft at a single instant of time [Wahb65]. The estimation process relies on two or more measurements in the body reference frame. Wahba formulated the problem as given two sets of m vectors denoted $\{\mathbf{r}_1, \mathbf{r}_{2\ldots}\ \mathbf{r}_m\}$ and $\{\tilde{\mathbf{b}}_1, \tilde{\mathbf{b}}_{2\ldots}\ \tilde{\mathbf{b}}_m\}$ with $m \geq 2$. Each pair $(\mathbf{r}_i, \tilde{\mathbf{b}}_i)$ corresponds to a generalized vector $\mathbf{x}_i$, where the main objective is to find the proper orthogonal matrix, $\mathbf{A}$, which approximates the first set into the best LS coincidence with the second; that is, find $\mathbf{A}$ which minimizes the cost function J [Chou03].

$$J(\mathbf{A}) = \sum_{i=1}^{m} a_i \left\| \tilde{\mathbf{b}}_i - \mathbf{A}\mathbf{r}_i \right\|^2 \tag{3.10}$$

$$J(\mathbf{q}) = \sum_{i=1}^{m} \frac{1}{\sigma_i^2} \left[\tilde{\mathbf{b}}_i - \mathbf{A}(\mathbf{q})\mathbf{r}_i \right]^T \left[\tilde{\mathbf{b}}_i - \mathbf{A}(\mathbf{q})\mathbf{r}_i \right] \tag{3.11}$$

subjected to the constraint $\mathbf{A}^T\mathbf{A} = \mathbf{1}_{3\times3}$ and $\det(\mathbf{A})=1$. a_i denotes tuning parameters and σ^2 represents the variance of the measurement noise.

Equations (3.10) and (3.11) define a constrained least-square cost function to be minimized, where $\mathbf{r}$ and $\tilde{\mathbf{b}}$ represent vector observations from two different coordinate frames. This function penalizes the error between the body-measured unit direction vector $\tilde{\mathbf{b}}_i$ and the transformation of the corresponding unit-reference vectors $\mathbf{r}_i$ from inertial coordinates using tuning parameters. Tuning parameters (denoted a_i) might be selected as the inverse variance of the measurement noise as indicated in Eq. (3.11) [MaMo00][Psia10]. One of the pitfalls of these cost functions is related to the tuning parameters. The selection of the tuning parameters is a heuristic choice; yet, a reformulation of the Wahba's problem as a

maximum likelihood estimation problem was conducted in published literature to determine the tuning parameters [Shus89]. These reformulations target *single-frame* attitude determination algorithms; that is, they assume that the vector measurements being processed to estimate the attitude have been taken from a constant attitude.

3.2.3 QUEST Algorithm

The *quaternion estimator* (QUEST) is a recursive estimator introduced to solve Wahba's problem based on the **q**-method developed by Davenport [Keat77]. This algorithm computes the optimal attitude based on a batch of *m* simultaneous observations. QUEST provides a way to process more than two directional measurements. It has found application for the first time in MAGSAT mission in 1979 [MaMo00].

The loss function shown in Eq. (3.10) can be rewritten as [MaCC05][CrMC07]

$$J(\mathbf{A}) = \lambda_0 - trace(\mathbf{A}\mathbf{B}^T) \tag{3.12}$$

with

$$\lambda_0 \triangleq \sum_{i=1}^{m} a_i \tag{3.13}$$

and

$$\mathbf{B} \triangleq \sum_{i=1}^{m} a_i \tilde{\mathbf{b}}_i \mathbf{r}_i^T \tag{3.14}$$

where *m* denotes the total number of measurements.

Minimizing (3.12) is similar to maximizing the $trace(\mathbf{AB}^T)$ in the same equation. Solving this problem yields [CrMC07]

$$trace(\mathbf{AB}^T) = \mathbf{q}^T \mathbf{K} \mathbf{q} \tag{3.15}$$

where **K** is the symmetric traceless matrix and **B** is given by

$$\mathbf{K} \triangleq \begin{bmatrix} \mathbf{B} + \mathbf{B}^T - trace(\mathbf{B})\mathbf{I}_{3\times 3} & \sum_{i=1}^{m} a_i \tilde{\mathbf{b}}_i \times \mathbf{r}_i \\ (\sum_{i=1}^{m} a_i \tilde{\mathbf{b}}_i \times \mathbf{r}_i)^T & trace(\mathbf{B}) \end{bmatrix} = -\sum_{i=1}^{m} a_i \Pi(\tilde{\mathbf{b}}_i)\Xi(\mathbf{r}_i) \tag{3.16a}$$

where

$$\Xi(\mathbf{r}_i) \triangleq \begin{bmatrix} [\mathbf{r}_i \times] & \mathbf{r}_i \\ -\mathbf{r}_i^T & 0 \end{bmatrix} \tag{3.16b}$$

The matrix **B** is propagated and updated sequentially. The optimal attitude is represented by the quaternion maximizing the right-hand side of Eq. (3.15)

$$\mathbf{K}\mathbf{q}_{opt} = \lambda_{\max} \mathbf{q}_{opt} \tag{3.17}$$

with Eqs. (3.12) and (3.15), the optimized loss function is given as

$$J(\mathbf{A}_{opt}) = \lambda_0 - \lambda_{\max} \tag{3.18}$$

where λ_{max} denotes the greatest eigenvalue of the **K** matrix.

$$\mathbf{B}(t_k) = \mu \mathbf{\Phi}(t_k, t_{k-1})\mathbf{B}(t_{k-1}) + \sum_{i=1}^{m_k} a_i \tilde{\mathbf{b}}_i \mathbf{r}_i^T \tag{3.19}$$

where $\mathbf{\Phi}_{3\times 3}(t_k, t_{k-1})$ represents the state transition matrix for the attitude matrix, μ denotes a fading memory factor (μ is assumed to be < 1), and m_k is the number of observations at time t_k. An optimal estimate of the attitude is found from $\mathbf{B}(t_k)$.

Alternative filters such as the *recursive quaternion estimator* (REQUEST) have been described also in [Bar96]. The REQUEST propagates and updates the **K** matrix instead of the **B** matrix. Thus, the QUEST and REQUEST are mathematically equivalent, but the REQUEST requires relatively more computations [ChBO04].

3.2.4 Extended QUEST

Unlike the QUEST algorithm, the *extended QUEST* operates in a two-stage process, namely prediction and correction. This allows for the inclusion of complicated dynamics model to estimate other critical parameters (in addition to the attitude) [Psia01]. This is accomplished by estimating the state-vector $\mathbf{x}_k$ (which includes the attitude quaternion $\mathbf{q}_k$ and the vector of auxiliary parameters along with the process noise $\mathbf{w}_{k\text{-}1}$) that minimizes the loss function [MaCC05]. This algorithm is known to be more computationally expensive; yet, more robust compared to the QUEST. Equation (3.20) shows the loss function to be minimized

$$J(\mathbf{A}) = \frac{1}{2}\sum_{i=1}^{m_k}\sigma_i^{-2}\left\|\tilde{\mathbf{b}}_i - \mathbf{A}(\mathbf{q}_k)\mathbf{r}_i\right\|^2 + \frac{1}{2}\left\|\mathbf{R}_{\mathbf{ww}}(k-1)\mathbf{w}_{k-1}\right\|^2 + \frac{1}{2}\left\|\mathbf{R}_{\mathbf{qq}}(k-1)(\mathbf{q}_{k-1} - \hat{\mathbf{q}}_{k-1})\right\|^2 + \frac{1}{2}\left\|\mathbf{R}_{\mathbf{xq}}(k-1)(\mathbf{q}_{k-1} - \hat{\mathbf{q}}_{k-1}) + \mathbf{R}_{\mathbf{xx}}(k-1)(\mathbf{x}_{k-1} - \hat{\mathbf{x}}_{k-1})\right\|^2 \tag{3.20}$$

subject to the attitude dynamics equation,

$$\mathbf{q}_k = \mathbf{\Phi}(t_k, t_{k-1}; \mathbf{q}_{k-1}, \mathbf{x}_{k-1}, \mathbf{w}_{k-1})\mathbf{q}_{k-1} \tag{3.21}$$

the transition equation for the auxiliary filter states,

$$\mathbf{x}_k = \mathbf{f}_{\mathbf{x}}(t_k, t_{k-1}; \mathbf{q}_{k-1}, \mathbf{x}_{k-1}, \mathbf{w}_{k-1}) \tag{3.22}$$

the vector $\mathbf{q}_{k-1}$ and $\mathbf{x}_{k-1}$ denotes the a posteriori estimate of $\mathbf{q}$ and $\mathbf{x}$ at sample time t_{k-1}, respectively. $\mathbf{f}$ denotes a known nonlinear function. $\mathbf{R}_{ww}$, $\mathbf{R}_{qq}$, $\mathbf{R}_{xq}$, and $\mathbf{R}_{xx}$ represent weights in the loss function.

The result of the propagation step is a modified form of the loss function [MaCC05]

$$J(\mathbf{q}_k,\mathbf{x}_k)=\frac{1}{2}\sum_{i=1}^{m_k}\sigma_i^{-2}\left\|\tilde{\mathbf{b}}_i-\mathbf{A}(\mathbf{q}_k)\mathbf{r}_i\right\|^2+\frac{1}{2}\left\|\tilde{\mathbf{R}}_{\mathbf{qq}}(k)(\mathbf{q}_k-\tilde{\mathbf{q}}_k)\right\|^2 + \frac{1}{2}\left\|\tilde{\mathbf{R}}_{\mathbf{xq}}(k)(\mathbf{q}_k-\tilde{\mathbf{q}}_k)+\tilde{\mathbf{R}}_{\mathbf{xx}}(k)(\mathbf{x}_k-\tilde{\mathbf{x}}_k)\right\|^2 \tag{3.23}$$

where the $\tilde{\mathbf{R}}$ matrices are obtained by a QR factorization in the propagation step that employs a linearization about a priori estimates at stage k-1. Eq. (3.24) is an approximation to Eq. (3.21), if the dynamics is nonlinear. Otherwise, they are equivalent.

The extended QUEST has a second phase referred to as the measurement update.

The optimum $\hat{\mathbf{x}}$ is given by

$$\mathbf{x}_k=\tilde{\mathbf{x}}_k-\tilde{\mathbf{R}}_{\mathbf{xx}}^{-1}(k)\tilde{\mathbf{R}}_{\mathbf{xq}}(k)(\mathbf{q}_k-\tilde{\mathbf{q}}_k) \tag{3.24}$$

$$J(\mathbf{q}_k,\hat{\mathbf{x}}_k)=-\mathbf{q}_k^T\left(\sum_{i=1}^{m_k}\sigma_i^{-2}\mathbf{K}_i\right)\mathbf{q}_k+\frac{1}{2}\left[\tilde{\mathbf{R}}_{\mathbf{qq}}(k)(\mathbf{q}_k-\tilde{\mathbf{q}}_k)\right]^T\left[\tilde{\mathbf{R}}_{\mathbf{qq}}(k)(\mathbf{q}_k-\tilde{\mathbf{q}}_k)\right] \tag{3.25}$$

Minimizing the loss function gives the best estimate of the quaternion $\hat{\mathbf{q}}_k$. Substituting into Eq. (3.23) yields

$$\hat{\mathbf{x}}_k=\tilde{\mathbf{x}}_k-\tilde{\mathbf{R}}_{\mathbf{xx}}^{-1}(k)\tilde{\mathbf{R}}_{\mathbf{xq}}(k)(\hat{\mathbf{q}}_k-\tilde{\mathbf{q}}_k) \tag{3.26}$$

where the hat denotes the expected value.

Though these algorithms have found a wide range of applications for the purpose of orbital guidance and navigation, alternative approaches based on probability theory have been introduced to provide more accurate and robust solutions. These approaches (such

as KFs) have proven to be more efficient than most deterministic approaches described so far. This is due to the sub-optimality of the fading memory approximation on the effect of the process noise. Fading memory concept for continuous operators refers to the case where two input signals which are close in the recent past, but not necessarily close in the remote past results in present outputs which are close [BoCh85].Computing the fading memory factor by a Kalman-gain-like algorithm provides a better performance at the expense of a higher computational cost [ChBO04][Bar96].

3.3 Probabilistic Approaches

3.3.1 Discrete Kalman Filter

KF is a recursive estimator based on a Bayesian filtering approach [WeBi06]. This approach provides a standard set of procedures to calculate the PDF of the state of a dynamic system given a prior distribution and all prior observables. Calculating the PDF allows not only to estimate the state-vector of the system, but also to provide a description of the associated uncertainties. Bayesian filtering method is conducted in an iterative way, namely propagation and update.

Assuming a prior PDF of the state-vector $\mathbf{x}_{k-1}$ given all measurements available at time step k–1, it is possible to calculate the posterior PDF at time step k given by [MoMK09]

$$P(\mathbf{x}_k \mid \mathbf{y}_{1:k-1}) = \int P(\mathbf{x}_k \mid \mathbf{x}_{k-1}) P(\mathbf{x}_{k-1} \mid \mathbf{y}_{1:k-1}) d\mathbf{x}_{k-1} \tag{3.27}$$

where $\int(\bullet)$ denotes the integral operator, $P(\mathbf{x}_{k-1}|\mathbf{y}_{1:k-1})$ represents prior PDF and $\mathbf{y}_{1:k-1}$ indicates the observables up to time step k–1.

When a new observable is available, the predicted PDF is corrected by applying Bayes' rule given by

$$P(\mathbf{x}_k \mid \mathbf{y}_{1:k}) = \frac{P(\mathbf{y}_k \mid \mathbf{x}_k)P(\mathbf{x}_k \mid \mathbf{y}_{1:k-1})}{P(\mathbf{y}_k \mid \mathbf{y}_{1:k-1})} \tag{3.28}$$

where the normalizing constant $P(\mathbf{y}_k|\mathbf{y}_{1:k-1})$ is obtained from

$$P(\mathbf{y}_k \mid \mathbf{y}_{1:k-1}) = \int P(\mathbf{y}_k \mid \mathbf{x}_k)P(\mathbf{x}_k \mid \mathbf{y}_{1:k-1})d\mathbf{x}_k \tag{3.29}$$

Similarly, a KF encompasses a two-stage process to estimate the current state based on the conditional mean theorem and the principle of orthogonality.

The principle of orthogonality indicates that if the stochastic processes $\{\boldsymbol{x}_k\}$ and $\{\boldsymbol{y}_k\}$ are either: (i) jointly Gaussian or (ii) the optimal estimate $\hat{\mathbf{x}}_k$ is restricted to be a linear function of the observables with mean-square error as a cost function then the optimal estimate $\hat{\mathbf{x}}_k$, given the observables $\boldsymbol{y}_1, \boldsymbol{y}_2, \ldots, \boldsymbol{y}_k$ is the orthogonal projection of $\mathbf{x}_k$ on the space spanned by these observables [WaMe01]. Figure 3.1 shows the principle of orthogonality in one-dimensional closed subspace. A visual inspection indicates that the optimal estimation with minimum square error in a closed subspace denoted **w** (representing all possible approximation) is obtained when the error vector **e** is perpendicular to the subspace.

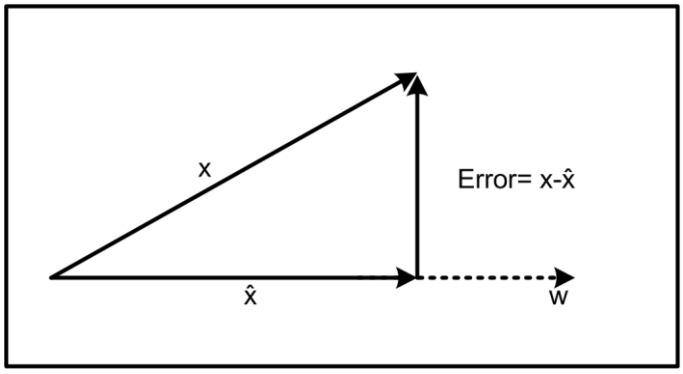

Fig. 3.1. Principal of orthogonality for one dimensional approximation subspace.

During the first stage (*i.e.*, the propagation) the filter predicts the state of the system based on the current state and measurement data. At each time step, the posterior PDF is assumed to be Gaussian. Then, the predicted state is corrected during the update stage when new absolute observations are collected [TrRo05]. The filter can update the first two moments of the conditional PDF of the state only. Figure 3.2 illustrates the iterative process followed by the KF to estimate the state of the system.

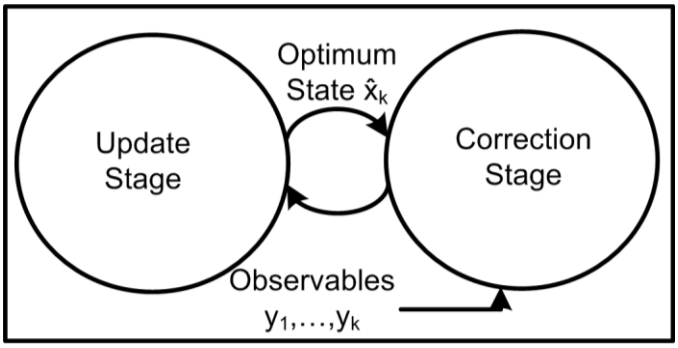

Fig. 3.2. Kalman filter estimation process.

The conditional mean estimator states that given stochastic processes $\{\boldsymbol{x}_k\}$ and $\{\boldsymbol{y}_k\}$ are jointly Gaussian, then the estimate $\hat{\mathbf{x}}_k$ that minimizes the mean-square error is the conditional mean estimator [WaMe01]

$$\hat{\mathbf{x}}_k = E\left[\mathbf{x}_k \mid \mathbf{y}_1, \mathbf{y}_2, \ldots, \mathbf{y}_k\right] \tag{3.30}$$

Let us consider the following linear discrete-time stochastic systems

$$\mathbf{x}_{k+1} = \boldsymbol{\Phi}\mathbf{x}_k + \mathbf{v}_k \tag{3.31}$$

$$\mathbf{y}_k = \mathbf{H}\mathbf{x}_k + \mathbf{u}_k \tag{3.32}$$

where $\mathbf{x}_k$ is the $n\times1$ state-vector, $\mathbf{u}_k$ is the control input, $\mathbf{y}_k$ is the $m\times1$ measurement vector, and $\mathbf{H}$ is a measurement matrix. The process noise $\mathbf{w}_k$ and the measurement noise $\mathbf{v}_k$ are assumed to be zero-mean Gaussian white noise with covariance given by [WaMe00]

$$E[\mathbf{w}_k \mathbf{w}_k^T] = \mathbf{Q}_k \tag{3.33}$$

The process noise $\mathbf{w}_k$ and the measurement noise $\mathbf{v}_k$ are uncorrelated. Thus, it follows that

$$E[\mathbf{v}_k \mathbf{w}_i^T] = 0 \tag{3.34}$$

The Kalman filtering approach attempts to jointly solve the process and measurement equations for the unknown state in an optimum manner. This is formally stated as follows. Using the last measured sensory data (assuming a white Gaussian process), find the minimum mean-square error estimate of the state $\mathbf{x}_i$.

This is accomplished through two different stages, which are the propagation and the update.

3.3.1.1 The Propagation Stage

The prediction stage encompasses predicting the state of the system and its covariance at time step k, given measurements collected at time step k–1. The state-vector is propagated using

$$\hat{\mathbf{x}}_{k|k-1} = \mathbf{F}_k \hat{\mathbf{x}}_{k-1|k-1} + \mathbf{C}_{k-1}\mathbf{u}_{k-1} \tag{3.35}$$

where $\mathbf{F}_k$ and $\mathbf{C}_{k\text{-}1}$ are known linear functions and $\hat{\mathbf{x}}_{k-1|k-1}$ is the corrected estimate of the state. The subscript $(\bullet)_{k|k\text{-}1}$ denotes the estimate at time step k conditioned on the previous measurement.

The covariance is propagated using

$$\mathbf{P}_{k|k-1} = \mathbf{F}_k \mathbf{P}_{k-1|k-1} \mathbf{F}_k^T + \mathbf{Q}_{k-1} \tag{3.36}$$

where $\mathbf{P}_{k-1|k-1}$ is the updated covariance matrix at time step k –1.

3.3.1.2 The Update Stage

In order to correct the estimated state and its covariance matrix, a residual vector has to be calculated using recent observations. This is given by

$$\hat{\mathbf{x}}_{k|k} = \hat{\mathbf{x}}_{k|k-1} + \mathbf{k}_k \tilde{\mathbf{y}}_k \tag{3.37}$$

where $\tilde{\mathbf{y}}_k$ is the innovation term that provides a measure of the new information contained in recent measurements.

The innovation covariance is given by

$$\mathbf{S}_k = \mathbf{H}_k \mathbf{P}_{k|k-1} \mathbf{H}_k^T + \mathbf{R}_k \tag{3.38}$$

Furthermore, the Kalman gain, which is a function of the relative certainty of the measurements and current state estimate, can be calculated from

$$\mathbf{k}_k = \mathbf{P}_{k|k-1} \mathbf{H}_k^T \mathbf{S}_k^{-1} \tag{3.39}$$

where $(\bullet)^{-1}$ denotes the inverse operator.

Finally, the state and error covariance are updated using

$$\hat{\mathbf{x}}_{k|k} = \hat{\mathbf{x}}_{k|k-1} + \mathbf{k}_k \tilde{\mathbf{y}}_k \tag{3.40}$$

$$\mathbf{P}_{k|k} = (\mathbf{1} - \mathbf{k}_k \mathbf{H}_k) \mathbf{P}_{k|k-1} \tag{3.41}$$

The state-error vector is defined by

$$\mathbf{e}_k = \mathbf{x}_k - \hat{\mathbf{x}}_k \tag{3.42}$$

Equation (3.42) satisfies the principle of orthogonality given by

$$E[\mathbf{e}_k \mathbf{y}^T] = 0 \tag{3.43}$$

3.3.2 Extended Kalman Filter

The attitude determination based on EKF is conducted in a two-stage process. During the first stage, an initial prediction of the attitude is conducted based on a kinematics model and measurements collected from onboard sensors. During the second stage, the filter corrects the predicted attitude based on the new absolute orientation measurements [SRKB08].

The filter described in [MoMK09] is based on the following model

$$\mathbf{x}_{k+1} = \mathbf{f}(\mathbf{x}_k, k) + \mathbf{G}_k \mathbf{w}_k \tag{3.44a}$$

$$\mathbf{y}_k = \mathbf{h}(\mathbf{x}_k, k) + \mathbf{v}_k \tag{3.44b}$$

where **f** and **h** are known nonlinear functions. **G** represents known matrix.

The spacecraft attitude state is given by a seven-state space model consisting of the quaternion appended with three more states to determine the drift in the gyroscopes

$$\mathbf{x}(t) = \begin{bmatrix} \mathbf{q}(t) & \boldsymbol{\beta}(t) \end{bmatrix}^T \tag{3.45}$$

The system can be described using the following model

$$\dot{\mathbf{q}} = \frac{1}{2}\Omega(\boldsymbol{\omega}_m - \boldsymbol{\beta} - \boldsymbol{\eta}_v)\mathbf{q} \tag{3.46}$$

$$\dot{\boldsymbol{\beta}} = \boldsymbol{\eta}_w(\mathbf{t}) \tag{3.47}$$

where the dot above the vectors indicate the derivative with respect to time. $\boldsymbol{\eta}_v$ and $\boldsymbol{\eta}_w$ represent the measurement and process noise.

The predicted state-vector is defined as in [LeMS82] by taking the expectation of (3.46) and (3.47). This yield

$$\dot{\hat{\mathbf{q}}} = \frac{1}{2}\Omega(\hat{\boldsymbol{\omega}})\mathbf{q} \tag{3.48}$$

$$\dot{\hat{\boldsymbol{\beta}}} = \mathbf{0}_{3\times 1} \tag{3.49}$$

The estimated rotational velocity is given by

$$\hat{\boldsymbol{\omega}} = \boldsymbol{\omega}_m - \hat{\boldsymbol{\beta}} \tag{3.50}$$

Equation (3.49) indicates that the bias is constant over the integration interval. As a result, assuming that the angular rate evolves linearly during the integration step Δt, a first-order numerical integrator can be used to propagate the quaternion. More details can be found in [TrRo05].

3.3.2.1 Continuous-Time Error-State Model

Based on the state-space model selected, the error state provides an error in the quaternion estimate and the bias [MTRH07]. The bias error is obtained by calculating the difference between the true and the estimated bias while a multiplicative-error representation has been selected for the quaternion. This representation requires the attitude error to be modeled as an infinitesimal rotation that causes the estimated attitude to match the true orientation [Greg04]. The error state can be expressed as

$$\Delta\boldsymbol{\beta} = \boldsymbol{\beta} - \hat{\boldsymbol{\beta}} \tag{3.51}$$

$$\mathbf{q} = \delta\mathbf{q} \otimes \hat{\mathbf{q}} \Leftrightarrow \delta\mathbf{q} = \mathbf{q} \otimes \hat{\mathbf{q}}^{-1} \tag{3.52}$$

where $\hat{\mathbf{q}}$ denotes the estimated quaternion and $\boldsymbol{\delta}\mathbf{q}$ represents the error in $\mathbf{q}$.

Using a multiplicative error representation reduces the attitude uncertainty to a 3×3 matrix. This reduction provides a solution to the loss of rank that would arise in a 4×4 covariance matrix due to the unit-quaternion constraint. However, this projection results in a loss of information [CrMC07].

The continuous-time error state is given by [TrRo05]

$$\dot{\tilde{\mathbf{x}}} = \mathbf{F}_C \tilde{\mathbf{x}} + \mathbf{G}_C \mathbf{n} \tag{3.53}$$

where

$$\mathbf{F}_C = \begin{bmatrix} -[\hat{\boldsymbol{\omega}}\times] & -\mathbf{1}_{3\times3} \\ \mathbf{0}_{3\times3} & \mathbf{0}_{3\times3} \end{bmatrix} \quad , \quad \mathbf{G}_C = \begin{bmatrix} -\mathbf{1}_{3\times3} & \mathbf{0}_{3\times3} \\ \mathbf{0}_{3\times3} & \mathbf{1}_{3\times3} \end{bmatrix} \tag{3.54}$$

are the system matrix and the noise matrix. The error-state is given by

$$\tilde{\mathbf{x}} = \begin{bmatrix} \delta\boldsymbol{\theta} \\ \Delta\boldsymbol{\beta} \end{bmatrix} \quad , \quad \mathbf{n} = \begin{bmatrix} \boldsymbol{\eta}_v \\ \boldsymbol{\eta}_w \end{bmatrix} \tag{3.55}$$

where $\boldsymbol{\delta\theta}$ is the error angle vector whose dimension is 3×1 and $\boldsymbol{\Delta\beta}$ is the error in the bias.

3.3.2.2 Discrete-Time Error-State Model

For a practical implementation, the discrete-time error model, the state transition matrix and the discrete-time system noise covariance are required.

According to [LeMS82][MTRH07], assuming a constant $\boldsymbol{\omega}$ over the integration time step Δt, the transition matrix can be obtained using

$$\boldsymbol{\Phi} = (t_{k+1}, t_k) = \exp\left(\int_{t_k}^{t_{k+1}} \mathbf{F}_C(\tau) d\tau\right) \tag{3.56}$$

The discrete-time system noise covariance is found using

$$\mathbf{Q}_d = \int_{t_k}^{t_{k+1}} \boldsymbol{\Phi}(t_{k+1}, t_k) \mathbf{G}_C(\tau) \mathbf{Q}_C \mathbf{G}_C^T(\tau) \boldsymbol{\Phi}^T(t_{k+1}, t_k) d\tau \tag{3.57}$$

A detailed description of the transition matrix and the discrete-time system noise covariance is provided in [TrRo05] and [MTRH07].

According to [TrRo05], the discrete-time transition matrix has the following form

$$\mathbf{\Phi}(t+\Delta t,t)=\begin{bmatrix}\mathbf{\Theta} & \mathbf{\Psi}\\ \mathbf{0} & \mathbf{1}\end{bmatrix} \tag{3.58}$$

where the matrix $\mathbf{\Theta}$ can be written as

$$\mathbf{\Theta}=\cos(|\boldsymbol{\omega}|\Delta t)\mathbf{1}_{3\times 3}-\sin(|\boldsymbol{\omega}|\Delta t)\left[\frac{\boldsymbol{\omega}}{|\boldsymbol{\omega}|}\times\right]+(1-\cos(|\boldsymbol{\omega}|\Delta t))\frac{\boldsymbol{\omega}}{|\boldsymbol{\omega}|}\frac{\boldsymbol{\omega}}{|\boldsymbol{\omega}|}^{T} \tag{3.59}$$

The matrix $\mathbf{\Psi}$ can be expressed by

$$\mathbf{\Psi}=-\mathbf{1}_{3\times 3}\Delta t+\frac{1}{|\boldsymbol{\omega}|^2}(1-\cos(|\boldsymbol{\omega}|\Delta t))[\hat{\boldsymbol{\omega}}\times]-\frac{1}{|\boldsymbol{\omega}|^3}(|\boldsymbol{\omega}|\Delta t-\sin(|\boldsymbol{\omega}|\Delta t))[\boldsymbol{\omega}\times]^2 \tag{3.60}$$

For small values of $|\boldsymbol{\omega}|$, the above expressions lead to a numerical instability. By taking the limit, and applying l'Hôpital's rule, (3.59) and (3.60) yield

$$\lim_{|\boldsymbol{\omega}|\to 0}\mathbf{\Psi}=-\mathbf{1}_{3\times 3}\Delta t+\frac{\Delta t^2}{2}[\boldsymbol{\omega}\times]-\frac{\Delta t^3}{6}[\boldsymbol{\omega}\times]^2 \tag{3.61}$$

$$\lim_{|\boldsymbol{\omega}|\to 0}\mathbf{\Theta}=\mathbf{1}_{3\times 3}-\Delta t[\boldsymbol{\omega}\times]+\frac{\Delta t^2}{2}[\boldsymbol{\omega}\times]^2 \tag{3.62}$$

The covariance of the noise in the discrete-time system has the following structure

$$\mathbf{Q_d}=\begin{bmatrix}\mathbf{Q_{11}} & \mathbf{Q_{12}}\\ \mathbf{Q_{12}} & \mathbf{Q_{22}}\end{bmatrix} \tag{3.63}$$

where

$$\mathbf{Q}_{11}=\sigma_v^2\Delta t\mathbf{1}_{3\times 3}+\sigma_w^2(\mathbf{1}_{3\times 3}\frac{\Delta t^3}{3}+\frac{\frac{(|\boldsymbol{\omega}|\Delta t)^3}{3}+2\sin(|\boldsymbol{\omega}|\Delta t)-2|\boldsymbol{\omega}|\Delta t}{|\boldsymbol{\omega}|^5}[\boldsymbol{\omega}\times]^2) \tag{3.64}$$

$$\mathbf{Q}_{12} = -\sigma_w^2(\mathbf{1}_{3\times3}\frac{\Delta t^2}{2} - \frac{|\boldsymbol{\omega}|\Delta t - \sin(|\boldsymbol{\omega}|\Delta t)}{|\boldsymbol{\omega}|^3}[\hat{\boldsymbol{\omega}}\times] + \frac{\frac{(|\boldsymbol{\omega}|\Delta t)^2}{2} + \cos(|\boldsymbol{\omega}|\Delta t) - 1}{|\boldsymbol{\omega}|^4}[\boldsymbol{\omega}\times]^2) \tag{3.65}$$

$$\mathbf{Q}_{22} = \sigma_w \Delta t \mathbf{1}_{3\times3} \tag{3.66}$$

$$\lim_{|\boldsymbol{\omega}|\to0} \mathbf{Q}_{11} = \sigma_v^2 \Delta t \mathbf{1}_{3\times3} + \sigma_w^2(\mathbf{1}_{3\times3}\frac{\Delta t^3}{3} + \frac{2\Delta t^5}{5!}[\omega\times]^2) \tag{3.67}$$

$$\lim_{|\boldsymbol{\omega}|\to0} \mathbf{Q}_{12} = -\sigma_w^2(\mathbf{1}_{3\times3}\frac{\Delta t^2}{2} - \frac{\Delta t}{3!}[\boldsymbol{\omega}\times] + \frac{\Delta t}{4!}[\boldsymbol{\omega}\times]^2) \tag{3.68}$$

3.3.2.3 The State and Covariance Propagation

The discrete-time gyroscope model is given by

$$\boldsymbol{\omega}_k = \boldsymbol{\omega}_{mk} - \boldsymbol{\beta}_k - \mathbf{v}_k \tag{3.69}$$

$$\boldsymbol{\beta}_{k+1} = \boldsymbol{\beta}_k + \mathbf{w}_k \tag{3.70}$$

The estimation of the rotational velocity and the drift can be calculated using

$$\hat{\boldsymbol{\omega}}_{k+1|k} = \boldsymbol{\omega}_{m_{k+1}} - \hat{\boldsymbol{\beta}}_{k+1|k} \tag{3.71}$$

$$\hat{\boldsymbol{\beta}}_{k+1|k} = \hat{\boldsymbol{\beta}}_{k|k} \tag{3.72}$$

As shown in [TrRo05], the covariance of the propagated state estimate is given by

$$\mathbf{P}_{k+1|k} = \boldsymbol{\Phi}_k \mathbf{P}_{k|k} \boldsymbol{\Phi}_k^T + \mathbf{Q}_d \tag{3.73}$$

3.3.2.4 The Update Stage

In order to update the estimated attitude, a residual vector has to be calculated from

$$\tilde{\mathbf{y}}_k = \frac{\mathbf{z}_k \times \hat{\mathbf{z}}_k}{\|\mathbf{z}_k\|\|\hat{\mathbf{z}}_k\|} \tag{3.74}$$

where $\mathbf{z}_k$ and $\hat{\mathbf{z}}_k$ are the measurement and the prior estimate of the measurement at time k, respectively.

The measurement matrix can be calculated according to [SRKB08]

$$\mathbf{H}(k) = \begin{bmatrix} \dfrac{-2\mathbf{b}_{ref}^{mag}\tilde{\mathbf{b}}_{meas}^{mag\ T}}{\|\tilde{\mathbf{b}}_{meas}^{mag}\|\|\mathbf{b}_{ref}^{mag}\|} & \mathbf{0}_{3\times3} \\ \dfrac{-2\mathbf{b}_{ref}^{sun}\tilde{\mathbf{b}}_{meas}^{sun\ T}}{\|\tilde{\mathbf{b}}_{meas}^{sun}\|\|\mathbf{b}_{ref}^{sun}\|} & \mathbf{0}_{3\times3} \end{bmatrix} \tag{3.75}$$

where $(\bullet)_{ref}$ and $(\bullet)_{meas}$ represent the data obtained from reference models and measurements collected using onboard sensors, respectively. Also $\mathbf{0}_{3\times3}$ represents a 3×3 matrix whose elements are zero.

Equation (3.74) defines the innovation of the EKF update. The covariance matrix of the innovation is given by

$$\mathbf{S} = \mathbf{H}\mathbf{P}\mathbf{H}^T + \mathbf{R} \tag{3.76}$$

The Kalman gain, which is a relative certainty between the current state and the measurement matrix, can be calculated using

$$\mathbf{k}_k = \mathbf{P}_k\mathbf{H}_k^T\mathbf{S}^{-1} \tag{3.77}$$

The correction terms are estimated from

$$\Delta\hat{\mathbf{x}}_k = \mathbf{k}_k\tilde{\mathbf{y}}_k \tag{3.78}$$

The update for the quaternion and the bias is given by

$$\hat{\mathbf{q}}_{k|k} = \begin{bmatrix} \frac{1}{2}\Delta\mathbf{q}_k \\ \sqrt{1 - \frac{1}{4}\Delta\mathbf{q}^T\Delta\mathbf{q}} \end{bmatrix} \mathbf{q}_{k|k\text{-}1} \tag{3.79}$$

$$\hat{\boldsymbol{\beta}}_{k|k} = \hat{\boldsymbol{\beta}}_{k|k\text{-}1} + \Delta\hat{\boldsymbol{\beta}}_k \tag{3.80}$$

Finally, the estimation of the error covariance is updated using

$$\mathbf{P}_{k|k} = (\mathbf{1}_{6\times 6} - \mathbf{k}_k\mathbf{H})\mathbf{P}_{k|k\text{-}1} \tag{3.81}$$

3.3.3 Unscented Kalman Filter

The EKF has performed very well in a variety of fields [LeMS82]; yet, it faces several limitations described in [WaMe00]. The limitations include: (i) nonlinear system functions approximated using a first-order Taylor approximation only (if it exists), (ii) divergence in case of a large initial error, and (iii) state PDF and covariance are represented using *Gaussian random variables* (GRV). This filter is prone to some major numerical difficulties (*e.g.*, instability and divergence). Furthermore, it is optimal for Gaussian distributions only [WaMe00]. Additionally, not only deriving the Jacobian matrices (if they exist) is a nontrivial operation in most processes, but also it may result in a significant complexity during its implementation. Moreover, it is impractical to represent a general PDF using only the mean and covariance of the function [JuUW95][CrMC07]. Consequently, the UKF is introduced as an alternative.

The UKF belongs to the class of *particle filters* (PFs). PFs do not require any linearization during the prediction stage [KoDj03]. However, a particle-based representation of a general distribution does not rely on a set of parameters such as the mean and covari-

ance. It is based on the premise that a general PDF can be represented using a large number of samples [WaCC09]. These filters deal with nonparametric distributions in a unique way and thrive with nonlinearities. PFs have performed well, specifically when the observations may get extremely corrupted with noise [Gold04]. However, this performance comes with a high cost associated with its computational complexity. Also, using PFs require calculating a certain number of particles [KaSG05]. Thus, PFs fail to represent the PDF and performs poorly in case the number of samples used is not enough. Figure 3.3 illustrates the estimation process followed by UKF.

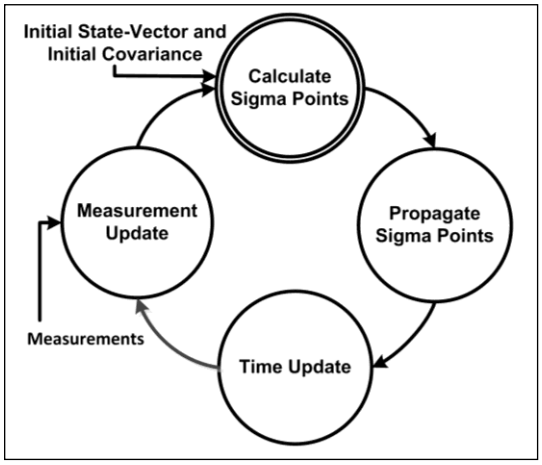

Fig. 3.3. Unscented Kalman filter estimation process.

The UKF is based on the unscented transform, which represents a Gaussian PDF using a set of $2n+1$ weighted sigma points (where n is the dimension of the state-vector) [Gold04]. Figure 3.4 shows the difference between the EKF and UKF in propagating the PDF. Using a set of fixed points to represent a general PDF is more practical than relying on its first and second moment (*i.e.*, the mean and variance) only. The mean and variance of a linearized function cannot map all the nonlinearities of a function. This can be explained by the important information contained in the original system, which is lost

through the linearization process. A particle-based representation can perform relatively better, if the number of particles used is sufficient.

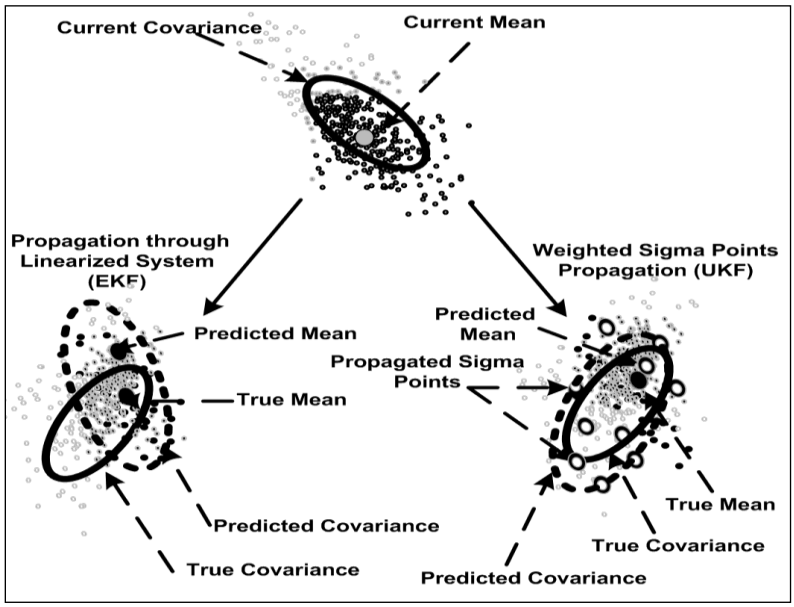

Fig. 3.4. Propagation process for (a) EKF and (b) UKF.

Given a system model similar to (3.44a) and (3.44b), the UKF starts the estimation process by calculating the sigma points to represent the PDF of the state-vector [CrMa82]

$$2n \text{ columns from } \pm\sqrt{(n+\bar{\lambda})[\mathbf{P}_{k|k}+\mathbf{Q}_k]} \rightarrow \boldsymbol{\chi}_k \tag{3.82}$$

where $\bar{\lambda}$ is a scaling factor and $\sqrt{\mathbf{M}}$ is a shorthand notation for a matrix **N** such that $\mathbf{N}\mathbf{N}^T=\mathbf{M}$. The matrix square-root **N** can be obtained using lower triangular Cholesky decomposition [PTVF07].

Due to the symmetric nature of the set of sigma points, its odd moments are equal to zero. Thus, the first three moments (i.e., the mean, the variance and the skew) represent exactly a Gaussian distribution. The scaling factor $\bar{\lambda}$ can be utilized to provide an accurate representation of higher-order moments for other types of distributions. $\bar{\lambda}$ has to be

selected in a way to ensure a positive semi-definite covariance matrix $\mathbf{P}_{k|k-1}$ [CrMa82][Juli02]**.** The set of sigma points, $\boldsymbol{\chi}_k$, is calculated using

$$\boldsymbol{\chi}_{0,k} = \hat{\mathbf{x}}_k \tag{3.83}$$

$$\boldsymbol{\chi}_{i,k} = \hat{\mathbf{x}}_k + (\sqrt{(n+\bar{\lambda})[\mathbf{P}_k + \mathbf{Q}_k]})_i \quad \text{for } i = 1,\ldots,n \tag{3.84}$$

$$\boldsymbol{\chi}_{i,k} = \hat{\mathbf{x}}_k - (\sqrt{(n+\bar{\lambda})[\mathbf{P}_k + \mathbf{Q}_k]})_i \quad \text{for } i = 1,\ldots,n \tag{3.85}$$

with

$$\bar{\lambda} = \bar{\alpha}^2(n+\bar{k}) - n \tag{3.86}$$

where $\boldsymbol{\chi}_{i,k}$ denotes the i^{th} column of $\boldsymbol{\chi}_{i,k}$, $\bar{\alpha}$ is a positive constant ($0 \leq \bar{\alpha} \leq 1$) that determines the spread of set of sigma points around $\hat{\mathbf{x}}_k$, and $\bar{k}$ is a third scaling parameter used to provide an accurate tuning of the higher order moments [ChKi07]. Thus, the matrix of $2n+1$ sigma points can be represented by

$$\boldsymbol{\chi}_k = \left[\hat{\mathbf{x}}_k \quad \hat{\mathbf{x}}_k + (\sqrt{(n+\bar{\lambda})[\mathbf{P}_k + \mathbf{Q}_k]}) \quad \hat{\mathbf{x}}_k - (\sqrt{(n+\bar{\lambda})[\mathbf{P}_k + \mathbf{Q}_k]})\right] \tag{3.87}$$

3.3.3.1 Propagation Stage

Once the sigma points have been calculated, they are propagated through the nonlinear function [WaMe00]

$$\boldsymbol{\chi}_{i,k} = \mathbf{f}(\boldsymbol{\chi}_{i,k-1}, k-1) \tag{3.88}$$

Using a weighted sample mean, the state-vector $\hat{\mathbf{x}}_{k+1|k}$ and its covariance are propagated as well

$$\hat{\mathbf{x}}_{k|k-1} = \sum_{i=0}^{2n} \mathbf{W}_i^{(m)} \boldsymbol{\chi}_{i,k} \tag{3.89}$$

$$\mathbf{P}_{k|k-1}^{\mathbf{xx}} = \sum_{i=0}^{2n} \mathbf{W}_i^{(c)} (\boldsymbol{\chi}_{i,k} - \hat{\mathbf{x}}_{k|k-1})(\boldsymbol{\chi}_{i,k} - \hat{\mathbf{x}}_{k|k-1})^T \tag{3.90}$$

Similarly, the predicted output covariance is obtained from

$$\mathbf{P}_{k|k-1}^{\mathbf{yy}} = \sum_{i=0}^{2n} \mathbf{W}_i^{(c)} (\mathbf{y}_{i,k} - \hat{\mathbf{y}}_{k|k-1})(\mathbf{y}_{i,k} - \hat{\mathbf{y}}_{k|k-1})^T \tag{3.91}$$

where $\mathbf{W}_i^m$ and $\mathbf{W}_i^c$ represent the weights for the mean and covariance respectively given by

$$\mathbf{W}_0^{(m)} = \frac{\bar{\lambda}}{\bar{\lambda} + n} \tag{3.92}$$

$$\mathbf{W}_0^{(c)} = \frac{\bar{\lambda}}{\bar{\lambda} + n} + (1 - \bar{a}^2 + \bar{k}) \tag{3.93}$$

$$\mathbf{W}_i^{(c)} = \mathbf{W}_i^{(m)} = \frac{\bar{\lambda}}{2(\bar{\lambda} + n)} \qquad \text{for } i=1,\ldots,2n \tag{3.94}$$

and $\hat{\mathbf{y}}$ denotes the predicted mean of the observation vector given by [CrMa82]

$$\hat{\mathbf{y}}_{k|k-1} = \sum_{i=0}^{2n} \mathbf{W}_i^{(m)} \mathbf{y}_{i,k} \tag{3.95}$$

where $\mathbf{Y}_{i,k+1}$ denotes the i^{th} column of the predicted observation matrix computed using

$$\mathbf{y}_{i,k} = \mathrm{h}(\boldsymbol{\chi}_{i,k}, k) \tag{3.96}$$

Next, the innovation covariance matrix is calculated from

$$\mathbf{P}_k^{\upsilon\upsilon} = \mathbf{P}_k^{\mathbf{yy}} + \mathbf{R}_k \tag{3.97}$$

where $\mathbf{P}_k^{\mathbf{yy}}$ denotes the output covariance. Then, the Kalman gain is given by

$$\mathbf{k}_k = \mathbf{P}_k^{\mathbf{xy}} (\mathbf{P}_k^{\upsilon\upsilon})^{-1} \tag{3.98}$$

where $\mathbf{P}_{k}^{\mathbf{xy}}$ denotes the cross-correlation function computed from

$$\mathbf{P}_{k|k-1}^{\mathbf{xy}} = \sum_{i=0}^{2n} \mathbf{W}_i^{(c)} (\boldsymbol{\chi}_{i,k} - \hat{\mathbf{x}}_{k|k-1})(\mathbf{y}_{i,k} - \hat{\mathbf{y}}_{k|k-1})^T \tag{3.99}$$

3.3.3.2 The Update Stage

Once the Kalman gain has been estimated and new measurements have been collected, the corrected state-vector is given by

$$\hat{\mathbf{x}}_{k|k} = \hat{\mathbf{x}}_{k|k-1} + \mathbf{k}(\mathbf{y}_k - \hat{\mathbf{y}}_k) \tag{3.100}$$

where $\mathbf{y}_k$ denotes the measurement vector, and the updated covariance is obtained from

$$\mathbf{P}_{k|k} = \mathbf{P}_{k|k-1} + \mathbf{k}_k \mathbf{P}_{k|k}^{\upsilon\upsilon} \mathbf{k}_k^T \tag{3.101}$$

3.3.4 Computational Complexity

This section addresses the time and space computational complexities of stochastic approaches and more specifically the EKF. *Time complexity* is defined as the number of characteristic operations it performs when given an input of size *n* [Kins10]. In addition to time complexity, space complexity plays a role of paramount importance as well. *Space complexity* is defined as the number of elementary objects that the algorithm needs to store during its execution.

3.3.4.1 Time Complexity

The computational complexity of carrying out the two-stage process associated with the EKF at step *k* involves a state prediction $\mathbf{x}_{k|k\text{-}1}$, calculation of the covariance of the propagated state $\mathbf{P}_{k|k\text{-}1}$, in which the transition matrix and the discrete-time noise covari-

ance matrix are needed. Additionally, the update stage requires the linearized measurement matrix **H**, the Kalman gain $\mathbf{k}_k$, which involves computing the residual $\mathbf{y}_k$ and its covariance **S**. Finally, the state $\mathbf{x}_{k|k}$ and the covariance $\mathbf{P}_{k|k}$ are updated.

The time complexity can be evaluated from the number of multiplications and additions required during the execution of an algorithm. Knowing that the number of operations needed for the multiplications of two $n \times n$ matrices is equal to $n^2(2n\text{-}1)$, we can estimate the number of operations involved for the different matrices. The results of the analysis are shown in Table 3.1. It is seen that the time complexity of the EKF is $O(n^3)$.

Table 3.1: Time complexity of the EKF.

Equation Number	Number of Operations	Complexity
(3.73)	$f(n) = 4n^3\text{-}n^2$	$O(n^3)$
(3.74)	$f(n) = 2n^2\text{-}n$	$O(n^2)$
(3.76)	$f(n) = 4n^3\text{-}n^2$	$O(n^3)$
(3.77)	$f(n) = 4n^3\text{-}2n^2$	$O(n^3)$
(3.79)	$f(n) = 3n^2\text{-}n$	$O(n^2)$
(3.81)	$f(n) = 4n^3\text{-}n^2$	$O(n^3)$
Total	$f(n) = 16n^3\text{-}3n^2\text{-}2n$	$O(n^3)$

3.3.4.2 Space Complexity

To address the space complexity of the EKF, we focus on the most demanding matrices in terms of memory requirements. Therefore, special attention is given to $\mathbf{P}_{k|k\text{-}1}$, $\mathbf{P}_{k|k}$, and **S** matrices.

In order to compute the covariance of the propagated states and residual, $\mathbf{P}_{k|k-1}$ and $\mathbf{S}$ respectively, four matrices of size $n \times n$ are required. Therefore, the space complexity is $O(n^2)$. Furthermore, updating the covariance, $\mathbf{P}_{k|k}$, demands the availability of three matrices of sizes $n \times n$. As a result, the space complexity is $O(n^2)$.

Therefore, we can conclude that the space complexity of the EKF is $O(n^2)$.

Similar evaluation can be applied to the UKF. The computational complexity of the UKF is of the same order as the EKF; that is, a time and space complexity are $O(n^3)$ and $O(n^2)$, respectively. However, the UKF requires a longer computational time to calculate the $2n+1$ sigma points.

3.4 Summary

This chapter introduced a review of important deterministic and stochastic algorithms for the purpose of attitude determination.

Deterministic algorithms revolve mostly around Wahba's problem formulated as a constrained LS problem. In order to solve this problem, several elegant closed-form algorithms have been introduced during the last 50 years. The highlight of these algorithms is that they require no a priori estimate of the attitude. Furthermore, the unit-norm constraint on $\mathbf{q}$ is reinforced in the formulation of the problem itself. On the other hand, these deterministic approaches yield estimators that suffer from a lack of probabilistic significance resulting in a poor performance when subjected to uncertainty in the process and measurement models. Furthermore, tuning the weighting coefficients is extremely challenging and represents another inherent pitfall of these approaches. Usually, the weights are chosen as scalars equal to the inverse of the associated vector measurement variance.

This choice is, however, heuristic. Efforts were made in order to recast Wahba's problem as a maximum likelihood estimation problem [Shus89]. This was achieved by assuming very special measurement noise probability distributions.

Stochastic filters have been presented as well. These filters have been used extensively for the purpose of orbital guidance. The highlight of these algorithms is their ability to estimate the attitude with auxiliary parameters. However, their main limitation is related to their computational cost. As seen throughout this chapter, KFs are computationally expensive in time and space.

In order to provide a grounded comparison, deterministic algorithms (TRIAD, QUEST, and extended QUEST) and stochastic ones (EKF and UKF) are implemented and evaluated using the same reference and measurement data in Chapter 4.

Chapter 4

EVALUATION OF CURRENT ATTITUDE DETERMINATION APPROACHES

The following simulations are designed to evaluate the performance and identify the limitations of all the deterministic and stochastic approaches introduced in Chapter 3. The different algorithms were developed and tested on Matlab version R2010b on Mac OS X version 10.6.8 using 2×2.4 GHz Quad-Core Intel Xeon processors with 12 GB of 1066 MHz DDR3 memory. The software implementation and source code are described in Appendix A.

4.1 Experimental Setup

Deterministic and stochastic approaches are applied to estimate the attitude of a pico-satellite. These approaches are evaluated based on two important performance measures; the accuracy and the transient response. The *accuracy* is defined as the knowledge and control of the spacecraft attitude with respect to a target attitude as defined relative to an absolute reference over a specified range of angular motion (under which determination and control performance must be met). The *transient response* provides the allowed set-

tling time or maximum attitude overshoot when new targets are acquired (or recovered from upsets).

The attitude determination hardware relies on sun sensors, TAM, and three-axis gyroscopic rate sensors. The magnetic field reference is modeled using a 13^{th} order IGRF. The TAM sensor noise is modeled by zero-mean Gaussian white noise with a standard deviation of 50 nT. The gyro measurements are simulated with noise term set to $\boldsymbol{\eta}_v = 5\times10^{-6}$ (rad/sec$^{1/2}$) for the gyros and $\boldsymbol{\eta}_w = 2\times10^{-8}$ (rad/sec$^{3/2}$) for the bias drift with a sampling time equal to 0.864 sec. Figure 4.1 shows the Earth magnetic field and sun data used in these simulations. Solid lines refers to the simulated data (denoted S-data) obtained from mathematical models by producing digital samples above nyquist frequency. Dotted lines represent the physical data (denoted P-data) obtained by adding a noise to the S-data. The noise added is an additive *white Gaussian noise* (WGN) whose value is set to 5% of the measurements unit norm per axis.

The different algorithms are evaluated with respect to the performance measures that have been defined already. The test cases are selected in a way to identify the limitations of each approach. For example, the robustness of deterministic and stochastic approaches to noisy measurements is addressed. This is accomplished by considering cases where an additional additive WGN is added. Furthermore, stochastic approaches are subjected to three additional performance test cases. The first one considers an exact knowledge of the initial attitude of the spacecraft, while the second one introduces an initial error in the attitude. Finally, the last case presents an extreme case where a large error exists in the initial orientation of the spacecraft.

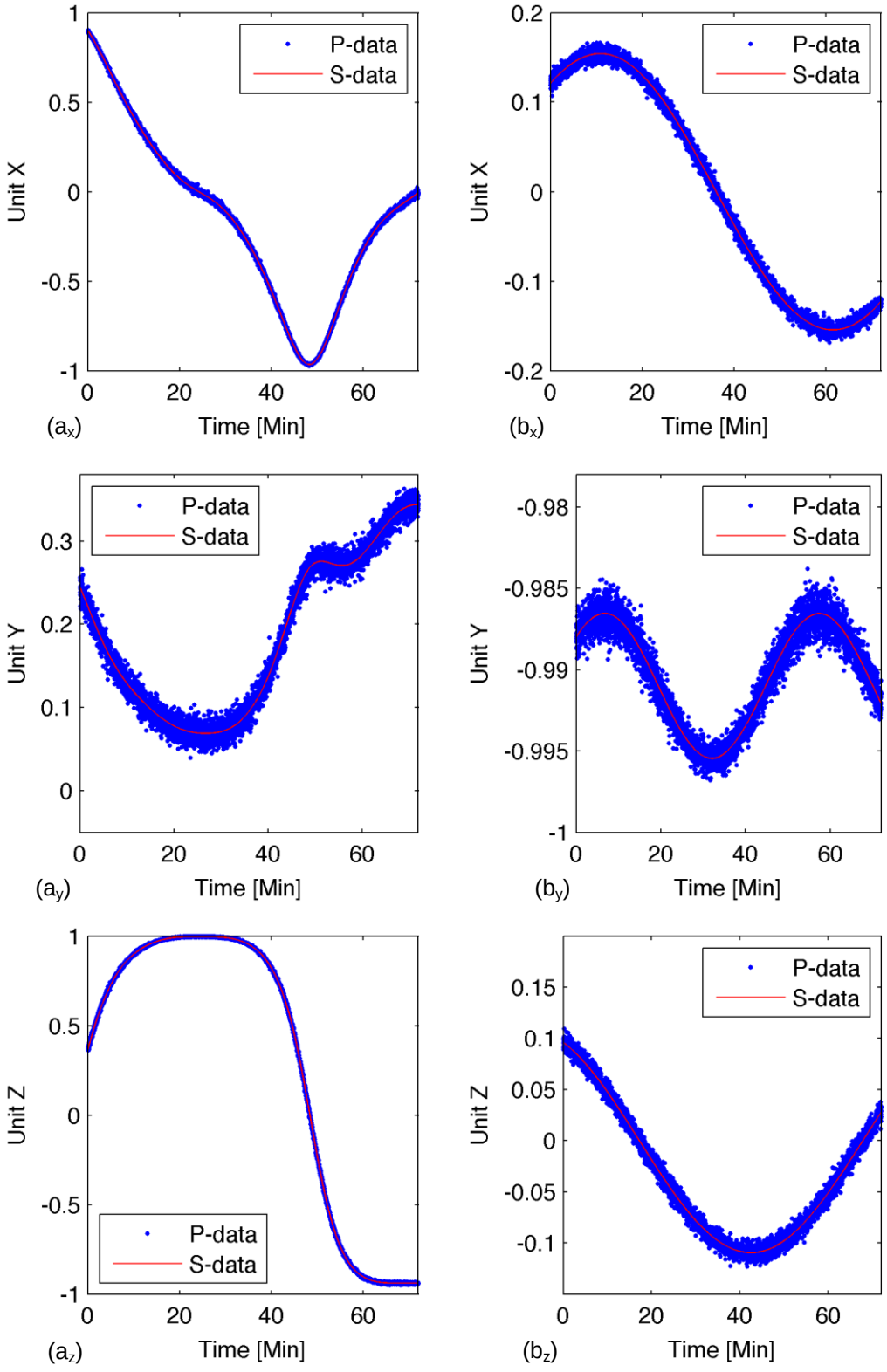

Fig. 4.1. S-data and P-data. (a_x), (a_y), and (a_z) magnetic field data in the x-, y-, and z-axis. (b_x), (b_y), and (b_z) sun sensor data in the x-, y-, and z-axis.

4.2 Simulation Study

4.2.1 Deterministic Approaches

The TRIAD, QUEST, and extended QUEST algorithms were simulated for the purpose of evaluating their pointing accuracy and transient response. Furthermore, the robustness of these algorithms while estimating the attitude of a spacecraft is addressed. This is accomplished by considering two experiments, where the measurements are buried in WGN (5% and 10% of the unit norm of the measurements).

4.2.1.1 TRIAD Algorithm

Using the development shown in Section 3.2.1, the TRIAD algorithm is summarized in Table 4.1. It is worth noting that this algorithm does not require a priori knowledge of the spacecraft attitude or any initialization parameters to process the measurements taken. Additionally, this algorithm is very attractive due to its simplicity and inexpensive time and memory requirements.

The first experiment considers the pointing accuracy of the TRIAD when the measurements processed are not corrupted with noise. Figure 4.2 shows the simulation results.

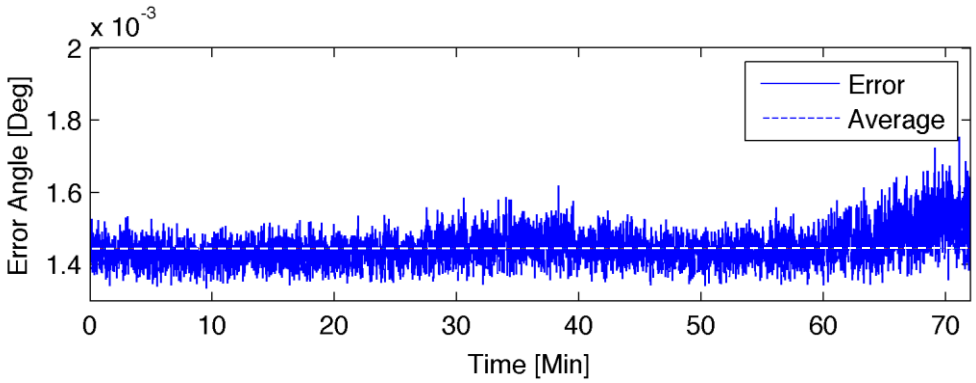

Fig. 4.2. Simulation results of the TRIAD algorithm.

Table 4.1: Summary of the TRIAD algorithm.

Algorithm 4.1 The TRIAD Algorithm

1: **Input**: $\tilde{\mathbf{b}}$, **r**

2: **repeat**

3: **Compute**

$$\mathbf{T}_{b1} = \tilde{\mathbf{b}}_1, \quad \mathbf{T}_{b2} = \frac{\tilde{\mathbf{b}}_1 \times \tilde{\mathbf{b}}_2}{|\mathbf{b}_1 \times \mathbf{b}_2|}, \quad \mathbf{T}_{b3} = \mathbf{T}_{b1} \times \mathbf{T}_{b2}$$

$$\mathbf{T}_{r1} = \mathbf{r}_1, \quad \mathbf{T}_{r2} = \frac{\mathbf{r}_1 \times \mathbf{r}_2}{|\mathbf{r}_1 \times \mathbf{r}_2|}, \quad \mathbf{T}_{r3} = \mathbf{T}_{r1} \times \mathbf{T}_{r2}$$

$$\mathbf{A} = \sum_{i=1}^{3} \mathbf{T}_{bi} \mathbf{T}_{ri}^{T}$$

4: **return A**

The trajectory of the error (shown in Fig. 4.2) illustrates that the estimated attitude agrees well with the actual attitude of the spacecraft with an average error of 1.4×10^{-3} deg. The estimation process exhibits some patterns and peaks. These observations can be explained by the formulation of the algorithm itself. Relying on two measurements at the time does not allow the estimation process to collect enough information about the environment. The term "*information*" refers to the evolution of the estimation process throughout the time. Moreover, the entire history of the measurements collected is not utilized; however, this point might also be seen as an advantage from the perspective that the history of the measurements does not need to be stored.

The second test case considers measurements corrupted with an additive WGN constituting a 5% and 10% of the magnetic field and sun data unit-norm per axis. The results of this test case are shown in Figure 4.3.

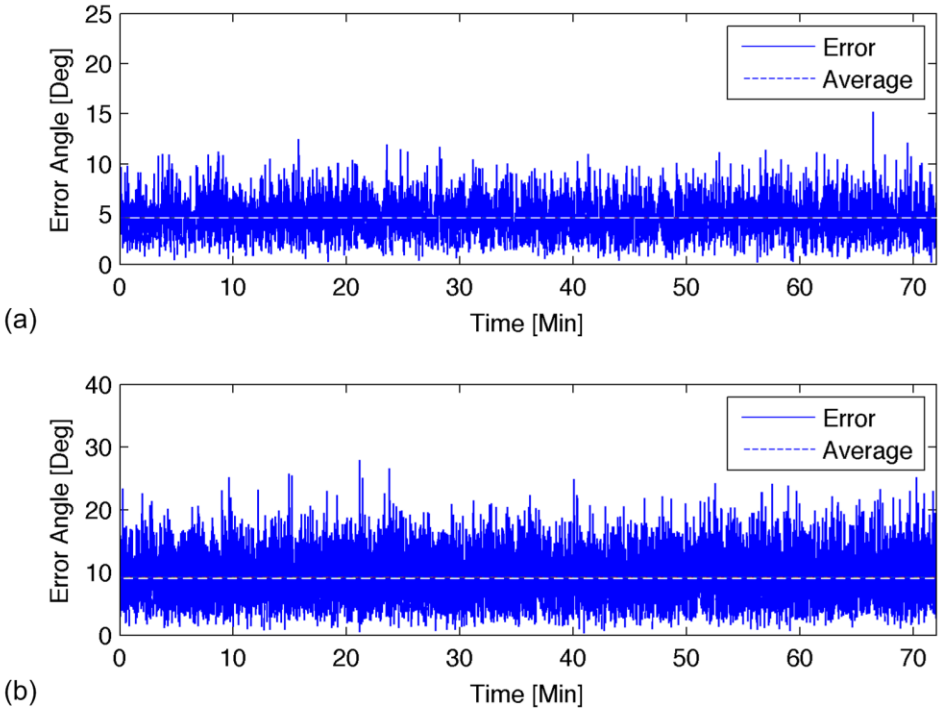

Fig. 4.3. Simulation results of the TRIAD algorithm with measurements corrupted with a (a) 5% additive WGN and (b) 10 % additive WGN.

A visual inspection of Fig. 4.3 shows a highly nonlinear and non-differentiable behaviour with an important loss in the pointing accuracy for both cases. Indeed, we can see that the average error reaches 4.6 and 9.23 deg., when the measurements are corrupted with high levels of WGN. This behaviour reflects the limitations of the TRIAD algorithm to deal with uncertainty in the measurements. This is a result of the lack of probabilistic significance of the algorithm itself, in which each measurement taken is assumed to be error-free. Consequently, the entire estimation process may collapse when measurements in the body frame are subjected to a high-level of noise. Finally, Table 4.2 summarizes the simulation results of the TRIAD algorithm.

Table 4.2: TRIAD simulation results.

Experiments	Average Error [Deg]
Uncorrupted Measurements	0.0014
5% Additive WGN	4.6
10% Additive WGN	9.23

4.2.1.2 The QUEST Algorithm

The QUEST algorithm (summarized in Table 4.3) is evaluated in a similar way as the TRIAD algorithm. The simulation results are shown in Figure 4.4.

Figure 4.4(a) illustrates the behaviour of the QUEST algorithm when the measurements are corrupted with a 5% WGN, while Figure 4.4(b) considers a 10% noise level.

A visual inspection of these results indicates a similar behaviour as the one observed with the TRIAD algorithm; that is, a highly nonlinear and non-differentiable trajectory (that does not converge throughout the entire estimation process). Similar to the TRIAD algorithm, the QUEST is also extremely sensitive to measurements corrupted with noise.

Table 4.4 summarizes the simulation results of the QUEST. These results indicate that the QUEST algorithm does not perform better than the TRIAD, though it involves more measurements and a higher computational cost. Furthermore, it points out the limitations encountered when deterministic approaches are subjected to uncertainty. These observations can be explained by the loss function considered (described in (3.10)) that does not account for the changes in the environment and the dynamics of the process.

Table 4.3: Summary of the QUEST algorithm.

Algorithm 4.2 The QUEST Algorithm

Input: $\tilde{\mathbf{b}}$, $\mathbf{r}$
repeat
  for i=1 to m do
    $\Pi(\tilde{\mathbf{b}}_i)$ using (2.17)
    $\Xi(\mathbf{r}_i)$ using (3.16b)
    $\mathbf{K}=\sum_{i=1}^{m}\mathbf{\Pi}(\tilde{\mathbf{b}}_i)\mathbf{\Xi}(\mathbf{r}_i)$
  end for
compute λ_{max} the greatest eigenvalue of the $\mathbf{K}$ matrix
compute q (the unit normalized eigenvector that corresponds to λ_{max})
return A(q)

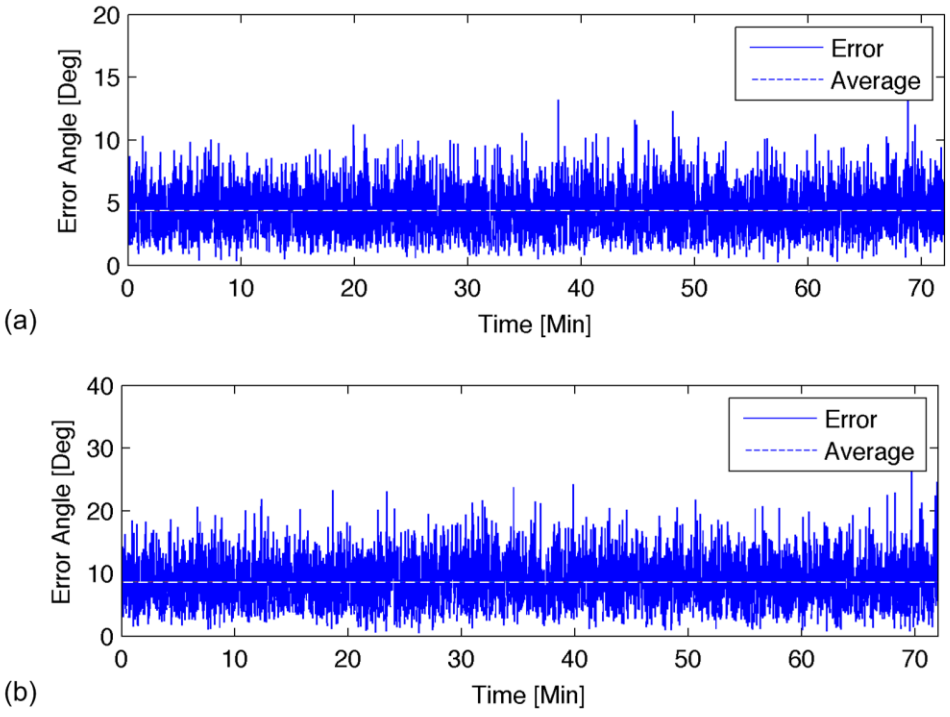

Fig. 4.4. Simulation results of the QUEST algorithm with measurements corrupted with a (a) 5% additive WGN and (b) 10 % additive WGN.

Table 4.4: QUEST simulation results.

Experiments	Average Error [Deg]
5% Additive WGN	4.53
10% Additive WGN	9.11

4.2.1.3 The Extended QUEST Algorithm

The extended QUEST algorithm (summarized in Table 4.5) employs an extended square-root information-filtering algorithm that proceeds in two phases. The first phase dynamically propagates a posteriori estimates at stage *k*-1 to compute a priori estimate at stage *k* [Psia10]. This algorithm is evaluated based on the same performance test cases as the TRIAD and the QUEST algorithms with the results shown in Figure 4.5.

The simulation results show similar behaviours as the ones observed with the previous deterministic algorithms (i.e., a highly nonlinear and non-differentiable trajectory that exhibits sharp peaks with some pattern). However, the extended QUEST is more robust when fed with noisy measurements providing a relatively more accurate estimate of the attitude.

The peaks and the nonlinearities in the deterministic algorithms error trajectories are due to the novelty and innovation in the process that cannot be estimated and captured by such approaches that suffer from a lack of probabilistic significance. Consequently, deterministic approaches face stringent limitations and pitfalls when subjected to uncertainty resulting from noisy measurements, ill-defined environments, and process dynamic models.

Table 4.5: Summary of the extended QUEST algorithm.

Algorithm 4.3 The Extended QUEST Algorithm

1: **input**: $\boldsymbol{\Phi}$, f, $\mathbf{q}_{k-1}$, $\mathbf{x}_{k-1}$, $\tilde{\mathbf{b}}$, $\mathbf{r}$
2: **repeat**
3: **predict** $\tilde{\mathbf{q}}_k$ and $\tilde{\mathbf{x}}_k$
4: $\tilde{\mathbf{q}}_{k|k} = \boldsymbol{\Phi}(t_k, t_{k-1}; \mathbf{q}_{k-1}, \mathbf{x}_{k-1}, \mathbf{w}_{k-1})\mathbf{q}_{k-1}$
5: $\tilde{\mathbf{x}}_{k|k} = f(t_k, t_{k-1}; \mathbf{q}_{k-1}, \mathbf{x}_{k-1}, \mathbf{w}_{k-1})$
6: **end predict**
7: **update** $\hat{\mathbf{q}}_{k|k}$ and $\hat{\mathbf{x}}_{k|k}$
8: **compute** $\hat{\mathbf{q}}_{k|k}$ by minimizing (3.25)
9: **compute** $\hat{\mathbf{x}}_{k|k}$ using (3.26)
10: **end update**
11: **return** $\mathbf{A}(\hat{\mathbf{q}}_{k|k})$

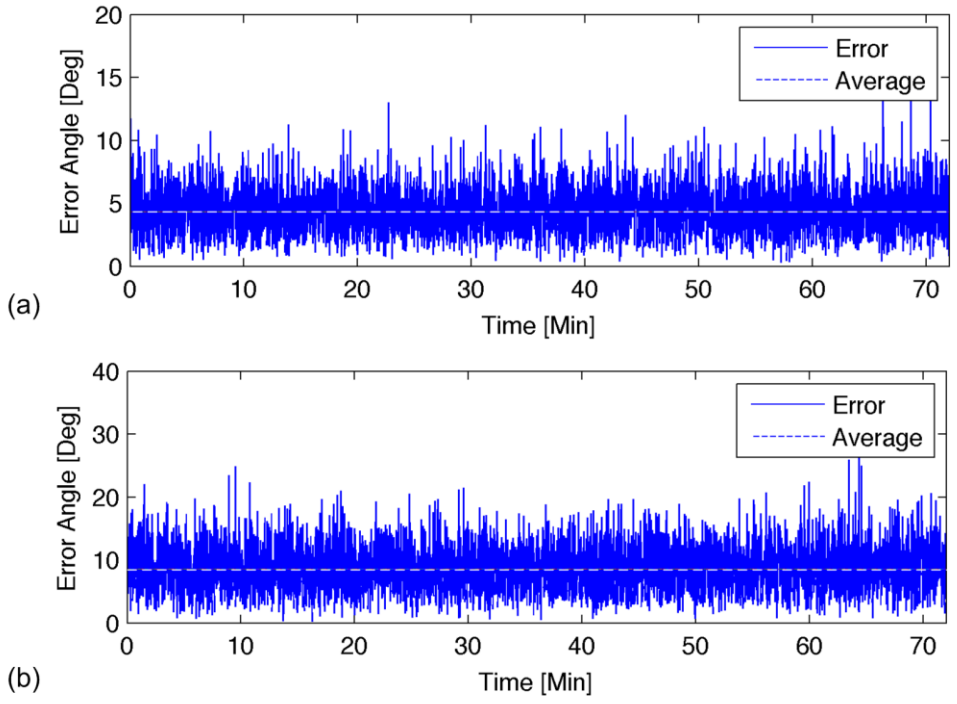

Fig. 4.5. Simulation results of the extended QUEST algorithm with measurements corrupted with a (a) 5% additive WGN and (b) 10 % additive WGN.

Table 4.6: Summary of the comparison between deterministic algorithms.

Algorithms	5% Additive WGN [Deg]	10% Additive WGN [Deg]
TRIAD	4.65	9.68
QUEST	4.58	9.02
Extended QUEST	4.35	7.96

4.2.2 Stochastic Approaches

The attitude determination based on KFs is conducted in a two-stage process. During the first stage, an initial estimate of the attitude is calculated based on a kinematics model and measurements collected from a three-axis gyroscope. During the second stage, the filter corrects the predicted attitude based on the new absolute orientation measurements [SRKB08]. A multiplicative quaternion-error approach is used to define the attitude error [Mark03]. This ensures that the quaternion normalization is maintained. The EKF and UKF are summarized in Tables (4.7) and (4.8), respectively.

For the first simulation, the EKF and UKF are executed with no initial attitude error, an initial bias set to zero, and measurements corrupted with a 10% WGN. Also, for the UKF $\bar{\alpha}$=1 and $\bar{\lambda}$=3. Figure 4.6 shows the time history of the error for: (a) the EKF and (b) the UKF.

The results indicate that the estimated attitude agrees with the actual one with an average error of 0.05 and 0.3 deg. for the EKF and UKF, respectively. Additionally, a non-linear diverging behaviour can be observed with a relatively larger variance for the UKF. Unlike the UKF, the error trajectory of the EKF does not exhibit any sharp peaks that may illustrate an innovation in the process; yet, a diverging behaviour is observed.

These results can be explained by the linearization procedure that the process and measurement models are subjected to when using the EKF. Such procedures do not allow the filter to identify the actual PDF of the process after propagation. Therefore, it accumulates an error over time leading to a diverging behaviour. Though the nonlinear dynamics of this process is represented using a Gaussian distribution described by its mean and variance only, the critical information of the process is not lost through the linearization process when the initial conditions provided are accurate. This explains the absence of any innovation in the trajectory of the error.

Compared to the EKF, the error trajectory of the UKF indicates that the process is not fully captured by the algorithm. This is due to the limited number of sigma particles that fail to represent the nonlinear process and measurement models accurately.

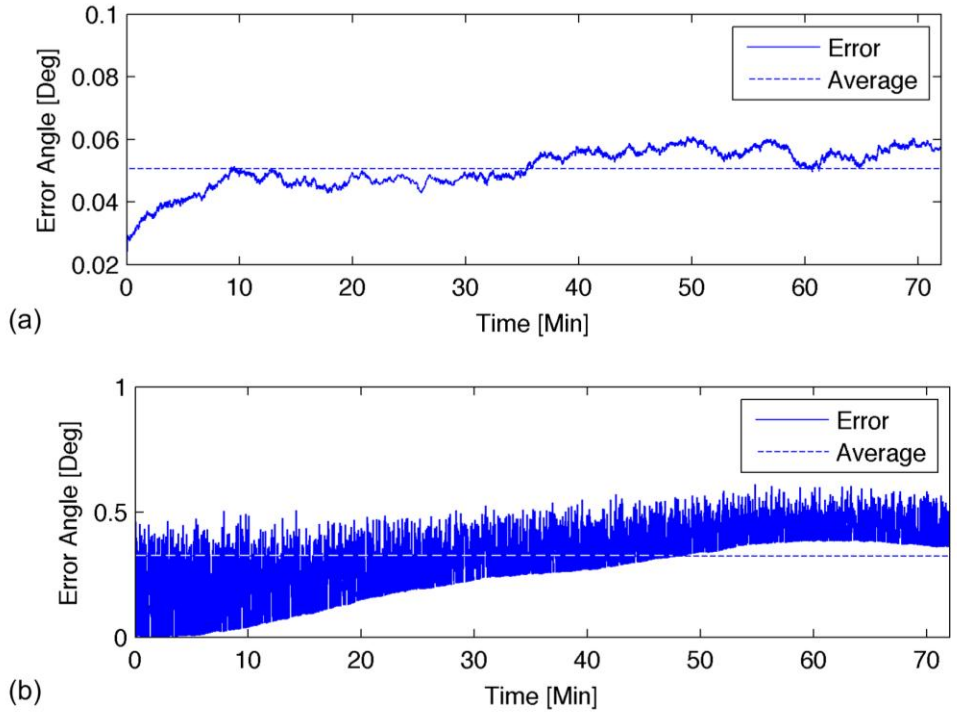

Fig. 4.6. Simulation results of (a) EKF and (b) UKF using exact initial conditions with measurements corrupted with a 10 % additive WGN.

Table 4.7: Summary of the extended Kalman filter algorithm.

Algorithm 4.4 The Extended Kalman Filter Algorithm

input: $\mathbf{x}_0$, Q, R, f, h, $\tilde{\mathbf{b}}$, **r**
$\mathbf{F}_k = \frac{\partial \mathrm{f}(\mathbf{x}_k, \mathbf{u}_k)}{\partial \mathrm{x}}\Big|_{\mathbf{x}=\hat{\mathbf{x}}k}$
$\mathbf{H}_k = \frac{\partial \mathrm{h}(\mathbf{x}_k)}{\partial \mathrm{x}}\Big|_{\mathbf{x}=\hat{\mathbf{x}}k}$
repeat
  predict $\tilde{\mathbf{q}}_{k|k\text{-}1}$ and $\tilde{\mathbf{x}}_{k|k\text{-}1}$
    propagate the state-vector (3.35)
    calculate the covariance of the propagated state-estimate (3.73)
  end predict
  update $\tilde{\mathbf{q}}_{k|k}$ and $\tilde{\mathbf{x}}_{k|k}$
    calculate the covariance matrix of the innovation (3.76)
    calculate the Kalman gain (3.77)
    compute $\hat{\mathbf{q}}_{k|k}$ using (3.79)
    update the covariance matrix (3.81)
  end update
return A($\hat{\mathbf{q}}_{k|k}$)

Table 4.8: Summary of the unscented Kalman filter algorithm.

Algorithm 4.5 The Unscented Kalman Filter Algorithm

input: $\mathbf{x}_0$, Q, R, f, h, $\tilde{\mathbf{b}}$, **r**
repeat
  predict $\tilde{\mathbf{q}}_{k|k\text{-}1}$ and $\tilde{\mathbf{x}}_{k|k\text{-}1}$
    calculate the sigma points (3.87)
    calculate the weights for the mean and covariance using (3.92) to (3.94)
    compute the covariance of the state-vector (3.90)
    compute the output covariance (3.91)
  end predict
  update $\tilde{\mathbf{q}}_{k|k}$ and $\tilde{\mathbf{x}}_{k|k}$
    calculate the Kalman gain (3.98)
    correct the attitude estimate $\hat{\mathbf{q}}_{k|k}$ using (3.100)
    update the covariance matrix (3.101)
  end update
return A($\hat{\mathbf{q}}_{k|k}$)

For the second test case, a more realistic scenario is considered. The filters are tested with an initial guess estimated using the TRIAD algorithm (evaluated in subsection 4.2.1.1). Figure 4.7 shows the time history of the attitude estimation error for the (a) EKF and (b) UKF, respectively. This test case considers the addition of a 5% WGN.

Both of the error trajectories are highly nonlinear. The EKF illustrates multiple transients exhibiting converging and diverging behaviours. The average error for the EKF is equal to 4.38 deg. These observations are a result of the linearized models used and the sensitivity to initial conditions of the model. The performance of a linearized model deteriorates when the system is subjected to an initial error. On the other hand, the UKF provides a more accurate estimate of the attitude with an average error of 0.3 deg. This is due to the sigma particles that were able to identify the actual PDF of the process during the prediction stage.

In order to evaluate the robustness of these stochastic approaches, another case is considered with a 10% WGN added to the measurements. The results are shown in Figure 4.8.

The EKF (shown in Fig. 4.8(a)) illustrates a very slow converging behaviour with an average error equal to 5.06 deg. The UKF (presented in Fig. 4.8(b)) provides a better performance with an average error of 0.4 deg. exhibiting robustness to noisy measurements. Using the sigma particles, the UKF has the unique ability to estimate the PDF after each recursion of the algorithm. Such characteristic is extremely attractive in noisy environments since it allows the algorithm to preserve its performance.

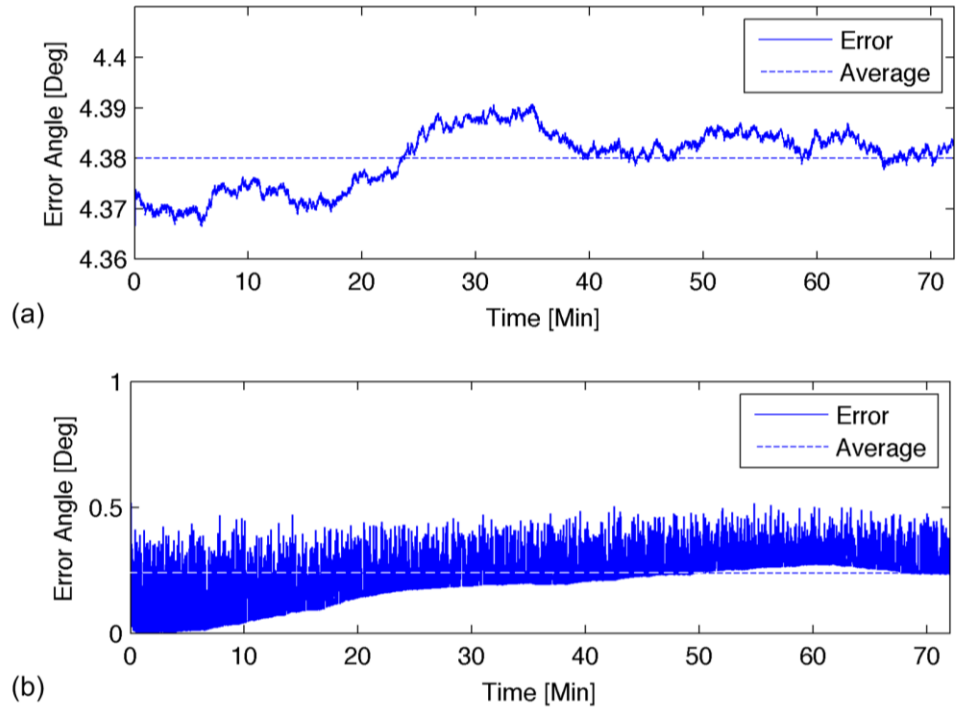

Fig. 4.7. Simulation results for (a) EKF and (b) UKF with initial conditions determined using the TRIAD algorithm and measurements corrupted with a 5% additive WGN.

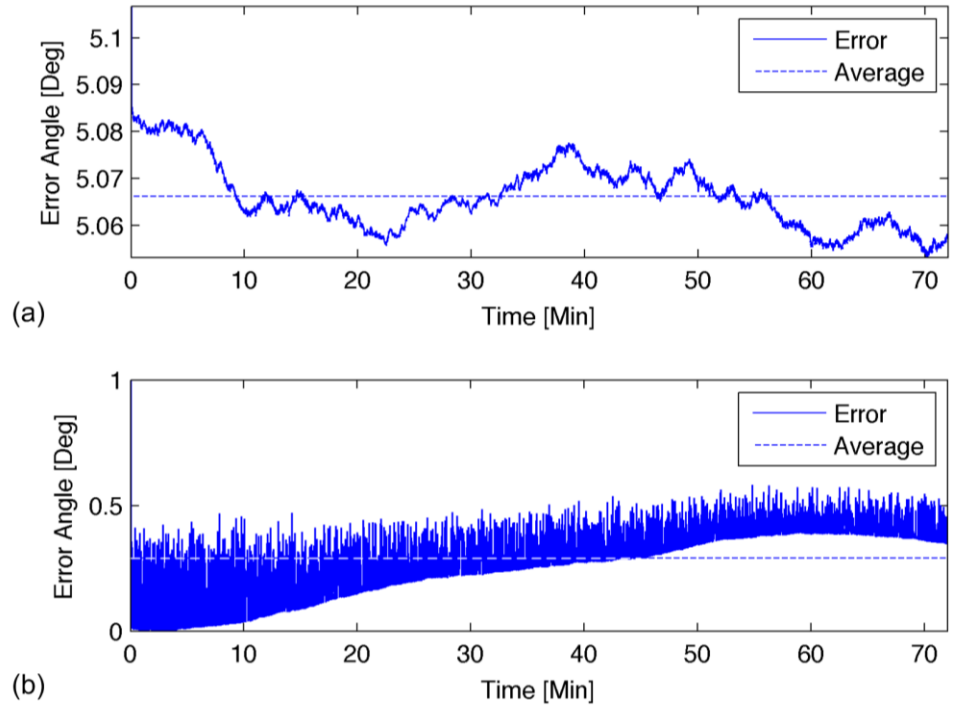

Fig. 4.8. Simulation results for (a) EKF and (b) UKF with initial conditions determined using the TRIAD algorithm and measurements corrupted with a 10 % additive WGN**.**

The third case considers the scenario where a large error of 36 deg. per axis is added to the initial attitude with an initial bias set to 0.2 (deg./hour) and no other parameter changed. Figure 4.9 depicts the estimation of the error for both of KFs.

The EKF exhibits an oscillatory behavior with an average error equal to 30 deg. Thus, the filter fails to estimate the actual attitude. This is due to the nonlinear nature of the process and sensitivity to initial conditions of the filter. A first-order linearization of the system model cannot contain large errors. Furthermore, nonlinear functions cannot be represented with the first and second moments only. Indeed, it works with a Gaussian distribution, but not with a general nonlinear function. The UKF was able to converge to the actual attitude with an error less than 0.4 deg. after one hour with a highly nonlinear response. It can be justified by the ability of the particles to approximate the nonlinearity of the process at hand more accurately.

The Kalman gain, which is a relative certainty between the current state and the measurement, is shown in Figure 4.10.

The results indicate that Kalman gain for the EKF is large for the first components of the attitude and the bias (denoted k_1 and k_2). This implies that the algorithm gives more weight to the measurements collected by the onboard sensors and ignores the linearized process and measurement models; thus, justifying the poor performance of the algorithm. On the other hand, the Kalman gain for the UKF is relatively small. This implies that the algorithm relies more on the models used and the sigma points calculated.

These results reinforce the following points. The approach followed by the EKF to estimate the state of a system is not suitable for highly nonlinear and dynamical environments [Kins09]. In particular, assuming a Gaussian distribution for the noise environment

and linearization may cause divergence and highly unstable filters [Juli02]. Additionally, both filters correct their estimate after collecting new absolute measurements only. This may result in processing delays.

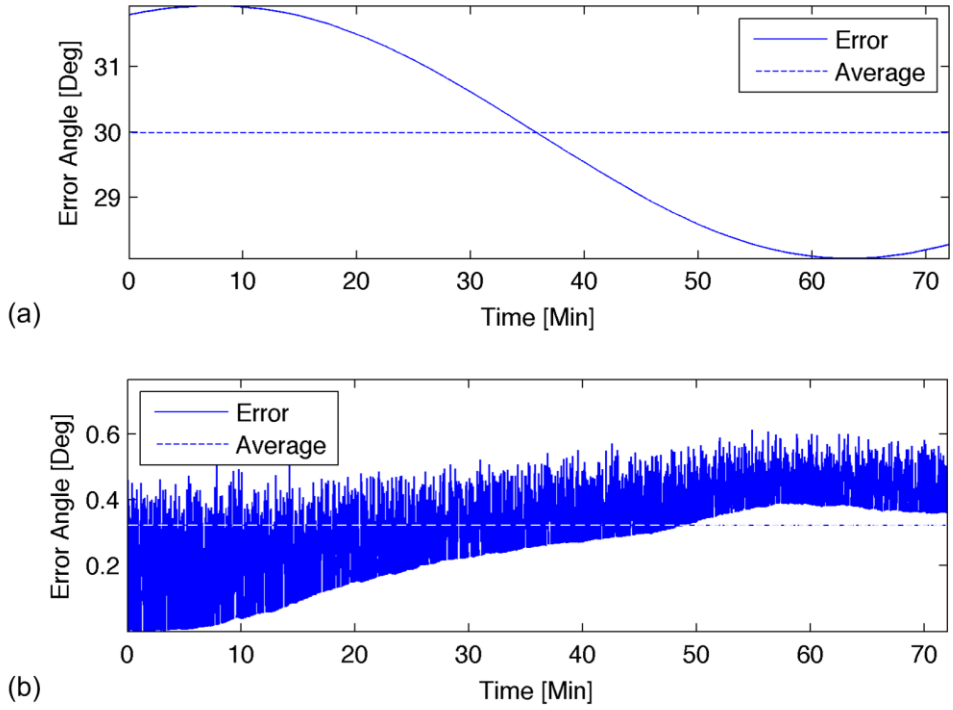

Fig. 4.9. Simulation results of (a) EKF and (b) UKF with a large initial error of 36 deg.

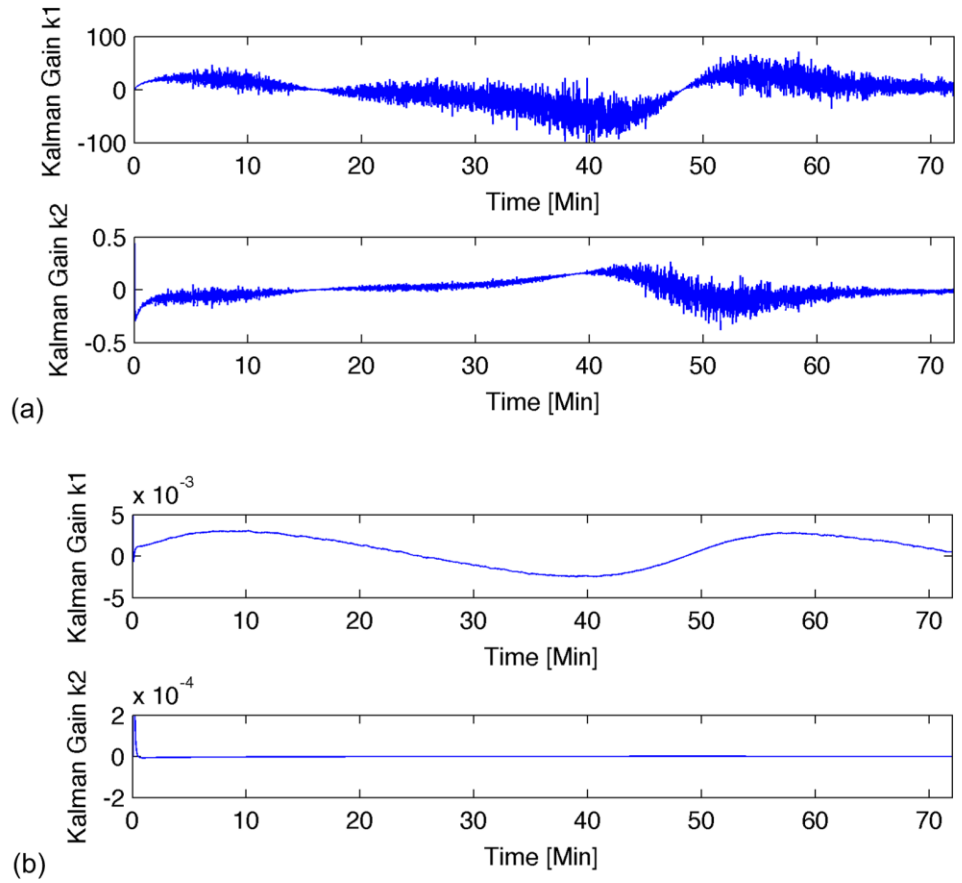

Fig. 4.10. Kalman gain for the third test case. (a) EKF and (b) UKF.

4.3 Comparison between Stochastic and Deterministic Approaches

All the algorithms presented possess some attractive properties, as well as inherent pitfalls. The limitations and highlights are summarized in this section.

4.3.1 Advantages

4.3.1.1 Deterministic Approaches

1. Offer elegant closed-form algorithms that provide a solution to Wahba's problem;
2. Do not require an initial guess of the attitude;
3. Are computationally inexpensive; and
4. Offer built-in quaternion normalization.

4.3.1.2 Stochastic Appraoches

1. Provide an attitude estimation accuracy within ±1 deg.;
2. Can fuse multiple sensory measurements; and
3. Can estimate auxiliary parameters in addition to the attitude optimally.

4.3.2 Disadvantages

4.3.2.1 Deterministic Approaches

1. Are sensitive to noisy measurements;
2. Provide a poor performance when the angle between the Earth magnetic field vector and the sun vector is small;

3. Can handle only vector-type of measurements (*e.g.*, QUEST algorithm);
4. Cannot estimate anything but the attitude (*e.g.*, QUEST algorithm); and
5. Can deal with simple dynamics model only.

4.3.2.2 Stochastic Approaches

1. Considers an additive white Gaussian noise only;
2. Covariance matrices have to be positive definite;
3. Relies on one measurement from the past only;
4. Approximates nonlinear systems using a first-order approximation (if it exists) represented using the first and second moments of a Gaussian distribution (*e.g.*, EKF) or with a fixed number of sigma particles (*e.g.*, UKF);
5. Suffer from sensitivity to initial conditions and divergence problems; and
6. May suffer from "brute-force" normalization of the quaternion when performed outside the filter algorithm. This normalization induces biases and may perturb the stochastic estimation process.

4.4 Summary

This chapter presented the evaluation of three deterministic algorithms (TRIAD, QUEST, and the extended QUEST) and two stochastic approaches (the extended and unscented KFs) for the estimation of a spacecraft attitude.

Deterministic approaches have shown attractive properties such as the ability to estimate the attitude without requiring any initialization process (*e.g.*, an initial guess of the attitude), while providing an elegant closed-form algorithm that offers an exact solution

to Wahba's problem. On the other hand, these approaches suffer from a major limitation, which is sensitivity to noisy measurements.

Stochastic approaches can provide a very accurate estimate of the attitude within ±1 deg. with the ability to fuse multiple measurements collected from onboard sensors; yet, they suffer from limitations as well. For example, the EKF linearizes nonlinear functions describing the process and measurement models so the standard KF can be applied. The linearization procedure induces biases and undesirable effects. Also, The UKF is based on a deterministic approach to select a limited number of weighted sigma points to represent the PDF.

All these algorithms constitute standard and state-of-the-art approaches for the purpose of attitude determination developed throughout the last 50 years. Indeed, under some cases, they provide a good performance that may satisfy a satellite's mission requirements. However, as discussed in the previous sections, they suffer from several limitations that impact directly their performance in a real-time environment. Furthermore, their computational cost constitutes another major drawback for small satellites. Consequently, alternative approaches ought to be considered for small satellites attitude determination.

Chapter 5

ATTITUDE DETERMINATION BASED ON POSSIBILISTIC APPROACHES

Current deterministic and stochastic approaches have shown attractive properties, as well as stringent limitations. This chapter introduces an improved approach for the estimation of the attitude based on a fuzzy logic. The objectives for this suggested solution can be summarized in twofold: (i) combine the advantages of deterministic and stochastic approaches under one umbrella (i.e., resilience to large error in the initial conditions and robustness to noisy measurements); and (ii) reduce the computational complexity for a potential implementation in small satellites.

5.1 Uncertainty in a Process

Uncertainty arises when the available information is imprecise due to the lack of knowledge, vagueness, and conflict of information. It is a situation, in which an action has to be taken based on premises for which reliability has not been clearly defined [Du-Ku13]. Uncertainty can be categorized into two main classes: (i) aleatory (objective) or (ii) epistemic (subjective). The first class of uncertainty deals with the representation of future events whose occurrence is governed by random phenomena (*e.g.*, spinning a rou-

lette wheel), while the second class express the uncertainty about the outcome of some events due to the lack of knowledge, ambiguity, or vagueness. Epistemic uncertainty (also known as reducible uncertainty, type B, or knowledge uncertainty) refers to a type of uncertainty that can be reduced through an increased understanding or more relevant data.

Processes containing uncertainty are analyzed with probabilistic methods, which assume that parameters of a model represent exactly the phenomenon modeled or the features of the real system. Consequently, their ability to deal with uncertainty or tolerate imprecision is limited, while their optimal performance is achieved when data is represented with absolute certainty as shown in Figure 5.1.

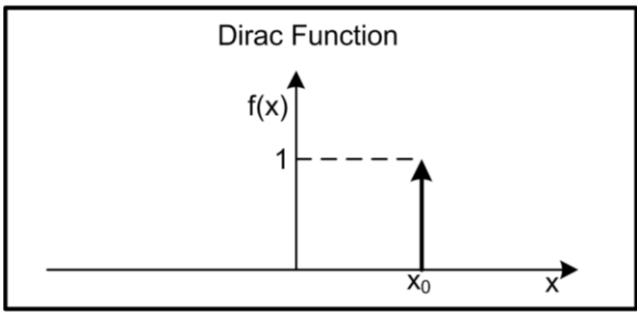

Fig. 5.1. Graphical representation of data with no uncertainty.

Fig.5.1 provides a graphical representation of data with no uncertainty denoted using the Dirac function. Similarly, the impact of uncertainty can be also be visualized. For example, using a probabilistic approach, the uncertainty causes the true value to be most likely within the space defined by 6σ, where σ represents the standard deviation of the PDF, as illustrated in Figure 5.2. A Gaussian distribution does not consider spikes of events that may occur outside 6σ. This shows the limitations of such distributions that are

inappropriate to represent chaotic processes. An in-depth description of different distributions is given in [Kins09].

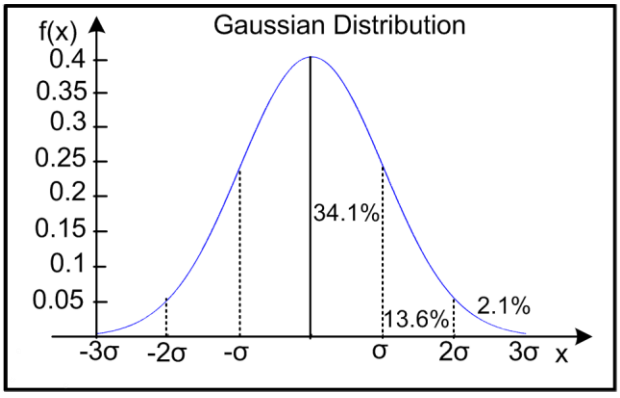

Fig. 5.2. Uncertainty represented using a Gaussian distribution.

Relying on probabilistic approaches requires quantifying probabilities. An important approach to do so is *Bayesian networks* (BN) also known as belief networks. These networks have become an important paradigm for reasoning under uncertainty. BN have found a number of applications (*e.g.*, reasoning about the oil market [Abra91]); however, they suffer from several constraints such as their limitations to: (i) represent propositional relationships between entities; and (ii) explicitly model temporal relationships. In order to deal with these limitations, other approaches such as dynamic belief networks [SMSM00], time nets [Kana91], modifiable temporal belief networks [WKYX11], and temporal nodes Bayesian networks have been introduced. These extensions provide more expressive power at the expense of efficient calculations. Another formal approach for dealing with uncertainty using probability theory is the *knowledge based model construction* (KBMC) [KYKY92]. The highlight of this approach is its ability to combine the strength of the probabilistic logics with computational advantages of BN relying on distinct models for knowledge specifications and probabilistic inference. However,

knowledge models are extremely difficult to define, specifically when the level of uncertainty is high and expert knowledge is not available.

As the complexity of a system increases, our ability to make precise, yet significant statements about its behaviour diminishes until a threshold is reached beyond which precision and significance becomes almost mutually exclusive characteristics. Consequently, the identification and the management of uncertainty becomes a challenging problem in such processes.

Alternative approaches based on a non-crisp type of soft computing have shown a tremendous potential in dealing with uncertainty, as well as providing attractive performance in poorly defined environments. Unlike probabilistic methods, these approaches are based on possibility and necessity measures to determine the occurrence of an event and granulation of data for a better reasoning under uncertainty [Yao04]. Though not used in this thesis, multi-granulation rough sets have been addressed in multiple publications for the purpose of data analysis [Pawl91]. This scheme is based on an optimistic and a pessimistic covering and the introduction of uncertainty measures (such as the degree of rough membership, approximation measure, and rough entropy) [LiLQ13]. Another interesting point with such approaches is that they do not involve probabilistic notions such as PDFs. However, they require defining entities referred to as membership functions in order to process the data. Figure 5.3 shows a graphical representation of different membership functions subjected to uncertainty.

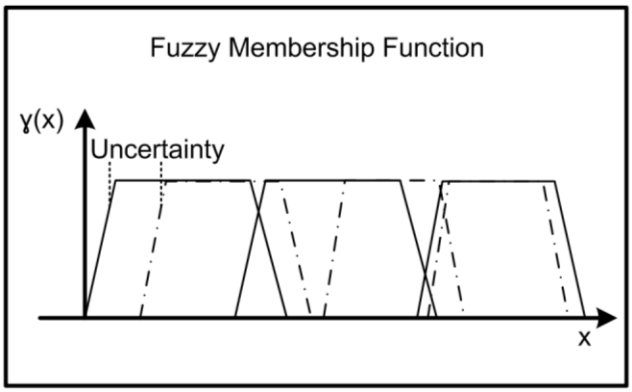

Fig. 5.3. Graphical representation of uncertainty in fuzzy systems.

Other types of classifier, such as Dempster-Sheifer classifier (based on a belief function, which is intimately related to the concept of fuzzy measures) can be considered [Kins04]. In essence, it provides a framework for the representation of knowledge about the value of an uncertain variable. Furthermore, several fuzzy measures (such as plausibility measure) can be associated with such type of classifiers [Yage02]. An important realization from this specific section can be summarized as follows. Traditional approaches, which are based on probability theory, are based and formulated upon very specific assumptions. These assumptions include the nature of the: (i) measurement and process models, (ii) environment and noise present, (iii) dynamic of the environment, as well as potential disturbances (if present). Furthermore, most assumptions evolve around Gaussian distributions referring to PDF and linearized models to represent the dynamics of the systems.

Finally, in addition to the different approach presented, several other techniques have been discussed in [LaLe01]. These techniques are based on nonparametric approaches, including but not limited to expert systems and neural networks. These approaches were

used for the purpose of implementing intelligent systems capable of speech and perception based on artificial intelligence.

5.2 Fuzzy Analysis

In 1965, fuzzy theory was introduced as a new paradigm of computing by Lotfi Zadeh (advisor of Rudolf Kalman) [Zade65]. Unlike classical computing techniques that would rely on crisp concepts only (i.e., membership or non-membership), fuzzy theory relies on class of sets that generalize the concept of memberships using a fuzzy number between 0 and 1 (where 0 means no membership and 1 full membership). It is based on the possibility theory that describes imprecise (sometimes contradictory) pieces of information, where the term "*imprecision*" means the value of a variable has been given, but not with the required statistical measure that describes the deviation between the true value and the estimated one (i.e., precision).

Possibility theory is a branch of the theory of evidence. Unlike probability analysis that relies on a single measure that provides the likelihood of a certain event to occur, possibility theory relies on two measures, namely: (i) possibility and (ii) necessity set of measures [Garm05]. Furthermore, fuzzy theory initiated a new paradigm of computing, which is *computing with words* (CW). This paradigm conveys the information using a collection of propositions based on a natural or synthetic language. Figure 5.4 shows a graphical representation of possibility and necessity. This figure indicates that any assumption might be false or true. Though an assumption might be correct, there might be some cases that violate the assumption. Nevertheless, there might be cases for which the

assumption is necessarily true. A similar description can be used when an assumption is considered false.

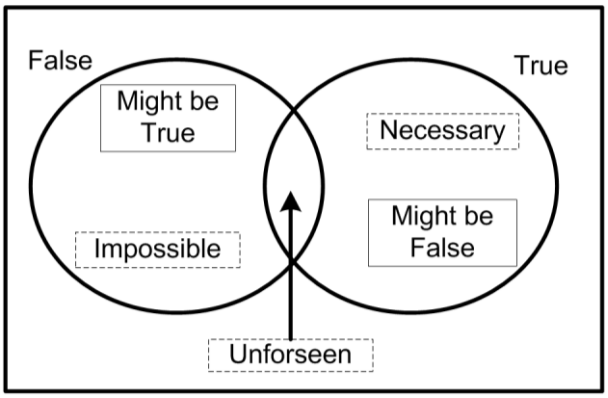

Fig. 5.4. Representation of possibilistic measures.

Granulation of data is critical for CW. As described by Zadeh, a granule is a fuzzy set of points having the form of a clump of elements drawn together by similarity (an example of a granule in software programming can be a program module). A granule in a higher level can be decomposed to smaller granules in lower levels, and conversely. Granulation is accomplished by constraining the values of variables. Moreover, using an *initial data set* (IDS), an answer to a specific query described using *terminal data set* (TDS) is derived using natural language also. Furthermore, it is domain specific and relies on the available knowledge. Therefore, it is critical to build models to provide both semantical and operational interpretations of these notions [Yao04]. Granulation of data is critical to cognitive computing since it plays an important role in mimicking human cognition [Zade96].

Granular computing (GrC) has received a tremendous attention from the scientific community due to its applications in data compression and extraction of information, which is critical for the design of cognitive machines. GrC consists of developing the appropriate mapping that links the different representations of the same problem at different levels of detail. Different models of GrC have been introduced in [Yao04]. Granular computing requires finding an optimal approach for establishing the granules. Also, it requires finding an appropriate method for establishing the granules' structures and their interpretation once constructed. Only then, a qualitative and quantitative characterization and analysis can take place. This will allow for the study of the different types of granulations by focusing on the properties of the mappings.

Different techniques for establishing the granule of data have been described in [EsVW06]. These schemes include: (i) mosaic (also known as table look-up), (ii) gradient decent, (iii) clustering with gradient decent, and (iv) evolutionary algorithms. A table look-up scheme constructs a fuzzy model based on pre-defined antecedents of the rules and establishes the consequences using a least-square approach. Gradient decent scheme provides more flexibility as the table look-up. It requires fixing the type and number of the memberships only, while it calculates their positions and the value of the consequences. By combining a clustering algorithm and a gradient decent scheme all the parameters become adjustable, but the type of the membership functions. The clustering and gradient decent method calculates the initial location of the membership functions by projecting the partition matrices obtained from a clustering applied to the input-output data. The consequences are generated from the centers of their covariance matrices and refined to improve the approximation by applying a gradient decent optimization technique

[EsVW06]. Finally, evolutionary approaches provide the unique ability to adjust all the parameters of the fuzzy models, including the set of inputs used to construct the model with the ability to consider complex constraints to enforce some desired features. The evolutionary strategies are computational algorithms that use methods derived from the concept of natural evolution, including reproduction, mutation and selection. These algorithms are very powerful during the investigation of a global solution in the search space. However, they are very expensive computationally. Consequently, they will not be considered in this thesis. The different characteristics of these approaches are summarized in Table 5.1. This table indicates the ability of each approach to adjust the type, number locations of the MFs, and the consequences.

Table 5.1: Different data granulation schemes and their characteristics.

Method	Type of MFs	Number of MFs	Location of the MFs	Consequences
Mosaic Scheme	Fixed	Fixed	Fixed	Adjusted
Gradient Descent	Fixed	Fixed	Adjusted	Adjusted
Clustering + Gradient Decent	Fixed	Adjusted	Adjusted	Adjusted
Evolutionary Strategies	Adjusted	Adjusted	Adjusted	Adjusted

5.3 Fuzzy Inference Systems

A *fuzzy inference system* (FIS) can be defined as the process of formulating the mapping from an input to an output using fuzzy logic. FISs are capable of approximating any continuous function into a compact domain with a high level of accuracy. Thus, they are considered as universal approximators. These approximators provide a unique dimension to define models and processes. One of which is their ability to equip their description with linguistic concepts that provide an intuitive sense of their behaviour. This process would require the development of critical building blocks such as: (i) membership functions, (ii) fuzzy logic operators, and (iii) rules.

Figure 5.5 shows a general block diagram describing the fuzzy inference system process. A more detailed block diagram is shown in Fig. 5.9. This process relies on an expert knowledge that allows for the development of the rules in a more efficient approach. Also, a defuzzification technique has to be selected in order to estimate the crisp output based on the degree of membership of the actual inputs with respect to the defined MFs.

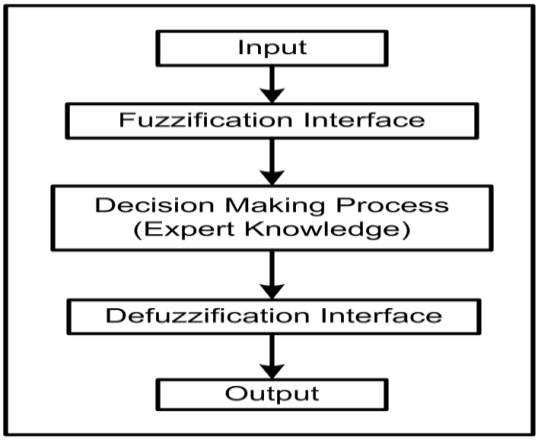

Fig. 5.5. A description of a fuzzy inference system.

5.3.1 Fuzzification Process

Fuzzification is the process of mapping the input data from crisp values (i.e., 0 or 1) to values between 0 and 1. In order to do so, MFs have to be utilized. These MFs can be: (i) triangular, (ii) trapezoidal, or (iii) Gaussian. Figure 5.6 shows two different classes of membership functions (trapezoidal and triangular) as an example.

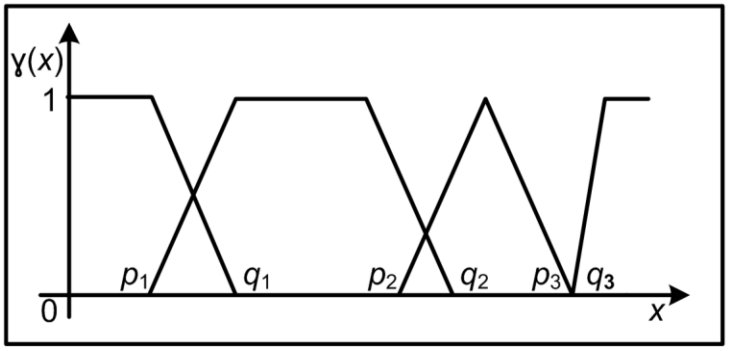

Fig. 5.6. Different membership functions used during the fuzzification process.

The use of one or other type of membership functions has to be selected carefully depending on several aspects. For example, Gaussian and polynomial MFs exhibit continuous derivatives facilitating sensitivity analysis and differentiability in the process. On the other hand, triangular ones provide simple linear interpolations and simple numerical evaluations, while local convergence might be guaranteed using triangular and polynomial MFs.

An input can belong to one or more MFs. Once the degree of membership has been established with respect to all MFs, a fuzzy arithmetic operator can be applied to determine the corresponding fuzzy level of the input variable. It is critical to mention that once all the computations of all the membership functions have been conducted, they do not need to be recalculated again, if unchanged. This is extremely important when dealing

with the computational complexity of algorithms based on a FIS. When the parameters describing the dynamics of the process are unchanged, the computational cost of the algorithm is minimized. Such feature is very attractive for our specific quest.

5.3.2 Decision-Making Process

The decision-making process maps fuzzy values of the inputs to fuzzy values of the outputs. It relies on a set of *if-then* rules based on an expert knowledge. They provide the resulting output based on the input data by combining and weighting a number of fuzzy sets (resulting from the fuzzy inference process during the estimation process) [Jang93].

The decision-making process is conducted for each rule through the following procedure: (i) estimate the degree of membership for the input data based on the defined MFs and fuzzy sets, (ii) establish the applicability for each rule based on the degree of membership and connectives, and (iii) calculate the output based on the applicability of each rule using a Max-Min or a Max-Product fuzzy inference system, as an example. The proper selection of these rules is critical to achieve an optimal performance. Figure 5.4 shows a graphical representation of the fuzzy rules. It indicates the value at the output based on the error and the change in the error.

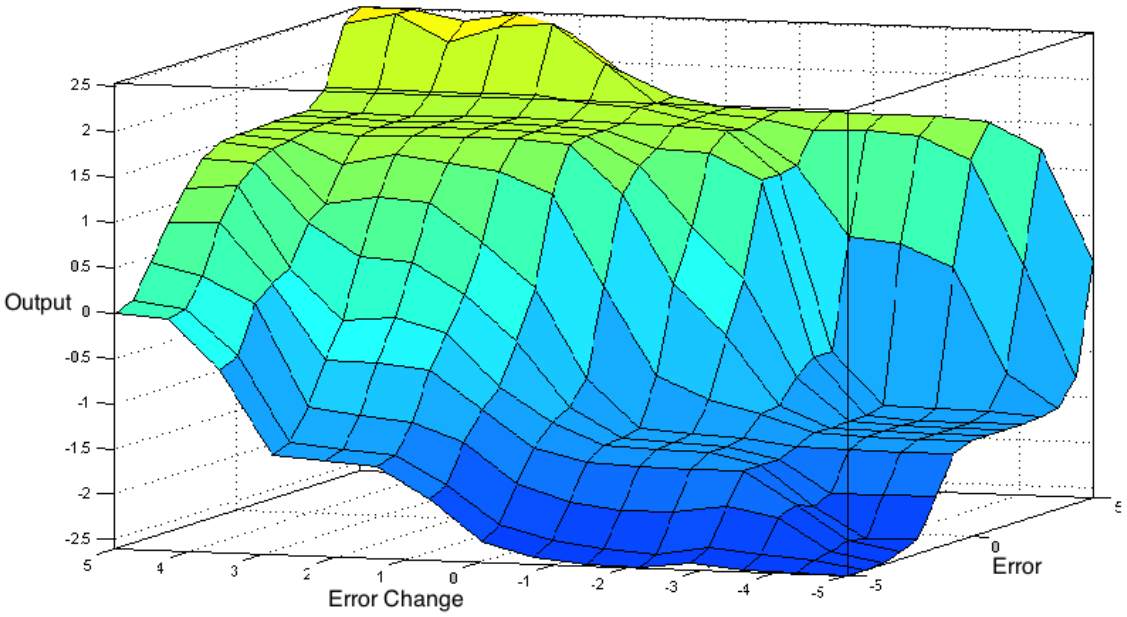

Fig. 5.7. Graphical representation of fuzzy rules.

5.3.3 Defuzzification

This process is responsible for combining and weighting a number of fuzzy sets resulting from the fuzzy inference system. This would result in a mapping from a space of fuzzy sets into a space of crisp values.

Different techniques for the purpose of defuzzification are available among which we find:

1. The Center of Area (Centroid): This technique calculates the center of the area of the combined membership functions, given by

$$w = \frac{\sum_{i=1}^{k} \gamma(x_i) x_i}{\gamma(x_i)} \tag{5.1}$$

where w is the crisp value and k is the number of items in the fuzzy set.

2. The Center of Sums: It considers the contribution of the area of each fuzzy set individually making it more computationally efficient compared to the centroid defuzzification technique; and
3. The First-of-Maxima: It calculates the crisp output by taking the union of the fuzzy sets and estimates the largest value of the domain with the maximal membership degree.

Other defuzzification techniques (*e.g.*, the last-of-maxima and the middle-of-maxima) can be found in [RaSa96]. Figure 5.8 shows a graphical representation of the defuzzification process using: (A) the centroid, (B) center of sums, and (C) first-of-maxima.

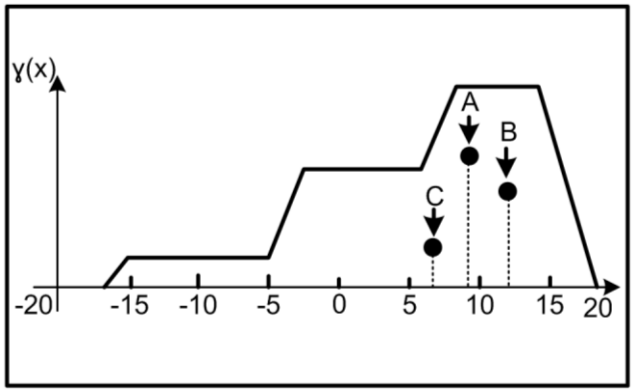

Fig. 5.8. An illustration of a defuzzification process.

5.4 Approximation Capabilities of a FIS

Fuzzy inference approach operates in a local way. This means that the information provided by each rule that belongs to the decision-making process is restricted to a compact region and the union of these local descriptions achieves the approximation of the developed function [EsVW06]. Consequently, a FIS can approximate and represent any mathematical function in a compact domain.

Given a FIS system with an arbitrary number of normal membership functions (triangular or trapezoidal) with centers c_{ji}, distributed over the intervals

$$[p_i, q_i] \ \forall i = 1, \ldots, N \tag{5.2}$$

and covering the interval such that at least one and at most two membership functions are different from zero for a given value x_i and let

$$g(x): \Re^n \to \Re \tag{5.3}$$

be an unknown function. If g(x) is continuously differentiable in the interval

$$U = [p_1, q_1] \times [p_2, q_2] \times \ldots \times [p_n, q_n] \tag{5.4}$$

then the fuzzy system f(x) can approximate the function g(x) with an arbitrary bounded error

$$\|\mathrm{g(x)} - \mathrm{f(x)}\|_\infty \leq \varepsilon \tag{5.5}$$

where $\|\bullet\|_\infty$ is defined as $\|\mathrm{e}(x)\|_\infty = \sup_{x \in U} |e(x)|$

5.5 Attitude Determination Based on a FIS

This section describes an estimation algorithm for the purpose of calculating the attitude of a spacecraft. To design a *fuzzy algorithm* (FA), it is critical to select the type of FIS; form a set of fuzzy rules; introduce the MFs in addition to fuzzy sets for the input data; select fuzzy logic operations and defuzzification rules. Moreover, a scheme to establish the granules of data has to be determined.

The FA constructed relies on triangular MFs and a gradient decent algorithm to adjust the location of the MFs and their consequences. Different optimization techniques were discussed in [BoVa04]. The selection of the gradient decent optimization scheme is driven by its low computational cost and the availability of the gradient of the process at hand with no intensive calculations. Consequently, reactive proportional actions can be inferred directly.

The initial position of the membership functions is another element that must be chosen. The procedure is given as follows:

1. Distribute the N_i triangular membership functions over the interval $[p_i, q_i]$. The membership functions cover the entire input interval (with at least two MFs covering each input domain);
2. Identify and generate all possible combinations among the antecedents in order to set the rules;

3. Optimize the parameters of the MFs and the consequences by minimizing the cost function shown in Eq. (5.6); that is, adjusting the membership functions of the antecedents. The cost function is given by

$$J = \frac{1}{2}\sum_{i=1}^{N}(w_i - \mathrm{f}(x^i, \boldsymbol{\Lambda}))^2 \tag{5.6}$$

where $\boldsymbol{\Lambda}$ denotes a vector representing all the parameters of the fuzzy algorithm that can be tuned (such as the consequences, parameters of the membership functions).

This minimization problem is extremely challenging and difficult due to its nature since it is a nonlinear and a non-convex optimization problem. Furthermore, a gradient decent scheme provides a local minima resulting in an acceptable performance and not necessarily the global minima of the cost function. Also, a convergence to the solution is not guaranteed. As a result, a variable parameter (denoted *r*) to improve the convergence rate and properties is considered and selected. This parameter can be estimated using Newton and quasi-Newton methods [EsVW06]

$$\boldsymbol{\Lambda}(k+1) = \boldsymbol{\Lambda}(k) + r\frac{\partial J}{\partial \boldsymbol{\Lambda}} \tag{5.7}$$

r is sometimes referred to as the learning rate. The gradient decent method calculates parameters on the antecedents and the consequences of the fuzzy inference system. The method requires the definition of the antecedents' initial location for the MFs. Additionally; it can be combined with a calculation of the consequences by using a least squares approach.

5.5.1 Gradient Updating for Triangular Membership Functions

The membership functions are parameterized using only their model values. This parameterization not only preserves the overlap but also reduces the number of parameters to be tuned. Triangular membership functions are parameterized by the position of their three vertices; but the condition of the overlap (which is set to 0.5) makes the lower right vertex of one membership function to be at the same position as the modal value of the next membership function. Consequently, instead of tuning three parameters (the vertices), only one parameter is tuned for each membership function.

The parameterization for a triangular membership function using the modal values as parameters is

$$\gamma_j^i(x_i, c_{j-1}^i, c_j^i, c_{j+1}^i) = \max[0,\ \min(\frac{x_i - c_{j-1}^i}{c_j^i - c_{j-1}^i}, \frac{x_i - c_j^i}{c_{j+1}^i - c_j^i})] \tag{5.8}$$

The updating formula will be

$$c_j^i(k+1) = c_j^i(k) + r\sum_{t=1}^{N}\left(\frac{(w^t - f(x^t))}{B}\right)$$
$$\left[\sum_{l\in u_1}(w^{-l} - f(x^t))\frac{\gamma_l(x^t)}{\gamma_{j-1}^i(x_i^t)}\frac{\partial\gamma_{j-1}^i(x_i^t)}{\partial c_j^i} + \sum_{l\in u_2}(w^{-l} - f(x^t))\frac{\gamma_l(x^t)}{\gamma_j^i(x_i^t)}\frac{\partial\gamma_{j-1}^i(x_i^t)}{\partial c_j^i} + \right.$$
$$\left. \sum_{l\in u_3}(w^{-l} - f(x^t))\frac{\gamma_l(x^t)}{\gamma_{j+1}^i(x_i^t)}\frac{\partial\gamma_{j-1}^i(x_i^t)}{\partial c_j^i}\right] \tag{5.9}$$

where u_1, u_2, and u_3 is the set of rules with antecedent term γ_j^i, γ_{j-1}^i, and γ_{j+1}^i.

$$\frac{\partial \gamma^i_{j-1}(x^t_i)}{\partial c^i_j} = \begin{cases} 0 & \text{if } x^t_i < c^i_{j-1} \\ \dfrac{x^t_i - c^i_j}{\left(c^i_j + c^i_{j-1}\right)^2} & \text{if } c^i_{j-1} < x^t_i < c^i_j \\ 0 & \text{if } x^t_i > c^i_j \end{cases} \tag{5.10a}$$

$$\frac{\partial \gamma^i_j(x^t_i)}{\partial c^i_j} = \begin{cases} 0 & \text{if } x^t_i < c^i_{j-1} \\ \dfrac{c^i_{j-1} - x^t_i}{\left(c^i_j + c^i_{j-1}\right)^2} & \text{if } c^i_{j-1} < x^t_i < c^i_j \\ \dfrac{c^i_{j+1} - x^t_i}{\left(c^i_j + c^i_j\right)^2} & \text{if } c^i_j < x^t_i < c^i_{j+1} \\ 0 & \text{if } x^t_i > c^i_j \end{cases} \tag{5.10b}$$

$$\frac{\partial \gamma^i_{j+1}(x^t_i)}{\partial c^i_j} = \begin{cases} 0 & \text{if } x^t_i < c^i_j \\ \dfrac{x^t_i - c^i_{j+1}}{\left(c^i_{j+1} + c^i_j\right)^2} & \text{if } c^i_j < x^t_i < c^i_{j+1} \\ 0 & \text{if } x^t_i > c^i_{j+1} \end{cases} \tag{5.10c}$$

$$B = \sum_{i=1}^{N} \gamma(x_i) x_i \tag{5.10d}$$

The adaptation must be constrained such that the condition $c^i_j \le c^i_{j+1}$ is preserved.

Now that all the building blocks have been introduced, an attitude estimation algorithm will be described based on Mamdani model [LoMa06]. This algorithm is referred to as the Delta-Fuzzy Algorithm

5.5.2 Mamdani Model

Two of the most common fuzzy controllers are: Mamdani and *Takagi-Sugeno* (TS) controllers. Mamdani and Assilian were attracted by the capabilities of fuzzy logic and introduced a Mamdani-type fuzzy control scheme in 1975 [MaAs75], in which a fuzzy controller was used to convert heuristic control rules stated by a human operator into an automatic control scheme. Unlike the Mamdani controller which employs fuzzy sets as the consequent, the TS fuzzy controller relies on a linear interpolation to calculate the consequent [TaSu85]. Consequently, the algorithm proposed relies on a Mamdani model to adjust for the consequent directly.

The suggested Delta-Fuzzy estimator is designed based on the four important components shown in Fig. 5.5.

5.5.2.1 The Fuzzification Process

This algorithm relies on the Earth magnetic field as the only sensory data collected on the body frame of the satellite. This choice was driven by the availability of the magnetic field throughout the entire LEO (which is not the case for the sun data). Additionally, it provides the algorithm with a unique stability when the angle between the Earth magnetic field and the sun is small. The fuzzification stage proceeds as follows:

1. Measure the Earth magnetic field using TAM;
2. Calculate the residual using the reference Earth magnetic field data (estimated from the IGRF) using (3.74); and
3. Conduct a scale mapping to transfer the range of the residual into the initial universe of discourse.

5.5.2.2 The Decision-Making Process

The decision-making process is conducted based on the rule base that encompasses knowledge of the application goals. This process consists of:

1. Identifying the corresponding linguistic variables and fuzzy levels (i.e., identify the antecedents); and
2. Characterizing the consequences based on the rules established.

5.5.2.3 The Defuzzification Process

This process can be seen as the inverse of the fuzzification stage. It proceeds by:

1. Converting the range of the consequences into the universe of discourse by conducting a scale mapping; and
2. Identifying the crisp output (correction term for the attitude) using the center of gravity technique given by Eq. (5.1).

5.5.2.4 Update the Parameters of the Fuzzy Sets

The parameters of the antecedents are adjusted using a gradient descent optimization technique. This technique relies on the error and the change in the error in the attitude as inputs. Feeding the information to the optimization algorithm provides a unique feature that consists of being cognizant of the changes in the environment. Such feature did not exist in deterministic and stochastic approaches introduced in Chapter 3.

The algorithm implemented is illustrated in Figure 5.9. The dashed frames (denoting the reference Earth magnetic field and the desired attitude) represent the stored data, which are not part of the algorithm itself.

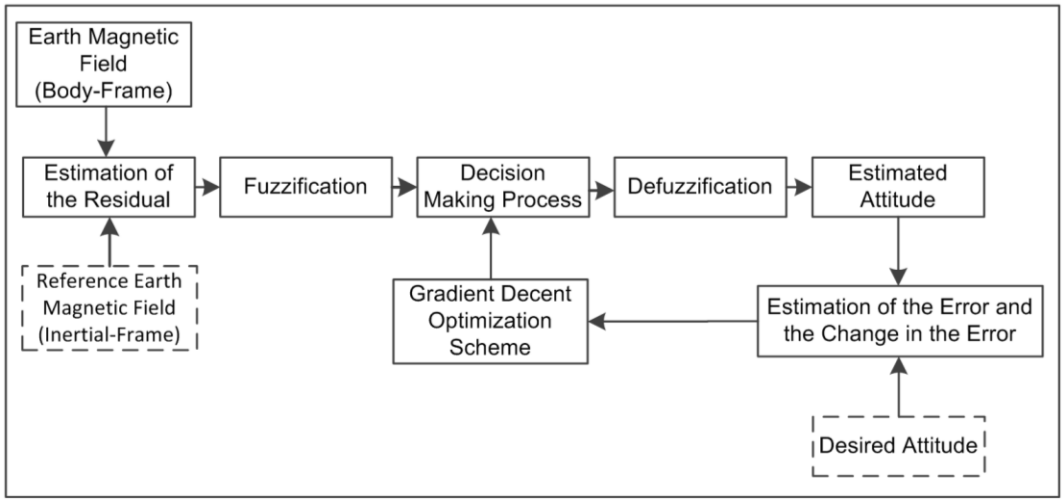

Fig. 5.9. Block diagram of the proposed Delta-Fuzzy algorithm.

5.6 Simulation Results

In this section several performance test cases are simulated to evaluate the performance of the FA implemented for the purpose of small satellites attitude determination. This algorithm relies on the S-data and P-date introduced in Chapter 4 for the evaluation of the different stochastic and deterministic algorithms. The simulations evaluate the algorithm against four performance measures, including: (i) the sensitivity to initial conditions, (ii) the robustness to noisy measurements, (iii) the transient response, and (iv) pointing accuracy. Figure 5.10 shows the time history of the attitude estimation error using the fuzzy algorithm with exact knowledge of the initial attitude. Results shown in Fig. 10(b) and Fig. 10(c) consider measurements corrupted with a 5% and a 10% additive WGN, respectively.

The error trajectory exhibits a smooth behaviour for the first 40 minutes of the simulations. Then, the estimation process exhibits a transient behaviour for 20 minutes before returning to the stable evolution encountered initially. The average error is 1.7 deg.

Similar behaviour can be observed when an additive WGN is added. These observations can be justified by the parameters used to tune the FA. These parameters may not provide a global solution. Additionally, the transient response is due to the gradient decent scheme updating its parameters to correct for the error and improve the estimation process. Furthermore, having an overlap of two MFs per input makes the FA more resilient to noisy measurements and imprecisions in the development of the FIS.

In order to visualize the impact of the gradient decent optimization technique, the error and the change in the error for each axis is monitored and displayed in Figures (5.11) and (5.12), respectively.

Figures (5.11) and (5.12) illustrate the response of the algorithm to the error and the change in the error. A nonlinear behaviour can be observed for the three axes. During such response, the FA redefines the widths of the input and output MFs. The FA algorithm suggested is fundamentally different from all the algorithms presented so far. As an example, the EKF tracks the initial conditions provided to converge to the exact attitude (in case the error is not large), while the FA can recover from large errors (as observed between 40 to 60 min. of Fig. (5.11) and (5.12)).

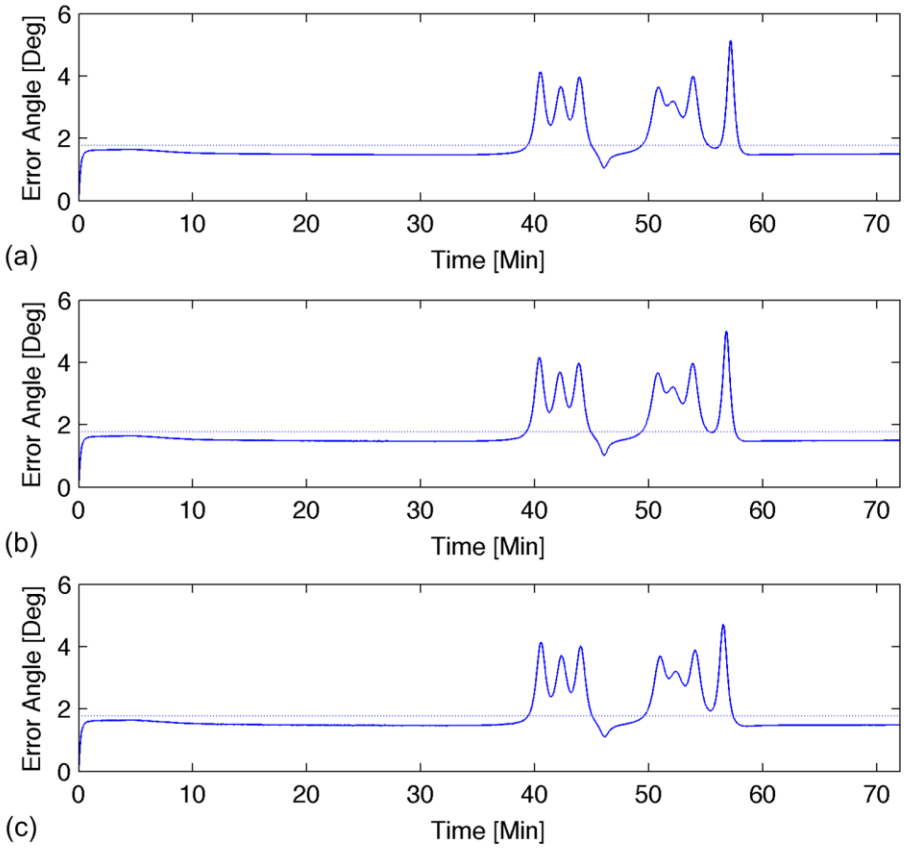

Fig. 5.10. Attitude determination using Delta-Fuzzy fuzzy algorithm with the exact initial attitude. (a) Uncorrupted measurements. (b) A 5% WGN added to the measurements. (c) A 10% WGN added to the measurements.

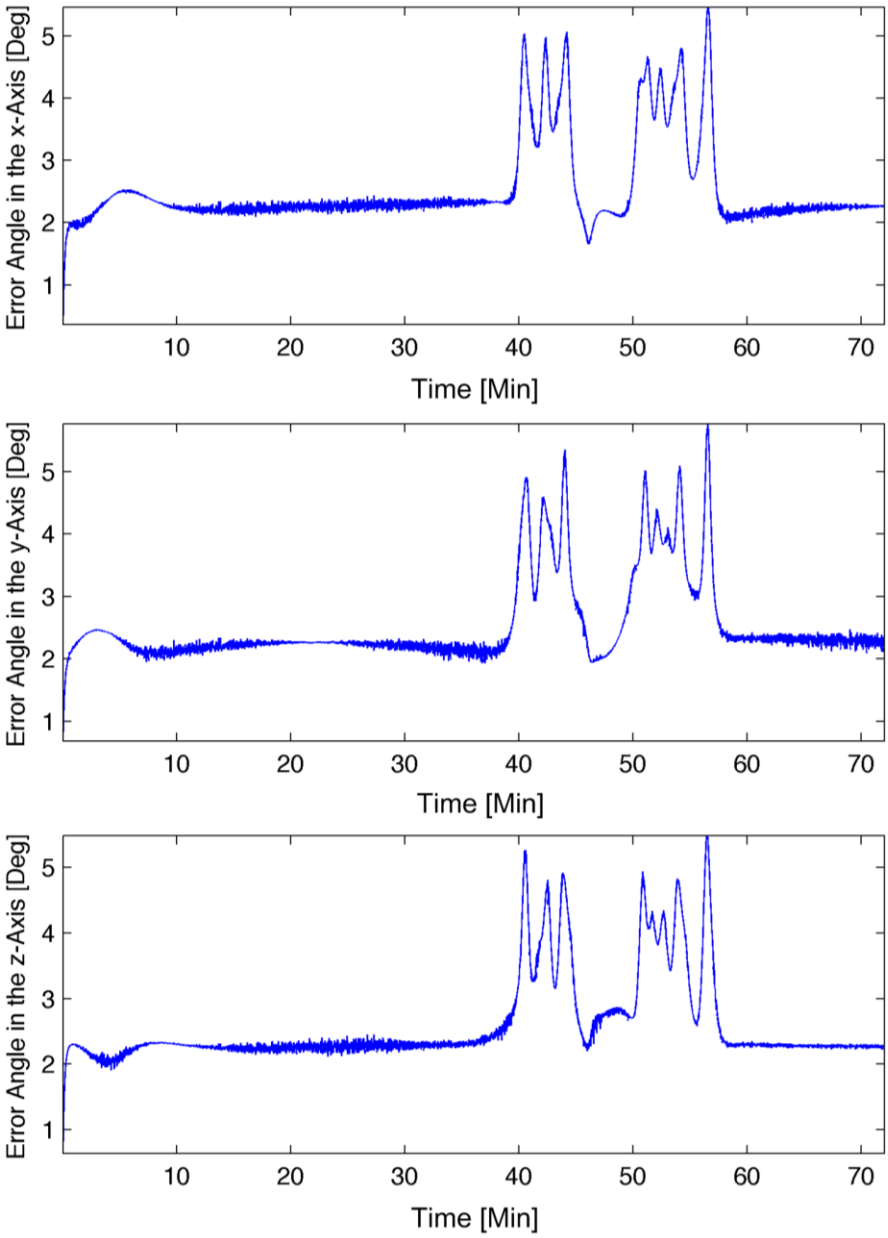

Fig. 5.11. The error in the x-, y-, and z- axes using the Delta-Fuzzy algorithm.

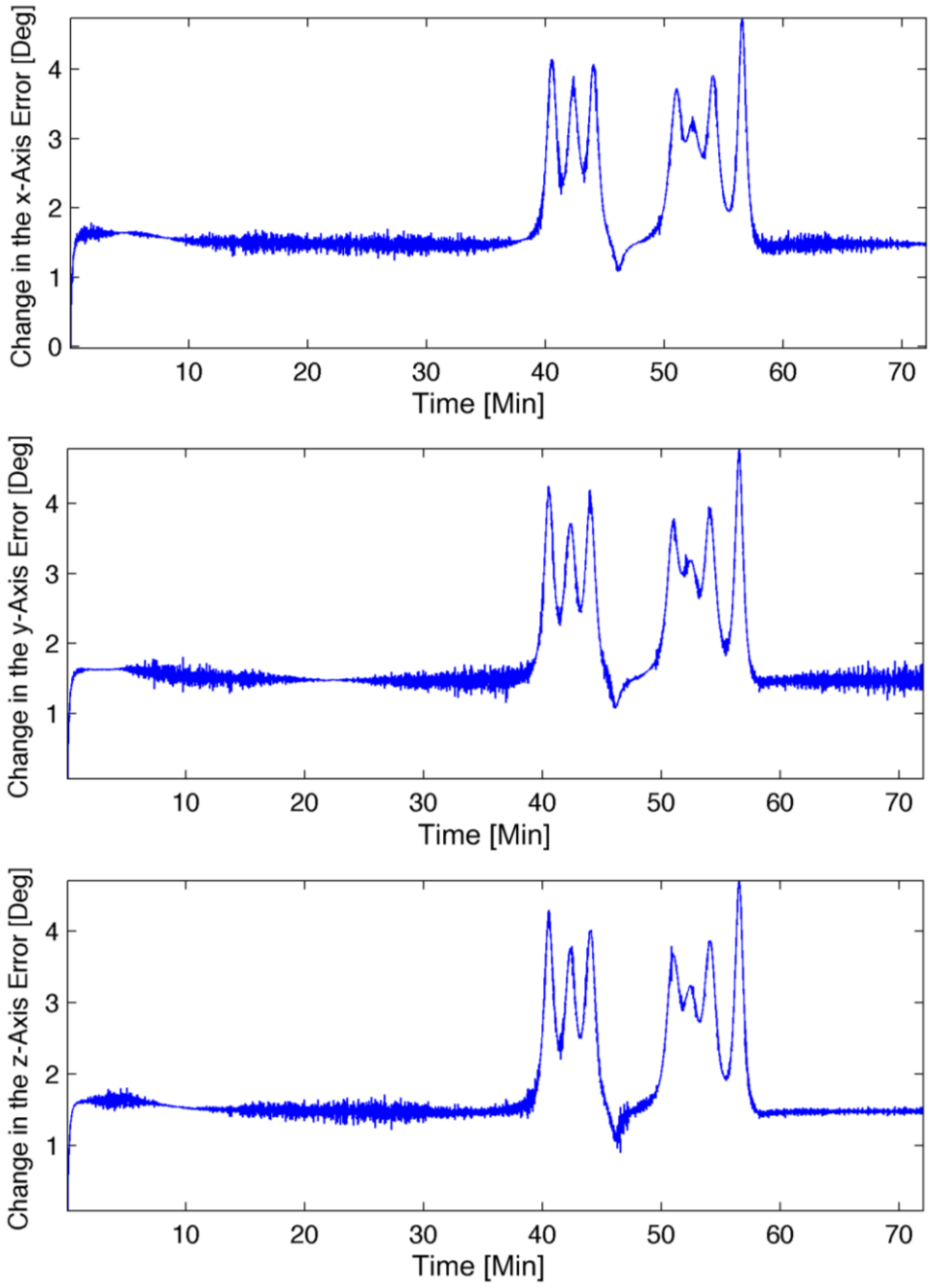

Fig. 5.12. The error change in the x-, y-, and z-axes using the Delta-Fuzzy algorithm.

Finally, Figure 5.13 illustrates the results of the estimation process when a large error is considered initially with and without the addition of a 5% WGN to the measurements per axis. Similar behaviour can be observed (in Fig 5.13(a) and Fig 5.13(b)) as in Fig. 5.10; that is, a smooth estimation process with some transients. The FA corrects very rapidly the error of the initial attitude by updating the MFs using the gradient decent scheme. The update stage of the scheme appears in the trajectory of the error as a deterioration of the performance of the algorithm. Once an optimal solution for the locations of the MFs and the consequences has been estimated (i.e., the error and the change in the error do not diverge), the FA resumes a smooth estimation process.

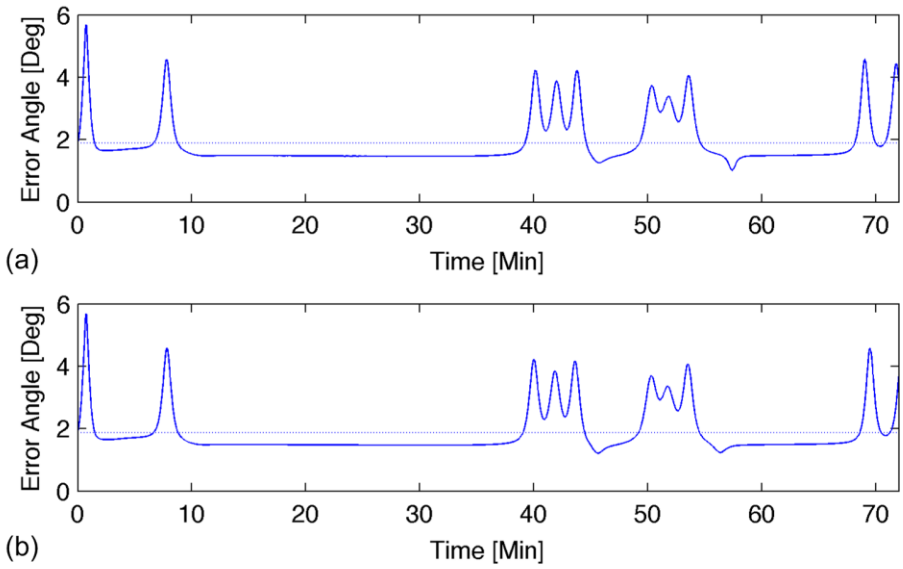

Fig. 5.13. Attitude determination using the Delta-Fuzzy algorithm with a large initial error. (a) Uncorrupted measurements. (b) A 5% WGN added to the measurements.

5.7 Discussion and Comparison

This section compares the proposed Delta-Fuzzy algorithm with deterministic and stochastic approaches introduced in Chapter 3 and evaluated in Chapter 4.

5.7.1 Algorithm Formulation

5.7.1.1 Fuzzy Algorithms require

1. The definition of the antecedents, MFs, as well as their initial locations;
2. The definition of all possible rules based on the different combinations of the antecedents; and
3. A scheme to optimize the location of the MFs and the consequences, if necessary.

5.7.1.2 Stochastic Algorithms

1. Require the specification of the process and measurement models;
2. Assume a process described using a GRV;
3. Assume a process and measurements corrupted with a WGN only;
4. Involve a two-stage process (thus computational delay); and
5. Require the approximation of a posteriori PDF.

5.7.1.3 Deterministic Algorithms

1. Require the definition of a loss function; and
2. Require a closed-form algorithm for the defined loss function.

5.7.2 Algorithms Performance and Computational Complexity

The next step in this comparison between all the approaches presented is to evaluate all the algorithms with respect to their performance in estimating the attitude, as well as their computational complexity. This comparison is summarized in Table 5.2.

Table 5.2: Performance and computational complexity of fuzzy, stochastic, and deterministic algorithms.

Performance Measures	Fuzzy Algorithm	Stochastic Approaches	Deterministic Approaches
Sensitivity to Initial Conditions	Can recover from large errors	Sensitive to initial conditions	Does not require initial conditions
Sensitivity to Noisy Measurements	Resilient to noisy measurements	Resilient to noisy measurements	Very sensitive
Transient Response	In the order of minutes	In the order of hours	In the order of hours
Time Complexity	$O(n^2)$	$O(n^3)$	$O(n^2)$
Space Complexity	$O(n)$	$O(n^2)$	$O(n)$

5.7.2.1 Discussion

The algorithmic formulation of each approach, as well as their performances and computational complexity illustrate the strength of fuzzy logic as compared to the alternatives studied. *Fuzzy algorithms* do not involve any notions of probability theory. Consequently, no a priori knowledge of the process and measurements PDF is required. Furthermore, they do not require a model of the environment or the process at hand. Additionally, the computational complexity of the suggested approach is much smaller than

stochastic approaches, while preserving its remarkable performance when subjected to large errors in the initial conditions and/or noisy measurements.

5.8 Summary

Chapter 5 introduced an improved approach to solve a class of nonlinear navigation problems for small satellites. This approach is based on fuzzy logic and a gradient decent optimization scheme for a granule-based type of computing. Unlike classical logic, fuzzy logic performs well when boundaries of a class are ill-defined (or blurred). Such characteristic was fully utilized in order to develop a robust algorithm showing an important tolerance to uncertainty and imprecision. Additionally, the gradient decent approach provide a unique feature to the suggested Delta-Fuzzy algorithm; that is, the ability to be cognizant of the changes in the environment; yet, preserving a low time and space computational costs. Now that the attitude determination was addressed, Chapter 6 will attempt to develop an optimal and energy efficient control scheme for the attitude.

Chapter 6

OPTIMAL CONTROL DESIGN

The controllability of the satellite at any given time is a task of tremendous importance for an optimal operation of the ADCS. To successfully accomplish this task, the attitude control must be extremely compact and light. Furthermore, an optimal controller ought to be designed to minimize: (i) the time delay, (ii) the overshoot, (iii) the transient response, and (iv) the steady-state error. Consequently, different control schemes have to be evaluated for an optimal selection of the control scheme to satisfy the aforementioned requirements.

6.1 Attitude Control of a Flexible Spacecraft

A compact control system implies a careful selection of the actuators. Usually, these actuators should not exceed 500g, as well as they should not require propellant (*e.g.*, thrusters). Additionally, they must be strong enough to counter-act all the disturbances encountered in LEO. These conditions can be satisfied by the use of magnetic torque rods as small satellites actuators.

Using magnetic torque rods for the purpose of attitude control is a challenging task. The controllability of the spacecraft attitude under magnetic actuation is addressed in [BhDh03]. The attitude dynamics of a spacecraft actuated by three magnetic torque rods and subjected to a time-varying magnetic field is strongly accessible and controllable, if the following conditions are satisfied. First, the magnetic field and its first two time-derivatives are linearly independent at every instant; second, the magnetic field is periodic in time. These properties are satisfied by the time variation of a constant dipole approximation of the geomagnetic field along a closed Keplerian (except in the case where the orbital plane does not coincide with the geomagnetic equatorial plane and does not contain the magnetic poles).

A time delay may be defined as the time interval between the start of the event at one point in a system and it resulting action at another point in the system. Delays (also known as transport lags or dead times) arise in physical systems, as well as during the computation process. Dealing with time-domain compensation can be accomplished through several approaches. These methods encompasses parameter optimized controllers and possibilistic algorithms, among others.

Parameters optimized controllers (such as *proportional integral derivative* controllers, PID) tune the controller's structure and parameters based on the process model to optimize its performance. These controllers have a solid heritage in aerospace engineering. For example, a PID controller has been implemented successfully in several missions for the purpose of attitude control [KuTB09]. Additionally, a self-tuning *integer-order PID* (IPID) controller for three-axis satellite stabilization with unknown parameters has been addressed in [Mora12]. Their results demonstrated the stability of a closed-loop sys-

tem in the presence of disturbances and uncertainties. Furthermore, a *fractional-order PID* (FPID) controller has received considerable attention due to its robustness and performance. For instance, a fractional regulator for spacecraft attitude stabilization was introduced in [KMAC04]. The FPID has revealed attractive characteristics such as additional flexibility compared to the IPID, which offers the opportunity to tune the parameters of the controller to a dynamical process by adjusting the order of the fractional derivative and integral.

Alternative controllers based on possibilistic approaches have proven to be critical for applications, in which the environment is unknown or ill-defined. For example, an adaptive fuzzy controller was applied to the attitude stabilization of a flexible satellite. The suggested approach does not depend on the exact model of the plant. It adjusts the rule parameter vector on-line. The drawbacks of this method have been illustrated by a chattering phenomenon and a large dissipation of power in an actual real implementation [LiGL05]. In [ScÖz94], a robust stabilization of a class of nonlinear systems that exhibits parametric uncertainty was introduced. The authors considered feedback linearizable nonlinear systems with a vector of unknown constant parameters perturbed about a known value. This work shows that linearization and stabilization of nonlinear systems exhibiting parametric uncertainty is possible via Lyapunov-based approach, if certain assumptions are satisfied (such as a structure matching condition). The main limitation for this approach is its respective computational cost in terms of space and time. Finally, a detailed literature review provides a range of nonlinear systems controlled by fuzzy logic showing usually superior results over conventional control [Lee90].

Now that the three controllers that are studied in this thesis are introduced, nonlinear model of the attitude dynamics is presented.

6.2 Nonlinear Model of the Attitude Dynamics

The attitude motion of a spacecraft can be represented using the Euler's equation for the motion of a rigid body under the influence of external moments, such as the control moment generated by the actuators. The attitude dynamic model can be described as [Psia01]

$$\mathbf{I}\dot{\boldsymbol{\omega}}(t) = -\boldsymbol{\omega}\times\mathbf{I}\boldsymbol{\omega} + \mathbf{N}_{\text{ctrl}} + \mathbf{N}_{\text{gg}} + \mathbf{N}_{\text{dist}} \tag{6.1}$$

$$\mathbf{N}_{\text{ctrl}} = \mathbf{m}_{\text{ctrl}} \times \mathbf{b}_{\text{body}}^{\text{mag}} \tag{6.2}$$

where $\mathbf{I}$ denotes the satellite's moment of inertia. $\mathbf{N}_{\text{ctrl}}$, $\mathbf{N}_{\text{gg}}$, and $\mathbf{N}_{\text{dist}}$ refer to the magnetic dipole produced in the magnetic coils, the gravity gradient torque, and disturbance torque, respectively. Finally, $\mathbf{m}_{\text{ctrl}}$ represents the magnetic moment and $\mathbf{b}_{\text{body}}^{\text{mag}}$ denotes the magnetic field in the body frame.

The different disturbance torques that affect small satellites in LEO are: (i) aerodynamic drag, (ii) gravity gradient, (iii) magnetic torque, and (iv) solar pressure, in order of magnitude. These disturbances are discussed in [Pete98].

The kinematics and dynamics models introduced in (3.48) and (6.1), respectively, are linearized about deviations from the nadir-pointing attitude assuming a circular orbit. The linearized equations, which accounts for gravity-gradient effects, aerodynamic drag torques and control torques are given by

$$\begin{bmatrix} \dot{\phi} \\ \dot{\theta} \\ \dot{\psi} \\ \dot{\omega}_1 \\ \dot{\omega}_2 \\ \dot{\omega}_3 \end{bmatrix} = \begin{bmatrix} 0 & 0 & 0 & 1 & 0 & 0 \\ 0 & 0 & 0 & 0 & 1 & 0 \\ 0 & 0 & 0 & 0 & 0 & 1 \\ -4\omega_0^2\nu_1 & 0 & 0 & 0 & 0 & \omega_0(1-\nu_1) \\ 0 & 3\omega_0^2\nu_2 & 0 & 0 & 0 & 0 \\ 0 & 0 & \omega_0^2\nu_3 & -\omega_0(1+\nu_3) & 0 & 0 \end{bmatrix} \begin{bmatrix} \phi \\ \theta \\ \psi \\ \omega_1 \\ \omega_2 \\ \omega_3 \end{bmatrix} + \begin{bmatrix} 0 & 0 & 0 \\ 0 & 0 & 0 \\ 0 & 0 & 0 \\ 0 & b_3(t)/I_{11} & -b_2(t)/I_{11} \\ -b_3(t)/I_{22} & 0 & b_1(t)/I_{22} \\ b_2(t)/I_{33} & -b_1(t)/I_{33} & 0 \end{bmatrix} \begin{bmatrix} m_1 \\ m_2 \\ m_3 \end{bmatrix} + \begin{bmatrix} 0 & 0 & 0 \\ 0 & 0 & 0 \\ 0 & 0 & 0 \\ 1/I_{11} & 0 & 0 \\ 0 & 1/I_{22} & 0 \\ 0 & 0 & 1/I_{33} \end{bmatrix} \mathbf{n}_d \tag{6.3}$$

where $\mathbf{n}_d$ refers to a vector of disturbances. b_1, b_2, and b_3 represent a dipole approximation of the Earth's magnetic field in the absence of the Earth's rotation in a local level frame. This approximation is given by:

$$\begin{bmatrix} b_1 \\ b_2 \\ b_3 \end{bmatrix} = \frac{\mu_f}{R_a^3} \begin{bmatrix} \cos\omega_0 t \sin i_m \\ \cos i_m \\ 2\sin\omega_0 t \cos i_m \end{bmatrix} \tag{6.4}$$

where μ_f is equal to 7.9×10^{15} Wb.m, ω_0 is the absolute angular velocity of the satellite and i_m is the inclination of the orbit with respect to the Earth's magnetic equator [KuCa04]. Also, ϕ, θ, and ψ represent the roll, pitch, and yaw deviations about the equilibrium nadir-pointing approach.

As indicated in (2.13), for small deviations the quaternion is given by:

$$\mathbf{q} \approx \begin{bmatrix} \phi/2 \\ \theta/2 \\ \psi/2 \\ 1 \end{bmatrix} \tag{6.5}$$

and

$$\nu_i = \frac{\left(\mathbf{I}_{jj} - \mathbf{I}_{kk}\right)}{\mathbf{I}_{ii}} \tag{6.6}$$

for the (i,j,k) index sets (1,2,3), (2,3,1), and (3,1, 2).

The linearized equations are valid only when the attitude angles remain small. Consequently, the controller designed is valid after detumbling only (also known as the scientific mode). In order to evaluate the performance and identify the different limitations of the different controllers, the characteristic equations of the dynamics describing the pitch and roll/yaw angles are needed. They are obtained using Laplace transform, as follows

$$s^2 + 3{\omega_0}^2 \frac{I_1 - I_3}{I_2} = 0 \tag{6.7a}$$

$$s^4 + (1 + 3\bar{\nu}_1 + \bar{\nu}_1\bar{\nu}_3){\omega_0}^2 s^2 + 4\bar{\nu}_1\bar{\nu}_3{\omega_0}^4 = 0 \tag{6.7b}$$

with

$$\bar{\nu}_1 = \frac{I_2 - I_3}{I_1} \tag{6.8a}$$

$$\bar{\nu}_3 = \frac{I_2 - I_1}{I_3} \tag{6.8b}$$

where s denotes Laplace variable [TiVe06].

6.3 Attitude Control, Theoretical Background

This section introduces the theoretical background behind the three different types of control schemes that are evaluated: (i) IPID, (ii) FPID, and (iii) fuzzy controller.

6.3.1 Integer-Order PID Controller

Control engineers practitioners have used PID controllers for a long time because of their simplicity and performance. They are considered to be the second most important control decision and communication instrument of the 20th century [Rhin00]. Throughout the years, the PID control scheme has dominated most of the industry applications. In fact, as indicated in [ViVi12], the use of PI and PID controllers is ubiquitous (they are found in more than 95% of process control applications). In this chapter, an ideal PID controller in a unity feedback block diagram is considered. The controller is given by

$$C(\mathrm{s}) = k_p + k_i s^{-1} + k_d s \tag{6.9}$$

where k_{p}, k_{i}, and k_{d} represent tuning parameters for the PID controller.

Figure 6.1 shows an ideal PID controller with unity feedback where $R(\mathrm{s})$, $E(\mathrm{s})$, $Y(\mathrm{s})$ represent the reference input, the error, and the output respectively. Several practical controllers are implemented based on this architecture, for example Honeywell TDC3000 Process Manager Type A [Hone03].

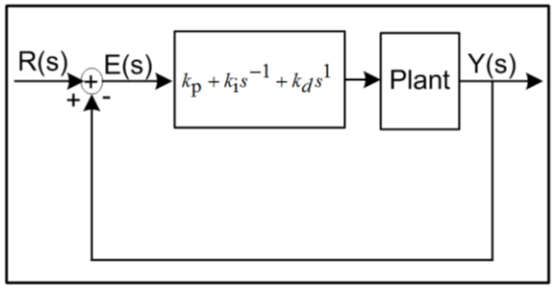

Fig. 6.1. Ideal block diagram of an IPID controller with unity feedback.

As mentioned in the beginning of this chapter, the PID consists of three different types of actions, namely the proportional, the derivative, and the integral ones. Their main effects on the controlled system behaviour can be summarized as follows:

1. The proportional action increases the speed of the response, while decreases the steady-state error and relative stability;
2. The integral action attempt to eliminate the steady-state error; but, decreases the relative stability; and
3. The derivative action increases the relative stability and sensitivity to noise.

The positive and negative effects of these actions can be visualized though a frequency analysis using bode plot as shown in Figure 6.2. For instance, the impact of the derivative action (increase of the relative stability) can be observed in the frequency-domain by introducing the $\pi/2$ phase lead, and the negative ones (increase of the sensitivity to high-frequency noise) by increasing the gain with a slope of 20 dB/dec. Similarly, for the integral action, the positive effects (elimination of the steady-state errors) can be deduced by an infinite gain at zero frequency, while the negative one (decrease of the relative stability) is indicated by a $\pi/2$ phase lag are introduced.

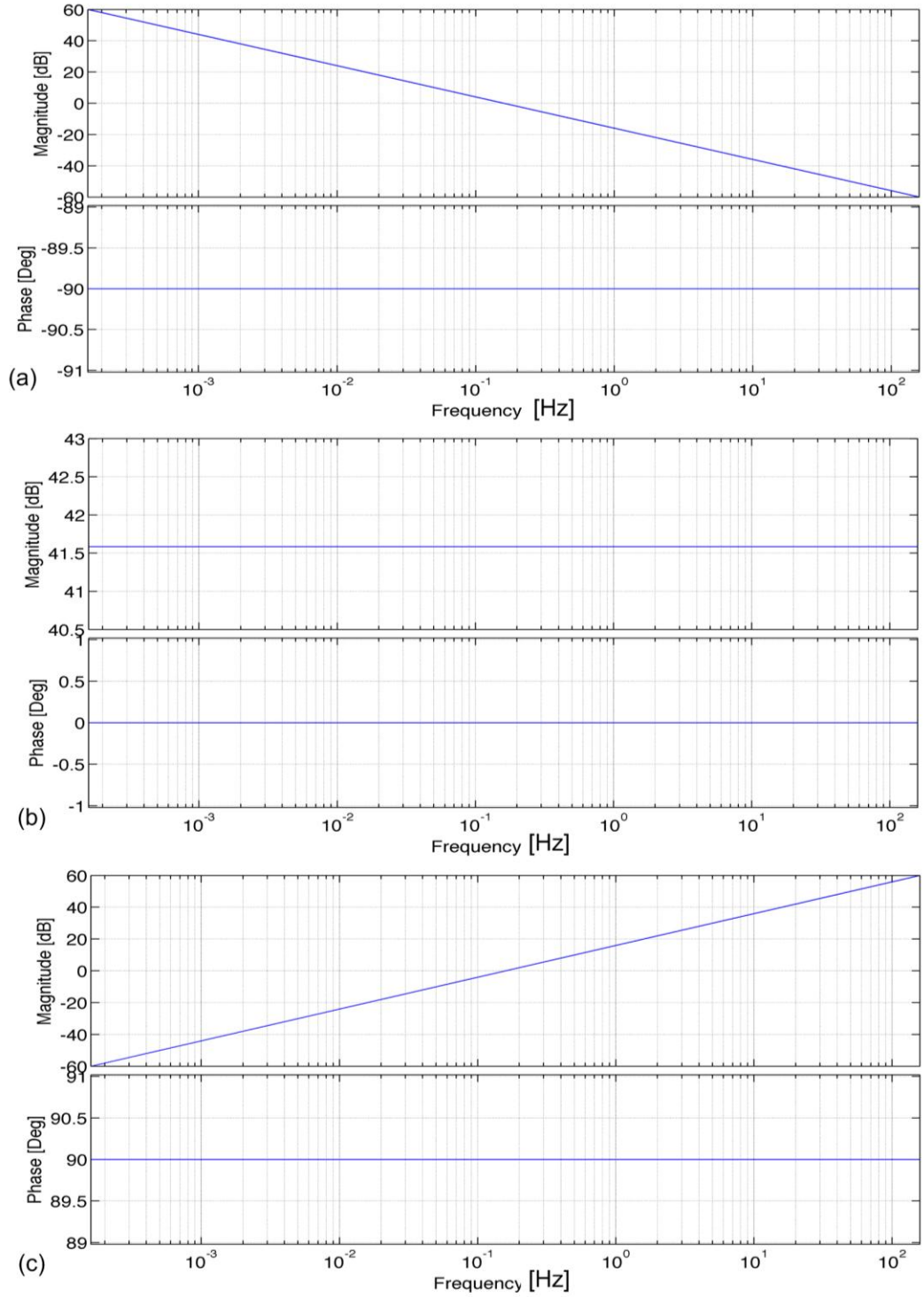

Fig. 6.2. Bode plot for the (a) integral, (b) proportional, and (c) derivative terms.

Using a PID controller, the control torque is given by

$$\mathbf{u}(t) = -k_{\mathrm{p}}\mathbf{q}_e - k_{\mathrm{i}}\int \mathbf{q}_e - k_d \frac{d}{dt}\boldsymbol{\omega}_e \tag{6.10}$$

where $\mathbf{q}_{\mathrm{e}}$ and $\boldsymbol{\omega}_{\mathrm{e}}$ refer to the error in the quaternion and angular velocity.

6.3.2 Fuzzy Controller

Another alternative for small satellites attitude control is based on fuzzy logic. This specific scheme has been used in numerous applications due to its robustness to parameter variations and system disturbances [AsAn12]. *Fuzzy control* (FC) exhibits very attractive characteristics (such as autonomy and modularity), while remaining robust to uncertainty in the process, as seen in Chapter 5.

FC has found numerous applications. In [Chia94], a fuzzy controller was developed for Cassini spacecraft with specific issues investigated (*e.g.*, tracking capability, thrusters' duty cycle). Also, the controller was compared with a conventional bang/bang scheme. A more complex example was introduced in [Ousa11], where a multi-axis attitude maneuver for a small satellite with variable inertia matrix using fuzzy logic strategy was investigated. The controller was implemented by means of a *multi-input multi-output* (MIMO) system with a knowledge base composed of 75 logic rules. This specific example reinforces the strength of fuzzy logic in dealing optimally with nonlinear navigation problems. The fuzzy controller designed has the following main components: (i) a fuzzification stage; (ii) a decision-making process; and (iii) a defuzzification stage, which are introduced in the next section.

6.3.2.1 The Fuzzification Process

The controller relies on five Gaussian membership functions to fuzzify the two inputs, which are the error and the change in the error.

6.3.2.2 The Decision-Making Process

The decision-making process is conducted based on the 16 rules derived to achieve the main goal; that is, minimizing the error and the change in the error. This is accomplished by:

1. Identifying the corresponding antecedents; and
2. Characterizing the consequences based on the rules of the domain experts.

6.3.2.3 The Defuzzification Process

This process converts the range of the consequences into a universe of discourse by conducting a scale mapping and identifying the crisp output (correction term for the control signal) based on the center of gravity technique using (5.1).

6.3.3 Fractional-Order PID Controller

The FPID controller provides more flexibility as compared to the IPID. In addition to the proportional, integral, and derivative gains, the order of the fractional derivative and integral have to be specified. Such flexibility allows for an optimal trade-off between the advantages and disadvantages of each term as seen in subsection 6.3.1; thus, leading to a more satisfying result, as well as a more powerful and flexible soft-computing design method to satisfy the stringent limitations found in small satellites.

FPID is based on a fractional-order calculus, which constitutes a trend of expanding integer operators to non-integer operators (*e.g.*, integrator and differentiator) [Love04]. As indicated in [PoDK97], the idea of using FPID controllers for the dynamic system control belongs to [Oust95], while a generalized FPID was proposed by Podlubny [Podl97]. Fractional-order dynamics and controls are relatively new research areas in control engineering used for the purpose of an accurate profile tracking in a controlled-output system. In this subsection, a review of some important notions about fractional calculus is introduced briefly.

6.3.3.1 Fractional-Order Calculus

Calculus refers to the mathematical study of change, which encompasses two major branches which are differential and integral calculus dealing with rates of changes and slope of curves and the summation of areas under curves, respectively.

The motivation for introducing fractional calculus is driven by the need to analyze and deal with non-smooth and non-continuous functions. For instance, the integer derivative gives the linear approximation of *smooth* functions. Smooth functions are defined as functions that have derivatives of all orders. Fractional derivative provides a power-law (nonlinear) approximation of the local behaviour of non-smooth functions (non-differentiable). Consequently, fractional calculus provides a more expressive power to deal with nonlinear behaviours.

A fractional integral is defined as:

$$I^{\xi}\,\mathrm{f(t)} = \frac{1}{\Gamma(\xi)}\int_0^t (\mathrm{t}-\tau)^{\xi-1}\,\mathrm{f}(\tau)\,\mathrm{d}\tau \qquad (6.11)$$

where $t > 0$ and ξ is a positive real number.

The current literature is rich in terms of the different definitions of fractional derivative; yet, the most used ones are Caputo and Riemann-Liouville definitions. Each definition has advantages, as well as disadvantages. For example, using a Riemann-Liouville derivative with a constant function is not zero. Additionally, if an arbitrary function is a constant at the origin, its fractional derivative has a singularity at the origin. Consequently, these disadvantages reduce the field of usage of the Riemann-Liouville definition. Therefore, the Caputo derivative has been selected for this specific application.

The fractional derivative, Caputo derivative, is defined as:

$$D^{\zeta}\,\mathrm{f(t)} = \frac{d^{\zeta} f(\mathrm{t})}{dt^{\zeta}} = \frac{1}{\Gamma(\zeta - n)} \int_0^t \frac{f^{(\mathrm{n})}(\tau)}{(\mathrm{t}-\tau)^{\zeta+1-n}}\,\mathrm{d}\tau \tag{6.12}$$

where ζ is a positive real number and Euler's Gamma function is given by

$$\Gamma(x) = \int_0^{\infty} e^{-t} t^{x-1} dt, \quad x > 0 \tag{6.13}$$

with the special case when x=n defined as

$$\Gamma(x) = (n-1)(n-2)\ldots(2)(1) = (n-1)! \tag{6.14}$$

Now, using the Laplace transformation we have

$$s^{-\xi} F(\mathrm{s}) = I^{\xi} f(\mathrm{t}) \tag{6.15}$$

and

$$s^{\zeta} F(\mathrm{s}) = \frac{d^{\zeta} f(\mathrm{t})}{dt} \tag{6.16}$$

Then, the fractional PID controller can be written as

$$C(\mathrm{s}) = k_{\mathrm{p}} + k_{\mathrm{i}} s^{-\xi} + k_{\mathrm{d}} s^{\zeta} \tag{6.17}$$

If we take ζ=ξ=1, then we obtain the classic PID controller. If ζ =0, a PI controller is obtained.

The control input using a FPID is given by

$$u(t) = -k_{\mathrm{p}}\mathbf{q}_e - k_{\mathrm{i}} I^{-\xi}\mathbf{q}_{\mathrm{e}} - k_{\mathrm{d}} D^{\zeta}\boldsymbol{\omega}_e \tag{6.18}$$

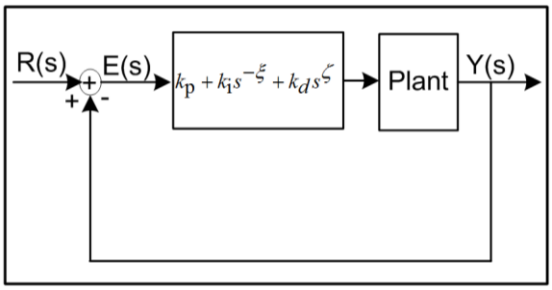

Fig. 6.3. Block diagram of a FPID controller with unity feedback.

Figure 6.3 shows a graphical representation of a FPID controller acting on a plant.

6.4 Simulation Results

These tests evaluate the ability of the different controllers to converge to the desired reference input. Based on the dynamics model introduced in (6.3), two different controllers have to be implemented. The first controller is optimized to control the pitch angle, while the second one adjusts the roll/yaw angles.

The transfer function describing the pitch angle is given by

$$\mathrm{T}_1(s) = \frac{1.3695\times10^{-3}}{s^2 - 5.3044\times10^{-10}} \tag{6.19a}$$

and the transfer function for the roll/yaw angles can be expressed using

$$T_2(s) = \frac{0.0002653s^2 - 1.19\times10^{-6}s - 8.995\times10^{-11}}{s^4 + 6.421\times10^{-19}s^3 + 0.0001827s^2 + 7.768\times10^{-23}s + 1.232\times10^{-13}} \tag{6.19b}$$

6.4.1 PID Controller

The first controller is designed to adjust the pitch angle optimally. The IPID controller was tuned after several iterations and the final parameters are shown in Table 6.1. One can observe that the contribution of the integer term is very small compared to the derivative and the proportional terms. Figure 6.4(a) shows the step response of the IPID controller implemented.

The simulation results indicate an 8% overshoot with a settling time of 170 sec. Furthermore, the steady-state error is less than 1%. This controller suffers from a long settling time, which will result in a long activation of the torque rods before generating the wanted actuation. Such behaviour would result in power wastage, as well as extra disturbances to the satellite. Consequently, a FPID controller is evaluated to adjust for the pitch angle. The tuning parameters are shown in Table 6.1.

The FPID controller provides a relatively better performance as illustrated in Figure 6.4(b). The settling time was reduced considerably. In fact, the transient response does not last more than 38 sec. However, the main limitation of this controller is related to its larger overshoot (17%). This comparison illustrates the relative merits of FPIDs over integer ones. This comparison constitutes one side of the answer only. The complete answer regarding the overall performance of such controllers has to be supported by an

analysis in the frequency-domain. For instance, using bode plots the sensitivity to noise and the distortion of the phase can be studied.

The frequency analysis is shown in Figure 6.5(a) and Figure 6.5(b) for the integer and fractional PID, respectively. A bode plot provides the frequency response of a linear time invariant system. These results consist of the frequency response gain and shift. They indicate that the IPID will be more sensitive to high frequency noise as compared to the FPID (18 dB/dec for the IPID and 5 dB/dec for the FPID). Additionally, a higher phase shift is experienced, when the frequency increases (17deg/dec for the IPID and 13deg/dec for the FPID).

Based on these results, the FPID is more robust than the IPID. Consequently, the FPID is used to control the pitch angle of the satellite. A summary of the comparison between each controller is shown in Table 6.2.

Table 6.1: Tuning parameters for IPID and FPID pitch controllers.

Parameters	k_p	k_i	k_d	ζ	ξ
IPID	0.70	9×10^{-5}	29	1	1
FPID	0.70	9×10^{-5}	50	0.6	0.9

Table 6.2: Summary of the comparison between IPID and FPID pitch controllers.

Parameters	Overshoot [%]	Transient Response [Sec]	Steady-State Error [%]	Frequency Response Gain [dB/Dec]	Phase Shift [Deg/Dec]
IPID	8	170	1	18	17
FPID	17	38	<1	5	13

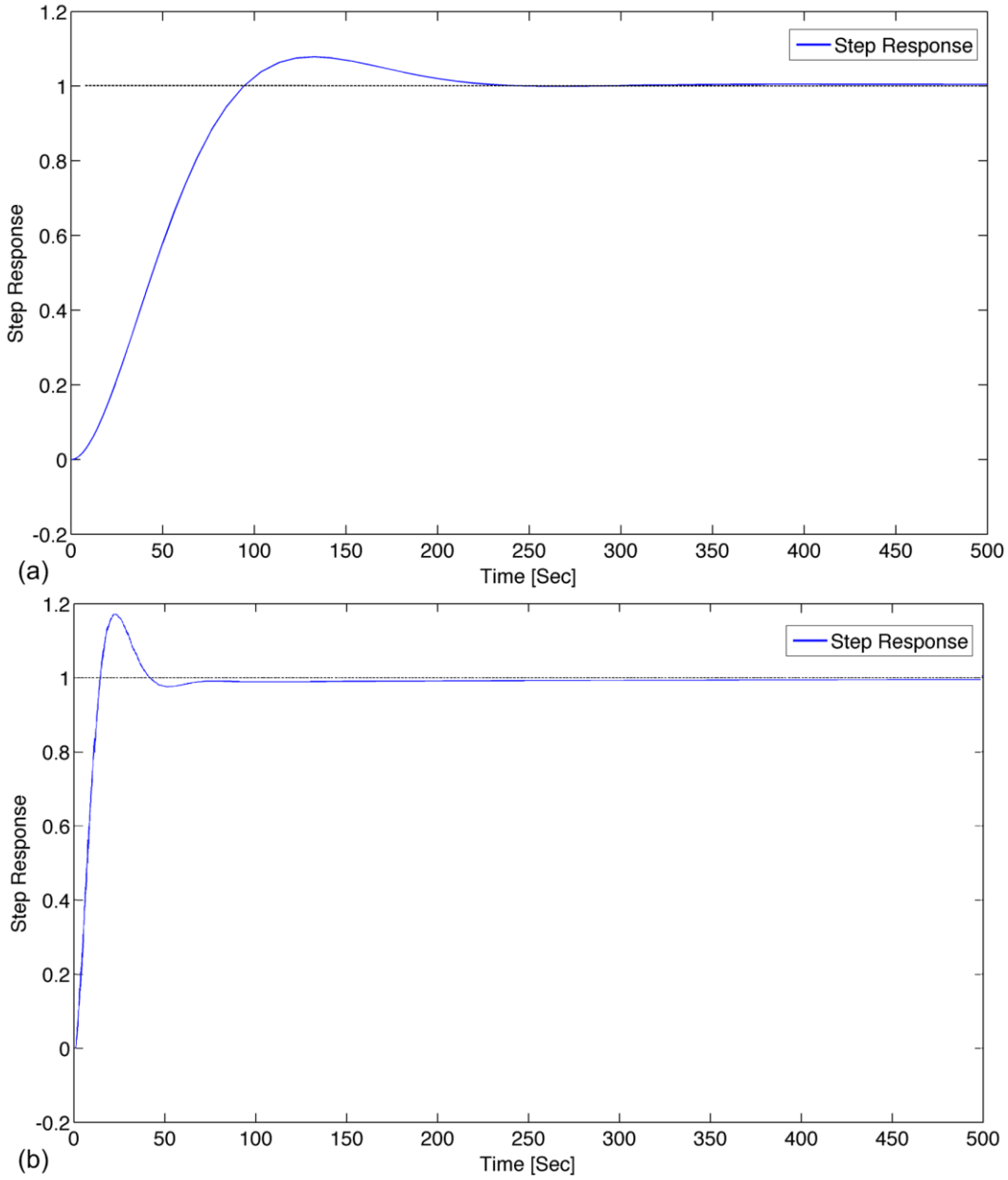

Fig. 6.4. Step response for the pitch controller. (a) IPID and (b) FPID controllers.

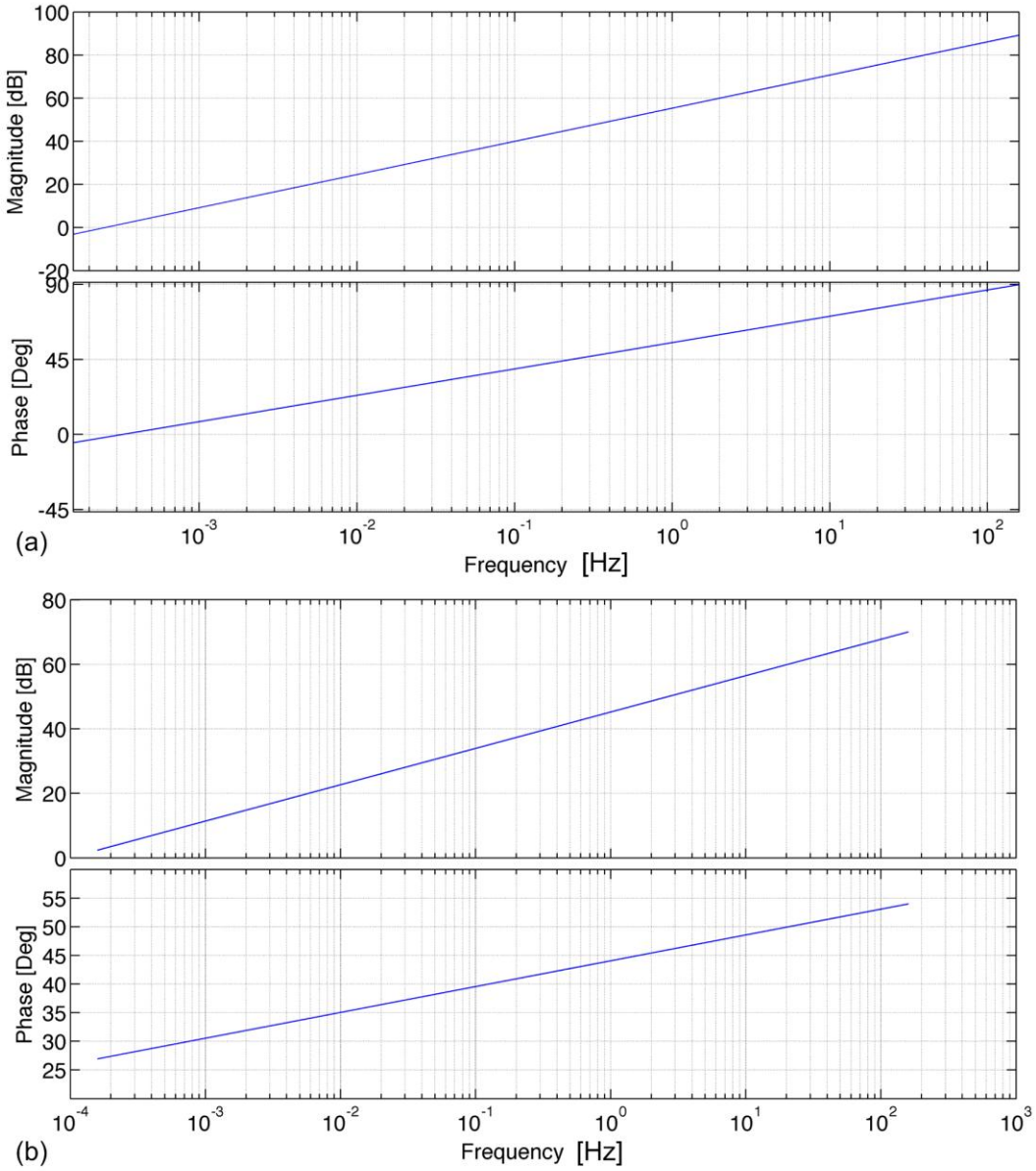

Fig. 6.5. Bode plots for (a) IPID and (b) FPID controllers.

In order to adjust for the roll/yaw angles another controller has to be designed. This controller is optimized by considering a plant described by (6.19b). Similarly both of the PID controllers are evaluated. The tuning parameters are provided in Table 6.3 and results presented in Figure 6.6.

A visual inspection of the results indicates that the IPID suffers from a large overshoot, settling time, and steady-state error as compared to the fractional one. The FPID exhibits a settling time of 53 sec (205 sec for the IPID), a 5% overshoot (44% for the IPID), and a steady-state error of 2% (7% for the IPID). Furthermore, a frequency analysis of both controllers reinforces the robustness of the FPID, as seen for the pitch controller. More specifically, the frequency gain is 12 dB/dec and 9 dB/dec with a phase shift of 15 deg/dec and 8 deg/dec for the integer-order and fractional-order PID controllers, respectively. A summary of this comparison is provided in Table 6.4.

Table 6.3: Tuning parameters for IPID and FPID roll/yaw controllers.

Parameters	k_p	k_i	k_d	ζ	ξ
Integer PID	10.619	8.09×10^{-9}	80	1	1
Fractional PID	18	8.09	350	0.6	0.7

Table 6.4: Summary of the comparison between FPID and IPID roll/yaw controllers.

Parameters	Overshoot [%]	Transient Response [Sec]	Steady-State Error [%]	Frequency Response Gain [dB/Dec]	Phase Shift [Deg/Dec]
IPID	44	205	2	12	15
FPID	5	53	7	9	8

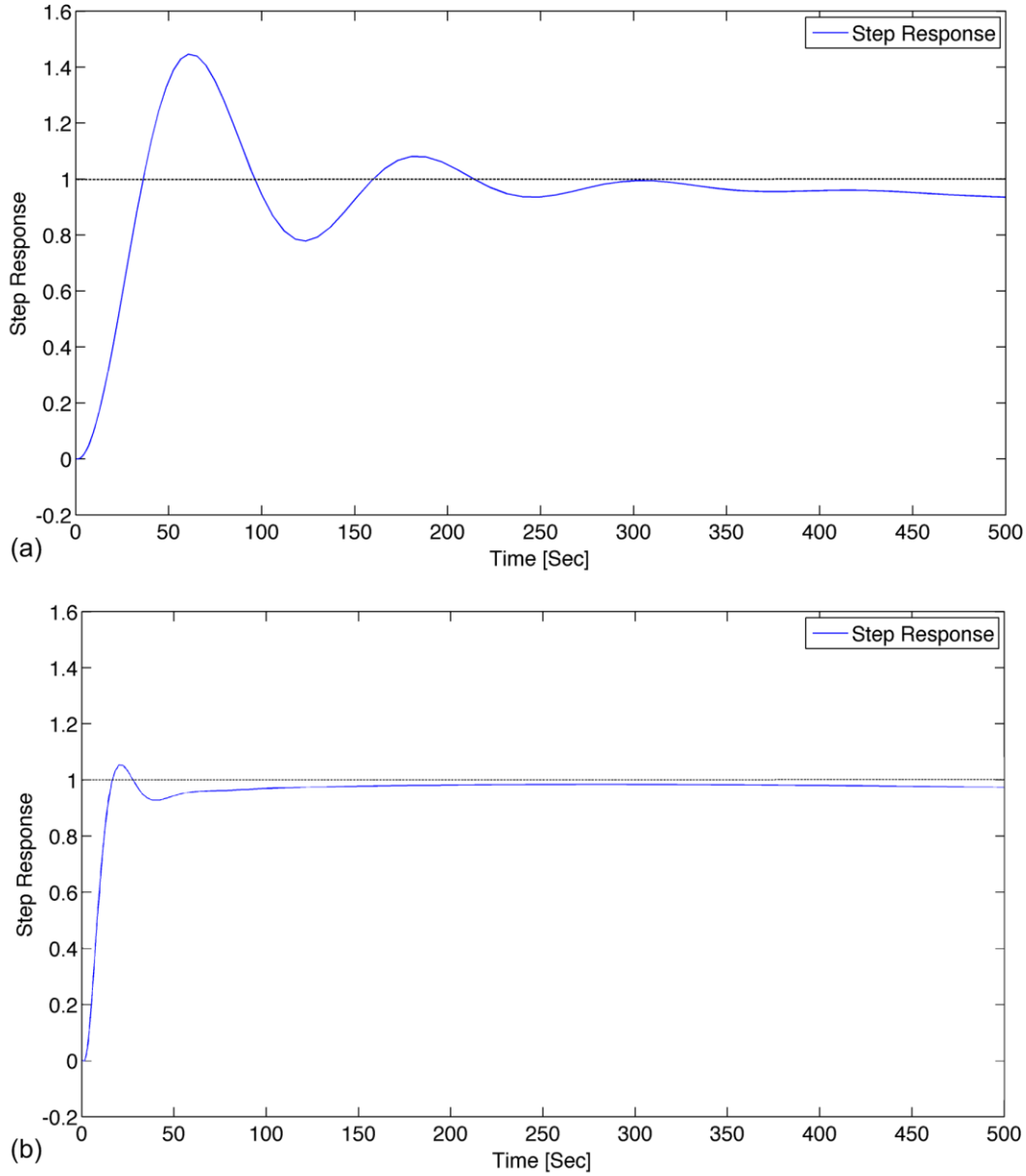

Fig. 6.6. Step response for the roll/ yaw controller. (a) IPID and (b) FPID controllers.

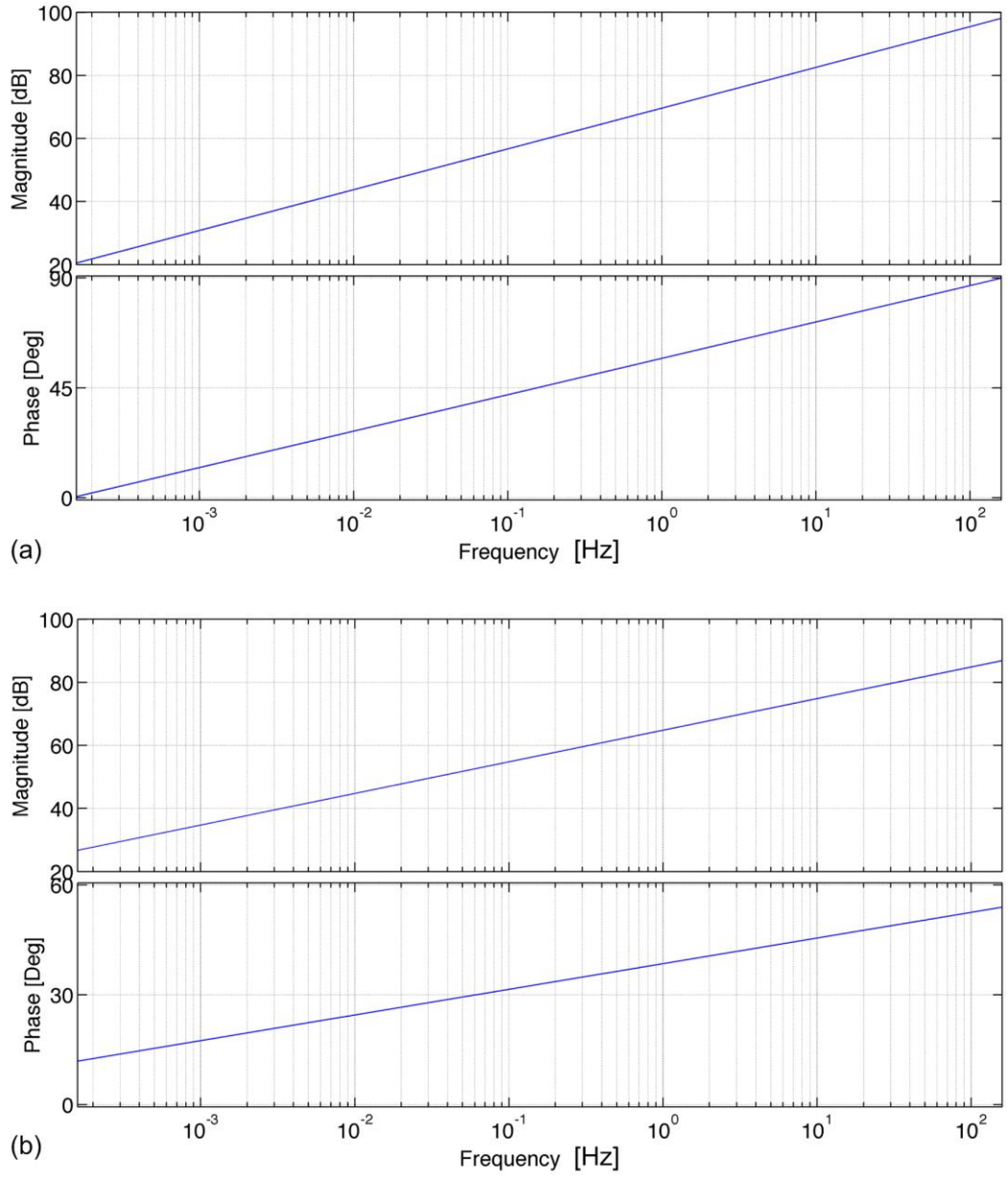

Fig. 6.7. Bode plot for (a) IPID and (b) FPID controllers.

Based on the comparison (summarized in Table 6.4), the FPID provides a better performance. This performance is not as optimal as the one obtained for the pitch controller (specifically for the settling time). Therefore, can an alternative type of controller (such fuzzy controller) provide a more attractive response?

6.4.2 Fuzzy Controller

As described in Section 6.3.2, a fuzzy algorithm was implemented in order to adjust for the roll/yaw angles. The results are shown in Figure 6.8.

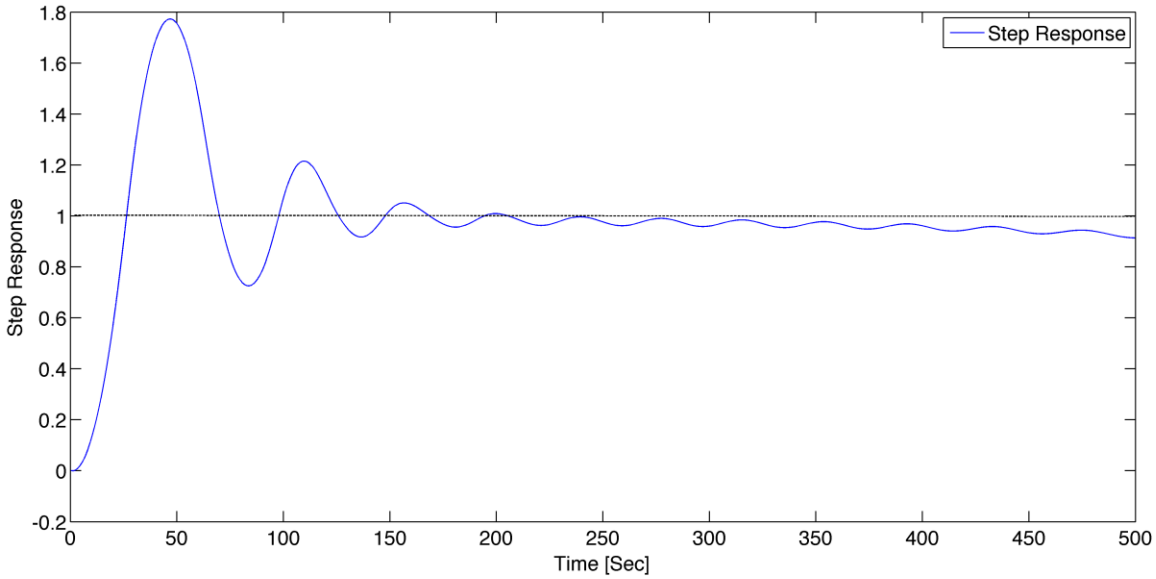

Fig. 6.8. Step response for the roll/yaw fuzzy controller.

Fuzzy controller performs relatively better than the IPID controller. However, it suffers from a large overshoot (75%); yet, the transient response has been reduced to 150 sec with a steady-state error of 5%. The transient response in this specific comparison constitutes the most desirable characteristic since it allows for an important power savings throughout the entire attitude control process.

One can notice that this controller does not provide a better performance than the FPID. Moreover, it exhibits an oscillatory behaviour with a diverging trajectory over time.

6.5 Observations and Discussions

Our main quest throughout this chapter was to design an optimal controller to correct for the orientation of the satellite by actuating the magnetic torque rods, while tackling one of the most severe limitations that small satellites suffer from; that is, the limitation in power. The main objectives were to minimize: (i) the overshoot, (ii) the settling time, (iii) the transient response, and (iv) the steady-state error.

Based on these requirements, the FPID controller exhibits the best performance as indicated in Tables 6.2 and 6.4. Moreover, the frequency analysis of the PID controllers has proved the relative robustness of the fractional-order controller as compared to the integer one. As a matter of fact, it exhibits a lower phase shift, which will result in less distorted output as compared to the input. Also, the gain is smaller as the frequency increases. This implies that high frequency noise will not impact the fractional-order PID as it would happen for the IPID. Finally, the FPID was compared to a fuzzy controller, as well. This comparison reinforced the relative merits and strengths of a FPID.

6.6 Summary

This chapter discussed the design of an optimal controller for the roll, pitch, and yaw angles. The dynamics model indicated that the roll and yaw angles follow the same evo-

lution in time, unlike the pitch angle. Consequently, two controllers have been implemented and optimized independently. Simulation results have shown that the FPID controller performs optimally in both cases, as compared to the IPID and fuzzy controllers.

Chapter 7

CONCLUSIONS

7.1 Overview

This thesis introduced an improved approach for the purpose of attitude determination and control. The attitude determination algorithm relies on a fuzzy approach in order to estimate the current error in the attitude, as well as a gradient decent approach to refine the locations of the membership functions. This work was motivated by the evaluation of the different deterministic algorithms (TRIAD, QUEST, and extended QUEST) and stochastic ones (EKF and UKF) described in Chapter 3. These approaches exhibit inherent pitfalls that were extracted through a numerical analysis in Chapter 4. For example, deterministic algorithms suffer from a lack of probabilistic significance and sensitivity to noisy measurements. On the other hand, stochastic algorithms are sensitive to initial conditions and subjected to divergence problems. In addition to these algorithmic pitfalls, the computational complexity represents an important factor in carrying this work.

The suggested solution illustrates attractive properties that were mutually exclusive to either deterministic or stochastic approaches. The new developed approach was able to

reconcile their advantages (such as robustness to noisy measurements, errors in the initial conditions, and a minimum steady-state error). Moreover, their respective limitations were minimized (*e.g.*, high computational cost and long convergence rate). As a result, the Delta-Fuzzy algorithm developed can recover in less than two minutes from large initial errors with an average pointing accuracy of 1.7 deg. Furthermore, it is more robust to large errors in the initial conditions, as well as to measurements corrupted with a significant level of WGN. Additionally, its performance does not deteriorate when the angle between the Earth magnetic field and the sun measured data is small.

The validation of the Delta-Fuzzy algorithm was conducted through different experiments that were established to test for the performance measures and the limitations of current approaches. In order to set certain thresholds for the initial error in the attitude and the added WGN to the measurements, the performance of current algorithms was used as a reference. The rationale behind such decision relates to the fact that these algorithms are used in industry and real-life space mission as indicated throughout this thesis.

This thesis addressed the design of an optimal control scheme to correct for the error in the relative orientation of the spacecraft. The optimal design was selected after the evaluation of different control schemes such as fuzzy, IPID, and FPID controllers as shown in Chapter 6. The introduction of a PID controller based on fractional calculus has provided an additional flexibility and a more expressive power. The evaluation conducted in the time domain provided measures such as overshoot, transient response, and steady-state error. The other evaluation conducted in the frequency domain was an indicator of the controller robustness based on the sensitivity to high frequency noise and distortion in

the phase. These evaluations resulted in the selection of a FPID controller to adjust for both of the pitch and roll/yaw angles.

7.2 Answers to the Research Questions Addressed

The thesis has raised several interesting research questions about the attitude determination and control for small satellites, as outlined in Section 1.2.3. This section links the results and observations to the research questions to provide insight into the answers and potential future research.

This work presented standard and state-of-the-art approaches for the purpose of attitude determination developed throughout the last 50 years. These approaches encompass deterministic and stochastic algorithms introduced in Chapter 3. Their study indicated that they are costly in time and space, as well as other inherent pitfalls. Also, knowing the different reference models needed, it might not be possible to rely on a single computing unit.

The EKF has shown very attractive characteristics when applied for the purpose of attitude determination. Such characteristics include: (i) very high pointing accuracy, (ii) robustness to noisy measurements, and (iii) the need of one measurement from the past only. These three main reasons constitute the main advantages of using the EKF for the purpose of orbital guidance and navigation.

The formulations of the different KFs (the EKF and UKF) allows for the study of their ability to deal with uncertainty in a dynamical non-stationary process. KFs can be applied to stationary, as well as non-stationary processes; yet, they are optimal for Gaussian processes only. As a result, Kalman filters cannot deal optimally with dynamical sys-

tems (which are characterized by power-law relationships). Finally, a visual inspection of the simulation results demonstrates the limitations of the filters to deal with epistemic uncertainty. For example, when an uncertainty related to the initial conditions (*e.g.*, the initial attitude) arises the filters' performance is affected directly. This can be observed through the deterioration of the performance, as well as a diverging behaviour of the estimation process.

Based on the different pitfalls of KFs (which are based on a probabilistic approach), several limitations have been identified. First, probabilistic approaches require the identification and specification of the exact PDF describing the process and measurement models. Additionally, the a priori PDF is required also. Such requirements are extremely difficult to satisfy, specifically for the space environment since it is ill-defined. For instance, initial conditions of the spacecraft after being released from the P-POD (*e.g.*, tumbling rate) are unknown. Such characteristics make it difficult for any probabilistic approach to perform optimally. These limitations were addressed and resolved through the use of a possibilistic approach (fuzzy logic). The main attribute of fuzzy logic is that they do not require the definition of any PDF. Furthermore, they provide a means to establish a new paradigm of computing; that is, computing with words. Such paradigm allows the applicability of an expert knowledge to the problem at hand.

Fuzzy and rough sets are based on possibility theory. Unlike probability analysis, possibility theory relies on two measures, namely (i) possibility and (ii) necessity for a better reasoning under uncertainty. As a result, a granule-based type of computing can be utilized. This computing requires the definition of MFs, which will establish the granulation of data. Based on the characteristics needed, different MFs are available as discussed

in Section 5.3.1. Once the MFs have been selected, different techniques can be used to define the optimality of the structures and configurations of data granules. Among these techniques, gradient decent optimization scheme is found. The highlight of this scheme is its low computational cost; yet, very effective to converge to an optimal solution. This technique has been used for the implementation of the Delta-Fuzzy algorithm in Section 5.5.1 showing a promising performance. As a result, a computationally efficient algorithm based on a FIS was implemented.

Other important questions addressed in this thesis are related to the power consumption associated with the actuators. An optimal control scheme has been defined as the one that minimizes the overshoot, time delay, transient response, and steady-state error in the time-domain. Also, a robust controlling scheme has to be characterized by a low sensitivity to high frequency noise and a low phase distortion in the frequency domain. These questions lead to the evaluation of three different controllers based on fuzzy logic, integer and fractional calculus. The evaluation of these controllers showed that a fractional-order proportional integral derivative controller has the unique capability of exhibiting the characteristics of an optimal control scheme. This is due to relative merits of fractional calculus over the integer one. Fractional calculus provides unique dimensions that did not exist with integer calculus; it possesses the unique ability to adjust the order of the integral and derivative operator.

7.3 Contributions and Main Findings

This thesis contributes to the knowledge of current small satellites attitude determination algorithms and control, as well as suggests an improved approach based on a granule-based computing for the purpose of estimating the attitude. The main contributions are:

1. The evaluation of current deterministic and stochastic algorithms under one umbrella and using a unified notation. This thesis provides uniquely three different deterministic and two stochastic algorithms for the purpose of orbital guidance. Furthermore, a detailed comparison that encompasses the algorithms formulation and their respective computational cost is presented;
2. For the first time, questions regarding the application of stochastic approaches (such as KFs) for pico- and nano-satellites due to their stringent limitations have been raised. Professor Witold Kinsner initiated these deep questions due to the algorithmic formulation of the EKF. In particular, the assumption of a Gaussian distribution of the space environment can no longer be valid. Consequently, another estimator based on alternative approaches has to be developed;
3. The novelty in this thesis encompass the development of an improved algorithm to estimate the relative orientation of the spacecraft based on a granule-based type of computing with a gradient decent optimization technique to refine the bounds of the MFs. This algorithm constitutes a novel approach to conduct attitude determination that has never been presented in published literature to the best of my knowledge. The suggested solution is computationally efficient and relies on the Earth magnetic field only with the unique ability of tracking the changes in the environment by updating the MFs.

Moreover, this algorithm is not only applicable to small satellites, but can also be used for larger spacecraft;

4. This thesis addressed for the first time the limitations in volume and power. In order to deal with these limitations, a comparison between fuzzy, integer-order, and fractional-order controllers was discussed. This comparison was conducted in time- and frequency-domains allowing for the identification of a robust control scheme for small satellites. As a result, two FPID controllers were designed to adjust for the pitch and roll/yaw angles providing a critical response with a low high-frequency noise sensitivity and phase shift distortion; and
5. Finally, the relative merits of fractional calculus over integer ones have been addressed for this specific application. Fractional calculus provides an extra flexibility to adjust the order of the integral and derivative operator to the dynamical process leading to an optimal response. Such performance could not be achieved by a fuzzy or an integer-order PID controller.

7.4 Limitations and Future Work

This humble work addressed one of the most challenging problems pico- and nano-satellites are facing nowadays. This problem has been tackled from all its angles; yet, some limitations are still present. These limitations can be summarized as follows:

1. The Delta-Fuzzy algorithm suffers from a constant error through the entire estimation process. This error has to be cancelled out without affecting the estimation process due to its nonlinear and non-convex nature. Consequently, the FIS used might be redefined or another granulation technique should be used; and

2. The control scheme relies on two FPID controllers. An important computational cost would be saved, if these controllers were combined to constitute one controller for the three angles.

References

[Abra91] Bruce Abramson, "ARCO1: An application of belief networks to the oil market," *Proc. of the Seventh Conf. on Uncertainty in Artificial Intelligence*, (Los Angeles, CA; Jul 13-15, 1991), pp. 1-8, 1991.

[AsAn12] Amirhossein Asadabadi and Amir Anvar, "Small satellite modeling and attitude *control* using fuzzy logic," *in World Academy of Science, Engineering and Technology*, vol. 72, 14-17, 2012.

[Aure12] Jacoba Auret, *Design of an Aerodynamic Attitude Control System for a CubeSat*. M.Sc. Thesis. Department of Electrical and Electronic Engineering, University of Stellenbosch, South Africa, March 2012, 110 pp.

[Bar96] Itzhack Y. Bar-Itzhack, "REQUEST- A recursive QUEST algorithm for sequential attitude determination," *in Journal of Guidance, Control, and Dynamics*, vol. 19, no. 5, pp. 1034-1038, 1996.

[BeMF07] Abdelaziz Benallegue, Abdellah Mokhtari, and Leonid Fridman, "High-order sliding mode observer for a quadrotor UAV," *in Intern. Journal of Robust and Nonlinear Control*, pp. 1- 4, 2008.

[BhDh03] Sanjay P. Bhat and Ajit S. Dham, "Controllability of spacecraft attitude under magnetic actuation," *Proc. 42nd IEEE Conf. on Decision and Control*, (Maui, USA; December, 2003), pp. 2383-2388, 2003.

[Blac64] H. D. Black, "A passive system for determining the attitude of a satellite," *in AIAA Journal*, vol. 2, pp. 1350–1351, July 1964.

[BoCh85] Stephen Boyd and Leon O. Chua, "Fading memory and the problem of approximating nonlinear operators with Volterra series," in *IEEE Trans. on Circuits and Systems*, vol. 32, no. 11, November 1985.

[BoVa04] Stephen Boyd and Lieven Vandenberghe, *Convex Optimization.* UK: Cambridge University Press, 2004, 727 pp. {ISBN-13: 978-0521833783}

[ChBO04] Daniel Choukroun, I. Y. Bar-Itzhack, and Y. Oshman, "Optimal-REQUEST algorithm for attitude determination," *in Journal of Guidance, Control, and Dynamics*, vol. 27, no. 3, pp. 418-425, 2004.

[Chia94] Richard Y. Chiang and Jyh-Shing Roger Jang, "Fuzzy logic attitude control for Cassini spacecraft," *Proc. 3rd IEEE Conf. on Computational Intelligence and Fuzzy Systems*, (Orlando, FL; June 26-29, 1994), pp. 1532-1537, 1994.

[ChKi07] Yee-Jin Cheon and Jong-Hwan Kim, "Unscented filtering in a unit quaternion space for spacecraft attitude determination," *Proc. of the IEEE Intern. Symposium Industrial Electronics*, (Vigo, Spain; June 04-07, 2007), pp. 66-71, 2007.

[Chou03] Daniel Choukroun, *Novel Methods for Attitude Determination Using Vector* Observations. Ph.D. Thesis. Israel Institute of Technology, Haifa, Israel, May 2003, 309 pp.

[CPKM03] Young-Keung Chang, Je-Hong Park, Young-Hyun Kim, Byoung-Young, and Myung-Il Min, "Design and development of HAUSAT-1 picosatellite system (CubeSat)", *Proc. of the intern. Conf. on Recent Advances in Space Technologies*, (Istanbul, Turkey; November, 2003), pp. 47-54, 2003.

[CrMa82] John Crassidis and Francis Landis Markley, "Unscented filtering for spacecraft attitude estimation," *in AIAA Journal of Guidance, Control, and Dynamics*, vol. 26, no. 4, pp. 536-542, July-Aug. 1982.

[CrMa96] J. L. Crassidis and F. L. Markley, "Attitude estimation using modified Rodrigues parameters," *Proc. of the Flight Mechanics/Estimation Theory Symposium*, NASA-Goddard Space Flight Center, Greenbelt, MD, May 1996, pp. 71-83.

[CrMC07] J. L. Crassidis, F. L. Markley, and Y. Cheng, "Survey of nonlinear attitude estimation methods," *in AIAA Journal of Guidance, Control and Dynamics*, vol. 30, no. 1, pp. 12–28, 2007.

[DDTA12] Arash Fazel-Darbandi, Jesse Doerksen, Jason Tayler, Udeesha Annakkage, Kasun Samarasekera, Mohammad Reza Fazel Darbandi, Pawel Glowacki, Dario Schor, Witold Kinsner, Diane Kotelko, Philip Ferguson, David Weber, and Samuel Kovnats, "Design and implementation of a power subsystem ," *Proc. of the 16th CASI Astronautics Conf.*, ASTRO12, (Quebec, Canada; April 24-26, 2012).

[Dieb06] James Diebel, *Representing Attitude: Euler Angles, Unit Quaternions, and Rotation Vectors*, Technical Report. USA: Stanford University, October 2006, 35 pp.

[DuKu13] Lakshmi S. Dutt and Mathew Kurian, "Handling of uncertainty- A survey," *in Intern. Journal of Scientific and Research Publications*, vol. 3, no. 1, pp. 1-3, 2013.

[EsVW06] Jairo Espinosa, Joos Vandewalle, and Vincent Wertz, *Fuzzy Logic, Identification and Predictive Control*. New York, NY: Springer, 2006, 273 pp. {ISBN 1846280877}.

[Garm05] Luis Garmendia, "The evolution of the concept of fuzzy measure," *in Studies in Computational Intelligence and Intelligent Data Mining*, vol. 5, pp. 185-200, 2005.

[Geoc09] Geocentrix Technologies Ltd., H.R. MacMillan Space Centre, and Jaymie M. *Matthews*, "A proposal to initiate a satellite design challenge for Canadian universities," Vancouver, BC: Geocentrix, January 13, 2009.

[Ghuf09] Sajid Ghuffar, *Design and Implementation of Attitude Determination Algorithm for the Cubesat UWE-3*. M.Sc. Thesis. Lulea University of Technology, Kiruna, Sweden, October 2009, 89 pp.

[Gold04] Eric Siome Klein Goldenstein, "A gentle introduction to predictive filters*," Revista de Informatica Teórica e Aplicada*, vol. 11, no.1, pp. 63-91, 2004.

[GrAn10] Mohinder S. Grewal and Angus P. Andrews, "Applications of Kalman filtering in *aerospace* 1960 to the present," *in IEEE Control Systems.*, vol. 30, no. 3, pp. 69-78, June 2010.

[Greg04] Bryan S. Gregory, *Attitude Control System Design for ION, The Illinois Observing Nanosatellite*. M.Sc. Thesis. University of Illinois, Urbana, Illinois, USA, 2004, 111 pp.

[Hone03] Honeywell, *Advanced Process Manager Control Functions and Algorithms*. Phoenix, AZ: Honeywell International Process Solutions, AP09-600 Release 650, December 5, 2003, 370 pp.

[HoRo80] Felix R. Hoots and Ronald L. Roehrich, *Models for Propagation of NOARD Elements Sets*, Technical Report. Aerospace Defense Center, 1980, 91 pp.

[HSAD98] L. Hongre, P. Sailhac, M. Alexandresca, and J. Dubois, "Nonlinear and mulitfractal approaches of the geomagnetic field," *Physics of the Earth and Planetary Interiors*, vol. 110, no. 1999, pp. 157-190, Sept. 1998.

[Jang93] Jyh-Shing Roger Jang, " ANFIS: Adaptive-network-based fuzzy inference system," in *IEEE Trans. Systems, Man, and Cybernetics*, vol. 23, no. 3, pp. 665-685, 1993

[JeVi10] Kasper Fuglsang Jensen and Kasper Vinther, *Attitude Determination and Control System for AAUSAT3*. M.Sc. Thesis. Department of Electronic Systems and Intelligent Autonomous Systems, Aalborg University, Danemark, June 2010, 224 pp.

[Juli02] Simon. Julier, "The scaled unscented transformation," *Proc. of the American Control Conf.*, vol. 6, pp. 4555-4559, 2002.

[JuUW95] Simon Julier, Jeffrey K. Uhlmann, and Hugh F. Durrant Whyte, "A new approach for filtering nonlinear systems," *Proc. of the American Control Conf.*, (Seatle, Washington; June 21-23, 1995), pp. 1628-1632, 1995.

[Kana91] Keiji Kanazawa, "A logic and time nets for probabilistic inference," *Proc. of the 10th National Conf. Artificial Intelligence* (AAAI), pp. 360-365, 1991.

[KaSG05] Rickard Karlsson, Thomas Schon, and Fredrick Gustafsson, "Complexity analysis of the marginalized particle filter," *in IEEE Trans. in Signal Processing,* vol. 53, no. 11, pp. 4408-4411, November 2005.

[Keat77] James E. Keat, *Analysis of Least-squares Determination Routine DOAOP,* Technical Report. Greenbelt, Maryland: Goddard Space Flight Center, National Aeronautics and Space Administration, 1977, 118 pp.

[Kins04] Witold Kinsner, "Is entropy suitable to characterize data signals for cognitive informatics?," *Proc. of the 3rd IEEE Intern. Conf. on Cognitive Informatics*, pp. 6-21, 2004.

[Kins07] W. Kinsner, "Challenges in the design of adaptive, intelligent and cognitive systems," *Proc. of the Sixth IEEE Intern. Conf. on Cognitive Informatics,* pp. 13-25, 2007.

[Kins09] W. Kinsner, *Fractal and Chaos Engineering*. Course Notes; Winnipeg MB; University of Manitoba, 2009, 900 pp.

[Kins10] W. Kinsner, *Switching and Automata Theory*. Course Notes; Winnipeg MB; University of Manitoba, 2010, 874 pp.

[KMAC04] A. Kailil, N. Mrani, M. Abid, S. Choukri, M. Mliha Touati, and N. Elalami, "Fractional regulators for spacecraft attitude stabilization," *in the* 22nd *AIAA Intern. Of Communications Satellite Systems Conf. and Exhibit*, (Monterey, California; May 9-12, 2004), pp. 1-11, 2004.

[KoDj03] Jayesh H. Kotecha and Petar M. Djuric, "Gaussian particle filtering," *in IEEE Trans. in Signal Processing*, vol. 51, no. 10, pp. 2592-2601, Oct. 2003.

[KSFC12] Witold Kinsner, Dario Schor, Mohammad Reza Fazel-Darbandi, Brendan Cade, Kane Anderson, Cody Friesen, Diane Kotelko, and Philip Ferguson, "The T-Sat1 nanosatellite

team of teams," *Proc. of the 11th IEEE Intern. Conf. on Cognitive Informatics and Cognitive Computing*, ICCI*CC 2012, (Kyoto, Japan; August 22-24, 2012), Paper 190, 2012.

[KuCa04] Jayant Kulkarni and Mark Campbell, "An approach to magnetic toque attitude control of satellites via 'H_∞' control for LTV systems," 43rd *IEEE Conf. on Decision and Control,* (Atlantis, Bahamas; December 14-17, 2004), pp. 273-277, 2004.

[KuTB09] K.D. Kumar, M. J. Tahk, and H. C. Bang, "Satellite attitude stabilization using solar radiation pressure and magnetotorquer," *in Journal of the Control Engineering Practice,* vol. 17, pp. 267-279, 2009.

[KYKY92] Takayasu Kasahara, Naoyuki Yamada, Yasuhiro Kobayashi, Katsuyuki Yoshino, and Kikuo Yoshimura, "Domain model for constructing a knowledge based system," *Proc. of the Fourth Intern. Conf. Tools with Artificial Intelligence*, (Arlington, VA; Nov 10-13, 1992), pp.467-468, November 1992.

[LaLe01] Kathryn B. Laskey and Tod S. Levitt, "Artificial intelligence: Uncertainty," *in Intern. Encyclopedia of the Social and Behavioural Sciences. Oxford, U.K.: Elsevier*, pp. 799-805, 2001.

[LeBS06] Zs. Lendek, R. Babuska, and B. De Schutter, *State Estimation under Uncertainty: A Survey*, Technical Report. Delft University of Technology: Delft Center for Systems and Control, February 2006, 73 pp.

[Lee90] Chuen Chien Lee, "Fuzzy logic in control systems: Fuzzy logic controller– part1," *in IEEE Trans. on Systems, Man, and Cybernetics*, vol. 20, no. 2, March-April 1990.

[LeMS82] E. J. Lefferts, F. L. Markley, and M. D. Shuster, "Kalman filtering for spacecraft *attitude* estimation," *in Journal of Guidance, Control, and Dynamics*, vol. 5, no.5, pp. 417–429, Sept.-Oct. 1982.

[LiGL05] X. J. Liu, P. Guan, and J. Z. Liu, "Fuzzy sliding mode attitude control of satellite," *Proc. of the 44th IEEE Conf. on Decision and Control,* (Seville, Spain; December 12-15, 2005), pp. 1970-1975, 2005.

[LiLQ13] Guoping Lin, Jiye Liang, and Yuhua Qian, "Multigranulation rough sets: From *partition* to covering," *in Information Sciences*, vol. 241, pp. 101-118, 2013.

[LoMa06] Alejandro Aceves-Lopez and Joseph Aguilar-Martin, "A simplified version of Mamdani's fuzzy control: The natural logic controller," *in IEEE Trans. on Fuzzy Systems*, vol. 14, no. 1, February 2006.

[Love04] Adam Loverro, *Fractional Calculus: History, Definitions and Applications for the* Engineer, Technical Report. USA: Department of Aerospace and Mechanical Engineering, University of Notre Dame, May 8, 2005, 28 pp.

[MaAs75] E.H. Mamdani and S. Assillian, "An experiment in linguistic synthesis with a fuzzy logic controller," *in International Journal of Man-Machine Studies*, vol. 7, no. 1, pp. 1-13, 1975.

[MaCC05] F. Landis Markley, John L. Crassidis, and Yang Cheng, "Nonlinear attitude filtering methods," *in AIAA Guidance, Navigation and Control Conf. and Exhibit*, (San Francisco, California; August, 2005), 32 pp, 2005.

[Magn13] *Total Magnetic Field in Nano-Teslass*. 2013 (Available as of October 2013 from http://www.epa.gov/esd/cmb/GeophysicsWebsite/pages/references)

[MaMa05] Susan Macmillan and Stefan Maus, "International geomagnetic reference field-the tenth generation," *in Earth Planets Space*, vol. 57, pp. 1135-1140, May 2005.

[MaMo00] F. L. Markley and D. Mortari, "Quaternion attitude estimation using vector observations," *in Journal of the Astronautical Sciences*, vol. 58, no. 2/3, pp. 359-380, 2000.

[Mark03] F. Landis Markley, *Multiplicative vs. Additive Filtering for Spacecraft Attitude* Determination. Technical Report. Greenbelt, MD: NASA's Goddard Space Flight Center Minneapolis, 2003, 8 pp.

[MoMK09] Jan Mochnac, Stanislav Marchevsky, and Pavol Kocan, "Bayesian filtering techniques: Kalman and extended Kalman filter basics," *Proc. of the 19th Intern. Radio Electronika Conf.*, (Bratislava; Apr. 22-23, 2009), pp. 119-122, Apr. 2009.

[Mora12] Morteza Moradi, "Self-tunning PID controller to three-axis stabilization of a satellite with unknown parameters," *in The Intern. Journal of Nonlinear Mechanics,* vol. 49, pp. 50–56, September 2012.

[MTRH07] Anastasios I. Mourikis, Nikolas Trawny, Stergios I. Roumeliotis, Daniel M. Helmick, and L. Matthies, "Autonomous stair climbing for tracked robots," *in The Intern. Journal of Robotics Research,* vol. 26, no.7, pp. 737–758, July 2007.

[NaKi13] Mohamed Temam Nasri and Witold Kinsner, "Extended Kalman filtering for pico-satellites attitude determination," *Proc. of the IEEE Conf. on Electrical and Computer Engineering, CCECE 2013,* (Regina, SK; May 5-8, 2013), 5 pp., 2013. {IEEE CN CFP13758-USB; ISBN 978-1-4799-0032-9}.

[NaNa11] M. Navabi and N. Nasiri, "Simulating the Earth magnetic field according to the 10th generation of IGRF coefficients for spacecraft attitude control applications," *the* 5th *Intern. Conf. on Recent Advances in Space Technologies,* (Istanbul, Turkey; June 9-11, 2011), pp. 584-588, 2011.

[NVTK03] Ioannis K. Nikolos, Kimon P. Valavanis, Nikos C. Tsourveloudis, and Anargyros N. Kostaras, "Evolutionary algorithm based offline/online path planner for UAV navigation," *in IEEE Trans. On Systems, Man, and Cybernetic, Part B: Cybernetics*, vol. 33, no. 6, Dec. 2003.

[OrZF06] Omar Orqueda, Xi Zhang, and Rafael Fierro, "An output feedback nonlinear decentralized controller for unmanned vehicle coordination," *Proc. of the American Control Conf.*, (Minneapolis, USA; June 14-16, 2006), pp. 1442-1445, 2006.

[Ousa11] Hamed Shahmohamadi Ousaloo, "Attitude control of a small satellite with uncertainly dynamic model using fuzzy logic strategy," 2nd *Intern. Conf. Control, Instrumentation and Automation* (ICCIA), (Shiraz, Iran; December 27-29, 2011), pp. 68-73, 2011.

[Oust95] Alain Oustaloup, *La dérivation non entière: Théorie, synthèse et applications.* Hermes, Paris: Hermes Sciencec Publications, 1995, 508 pp. {ISBN: 978-2866014568}.

[Pawl91] Zdzislaw Pawlak, *Rough Sets: Theoretical Aspects of Reasoning about Data*. Netherlands: Kluwer Academic Publishers, 1991, 229 pp. {ISBN 0792314727}

[Pete98] Bertrand Petermann, *Attitude Control of Small Satellites Using Fuzzy Logic*. M.Sc. Thesis. McGill University, Montreal, Canada, 1997, 111 pp.

[PoDK97] Igor Podlubny, L. Dorcak, and I. Kostial, "On fractional derivatives, fractional-order dynamic systems and $P^{\lambda}I^{\mu}D$," *Proc. of the 36th IEEE Conf. on Decision and Control,* (San Diego, CA; December 1, 1997), pp. 4985-4990, 1997.

[Podl97] Igor Podlubny, *Fractional-Order Systems and Fractional-Order Controllers.* Kosice, Slovakia: Institute of Experimental Physics, Slovak Academy of Sciences, UEF-03-94, 1994.

[Psia01] Mark L. Psiaki, "Magnetic torquer attitude control via asymptotic periodic linear quadratic regulation," *in Journal of Guidance, Control, and Dynamics*, vol. 24, no.2, pp. 386-394, 2001.

[Psia10] Mark L. Psiaki, "Generalized Wahba problems for spinning spacecraft attitude and rate determination," in *Journal of the Astronautical Sciences,* vol. 57, no. 2, pp. 73-92, January- June 2010.

[PTVF07] William H. Press, Saul A. Teukolsky, William T. Vetterling, and Brian P. Flannery, *Numerical Recipes: The Art of Scientific Computing.* New York, NY: Cambridge University Press, 2007 (3rd ed.), 1256 pp.{ ISBN 0521880688}.

[RaSa96] D. H. Rao and S. S. Saraf, "Study of defuzzification methods of fuzzy logic controller for speed control of a DC motor," *Proc. of the 1996 Intern. Conf. on Power Electronics, Drives and Energy Systems for Industrial Growth*, (New Delhi; January 8-11, 1996), vol. 2, pp. 782-787, 1996.

[RCHB13] Brady Russell, Lee Clement, Joshua Hernandez, Ahmad Byagowi, Dario Schor, and Witold Kinsner, "Implementation of a nanosatellite attitude determination and control system for the T-Sat1 mission," *Proc. of the IEEE Conf. on Electrical and Computer Engineering, CCECE 2013*, (Regina, SK; May 5-8, 2013), 5 pp., 2013. {IEEE CN CFP13758-USB; ISBN 978-1-4799-0033-6}

[Rhin00] R. Russell Rhinehart, "The century's greatest contributions to control practice," in *ISA Trans.*, vol. 39, pp. 3-13, 2000.

[Rohd07] Jan Rohde, *Kalman filter for attitude determination of student satellite*. M.Sc. Thesis. Norwegian University of Science and Technology, Trondheim, Norway, July 2010, 96 pp.

[SAFG12] Dario Schor, Kane Anderson, Cody Friesen, Kris Goodmanson, Morgan May, Arash Fazel-Darbandi, Witold Kinsner, M.D. (Ron) Britton, and Malcolm Symonds, "Complex system design exposure through a satellite design competition," *Proc. of the Canadian Engineering Education Association Conf.* (CEEA 2012), (Winnipeg, MB, Canada; June 17–20, 2012), pp. 1-5, 2012.

[ScÖz94] D. A. Schoenwald and Ü Özgüner, "Robust stabilization of nonlinear systems with parametric uncertainty," *in IEEE Trans. on Automatic Control*, vol. 39, no. 8, August 1994.

[ShOh81] M. D. Shuster and S. D. Oh, “Three-axis attitude determination from vector observations,” *in Journal of Guidance and Control*, vol. 4, no. 1, pp. 70–77, January - February 1981.

[Shus89] Malcolm D. Shuster, “Maximum likelihood estimation of spacecraft attitude,” in Journal *of the Astronautical Sciences*, vol. 37, no. 1, pp. 79-88, January- March 1989.

[Shus93] Malcom D. Shuster, “A survey of attitude representations,” *in Journal of the* Astronautical *Sciences*, vol. 41, no. 4, pp. 439-517, 1993.

[SMSM00] R. Sterritt, A. H. Marshall, C. M. Shapcott, and S. I. McClean, “Exploring dynamic Bayesian belief networks for intelligent fault management systems,” *in Intern. IEEE Conf. onSyst., Man, and Cybern*., (Nashville, TN; Oct 08-11, 2000), vol. 5, no., pp.3646-3652, 2000.

[SRKB08] M. Schmidt, K. Ravandoor, O. Kurz, S. Busch, and K. Schilling, “Attitude determination for the pico-satellite UWE-2,” *Proc. of the* 17^{th} *World Congress of The Intern. Federation of Automatic* Control, (Seoul, South Korea; July 6-11, 2008), pp. 14036- 14041, 2008.

[TaSh07] Sergei Tanygin and Malcolm D. Shuster, “The many TRIAD algorithms,” *Proc. of the Advances Astronautical Sciences*, (Sedona, Arizona; January 28– February 2, 2007), vol. 127, pp. 81-99, 2007.

[TaSu85] Tomohiro Takagi and Michio Sugeno, “ Fuzzy identification of systems and its *applications* to modeling and control,” *in IEEE Trans. on Syst., Man, and Cybern.*, vol. SMC-15, no. 1, pp. 116-132, 1985.

[ThSh10] Purvesh Thakker and Wayne A. Shiroma (eds.), *Emergence of Pico- and Nanosatellites for Atmospheric Research and Technology Testing.* Reston, Virginia: American Institute of Aeronautics and Astronautics, 2010, 599 pp. {ISBN: 978-1-60086-768-2}

[TiVe06] Paul Tisa and Paul Vergez, *Performance Analysis of Control Algorithms for FalconSat-3*. Technical Report. Tampa, Florida: 16th AAS/AIAA Space Flight Mechanics Conf., January 22-26, 2006, 18 pp.

[TrRo05] Nikolas Trawny and Stergios I. Roumeliotis, *Indirect Kalman Filter for 3D Attitude Estimation*. Technical Report. Minneapolis, MN: Department of Computer Science and Engineering, University of Minnesota, 2005, 25 pp.

[ViVi12] Ramon Vilanova and Antonio Visioli (eds.), *PID Control in the Third Millennium.* New York, NY: Springer, 2012, 599 pp. {ISBN: 978-1-4471-2424-5}.

[WaCC09] Tzu-Hang Wang, Jing-Ying Chang, and Liang-Gee Chen, "Algorithm and architecture for object tracking using particle filter," *Proc. of the IEEE Intern. Conf. on Multimedia and Expo.*, (New York, NY; June 28-July 3, 2009), pp. 1347-1377, 2009.

[Wahb65] Grace Wahba, "A least squares estimate of satellite attitude," *in SIAM Review*, vol. 7, no. 3, pp. 409, July 1965.

[WaMe00] Eric A. Wan and Rudolph van der Merwe, "The unscented Kalman filter for nonlinear estimation," *Proc. of the IEEE Adaptive Systems for Signal Processing, Communications, and Control Symposium*, (Lake Louise, Alta.; Oct. 01-04, 2000), pp. 153-158, 2000.

[WaMe01] Eric Wan and Rudolph van der Merwe, *Kalman Filtering and Neural Networks*, New York, NY: John Wiley & Sons, 2001, 298 pp.

[Wats01] Kirby Michael Watson, Microdot, *a 4-Bit Synchronous Microcontroller for Space Applications*. M.Sc. Thesis. Department of Electrical and Computer Engineering, Air University, USA, March 2001, 171 pp.

[WeBi06] Greg Welch and Gary Bishop, *An Introduction to the Kalman Filter*, Technical Report. North Carolina: Department of Computer Science, University of North Carolina, 2006, 16 pp.

[WeLa99] James R. Wertz and Wiley J. Larson (eds.), *Space Mission Analysis and Design*. El Segundo, CA: Microcosm Press, 1999 (3rd ed.), 969 pp. {ISBN-10: 1-881883-10-8}

[WKYX11] Zhaowen Wang, Ercan E. Kuruoglu, Xiaokang Yang, Yi Xu, and Thomas S. Huang, "Time varying dynamic Bayesian network for nonstationary events modeling and online inference," *in IEEE Trans. on Signal Processing*, vol. 59, no. 4, pp. 1553-1568, 2011.

[Yage02] R. R. Yager, "Uncertainty representation using fuzzy measures," *in IEEE Trans. on Syst., Man, Cybern. B, Cybern.*, vol. 32, no. 1, pp. 10-23, Feb. 2002.

[Yao04] Y. Y. Yao, "Granular computing," *Proc. 4th Chinese National Conf. on Rough Sets and Soft Computing*, vol. 31, pp. 1-7, 2004.

[Yash98] Gregory Yashko, *Ion Micro-Propulsion and Cost Modeling for Satellite Clusters*. M.Sc. Thesis. Department of Aeronautics and Astronautics, Massachusetts Institute of Technology, United States of Americas, June 1998, 110 pp.

[Zade65] Lotfi A. Zadeh, "Fuzzy sets," in *Information Control*, vol. 8, no. 3, pp. 338-353, 1965.

[Zade96] L. A. Zadeh, "Fuzzy logic = Computing with words," *in IEEE Trans. on Fuzzy Systems*, vol. 4, no. 2, pp. 103-111, 1996.

[ZeKS03] Shannon Zelinski, John T. Koo, and Shankar Sastry, "Optimization-based formation reconfiguration planning for autonomous vehicles," *Proc. of the IEEE Intern. Conf. on Robotics and Automation*, (Taipei, Taiwan; September, 2003), pp. 3758-3763, 2003.

Appendix A

Software

This chapter provides a description of the attitude determination algorithms implemented in this thesis. The source code described in this appendix is included in the DVD uploaded on my MSpace under a folder entitled *AD_Algorithms*. Matlab 2010b or later is recommended for these applications.

A.1 Stochastic Algorithms

The extended and unscented Kalman filters algorithms were implemented based on the block diagram shown in Fig. A.1. The source code shares common functional blocks (such as the sensory measurements and reference models) and differs in the implementation of the Kalman filter algorithms only. The EKF is implemented as described in Table 4.7 and the UKF is based on Table 4.8. The Matlab file for the EKF and UKF are named *AD_EKF.m* and *AD_UKF.m*, respectively.

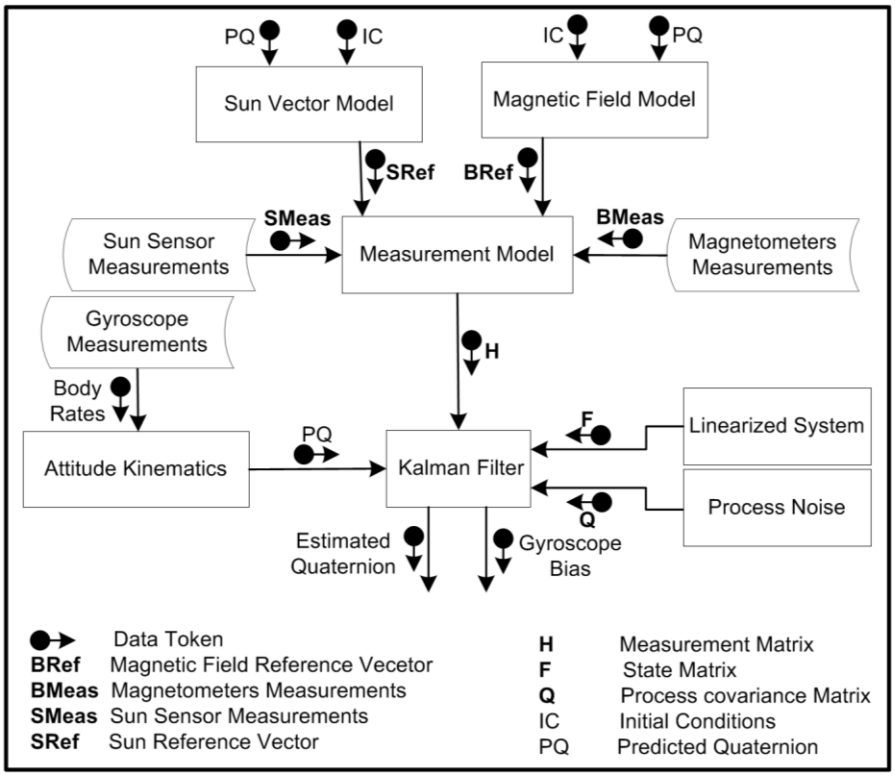

Fig. A.1. Block diagram of the Kalman filters software implementation.

A.2 Deterministic Algorithms

A.2.1 TRIAD Algorithm

The TRIAD algorithm was implemented based on the block diagram shown in Fig.A.2. The algorithm estimates the relative attitude as described in Table 4.1. The source code is found in *AD_TRIAD.m.*

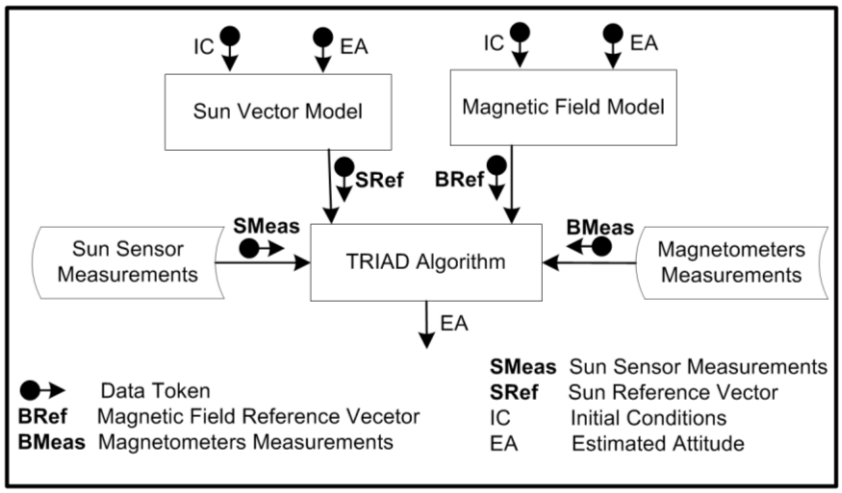

Fig. A.2. Block diagram of the TRIAD software implementation.

A.2.1 QUEST Algorithm

The QUEST implementation is similar to the TRIAD one from the perspective of the required functional blocks. The QUEST algorithm is based on Table 4.3. The source code of this algorithm is entitled *AD_QUEST.m*.

A.2.1 Extended QUEST Algorithm

Similar to Kalman filters, the extended QUEST estimates the attitude by applying a two-stage process (propagation and update). The propagation stage is conducted through a linearized model of the attitude kinematics, while the update stage is based on the QUEST algorithm as described in Table 4.5. The source code is available in *AD_EQUEST.m.*

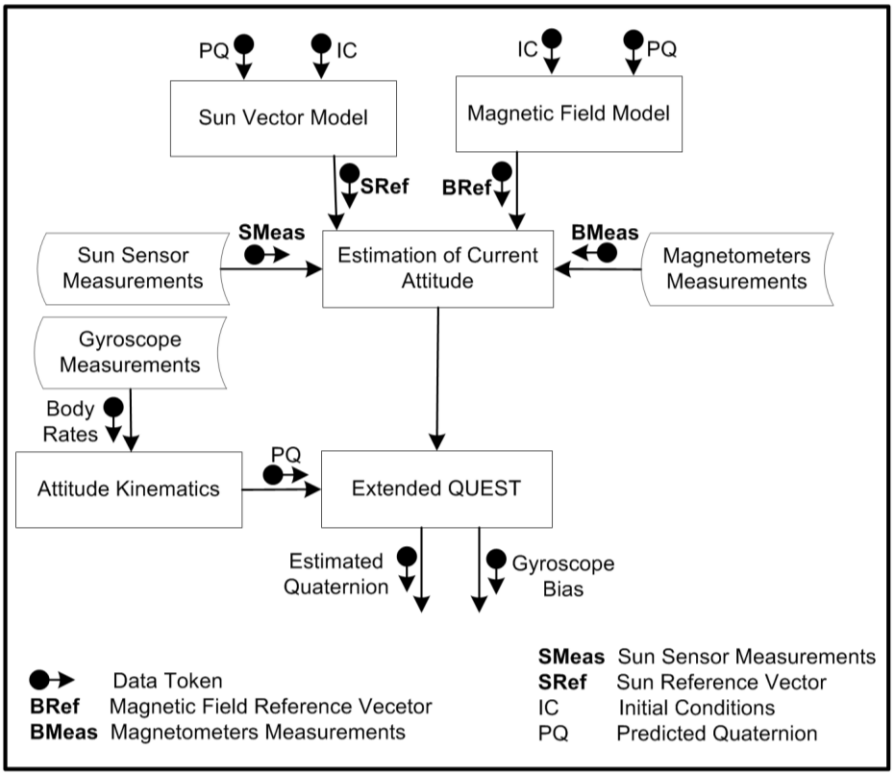

Fig. A.3. Block diagram of the extended QUEST software implementation.

A.3 Delta Fuzzy Algorithm

The Delta-fuzzy algorithm implemented is shown in Figure A.4. As opposed to the other algorithms, the algorithm relies on the Earth magnetic field only. The estimation process relies on a fuzzy inference system to calculate the error in the a priori attitude. Also, this algorithm indicates the presence of a control token. This token activates the gradient decent optimization scheme which recalculates the boundaries of the MFs. Such reaction allows the algorithm to the changes in the environment; Thus, leading to an improved estimate of the attitude. The source code is available in *AD-Delta-Fuzzy.m.*

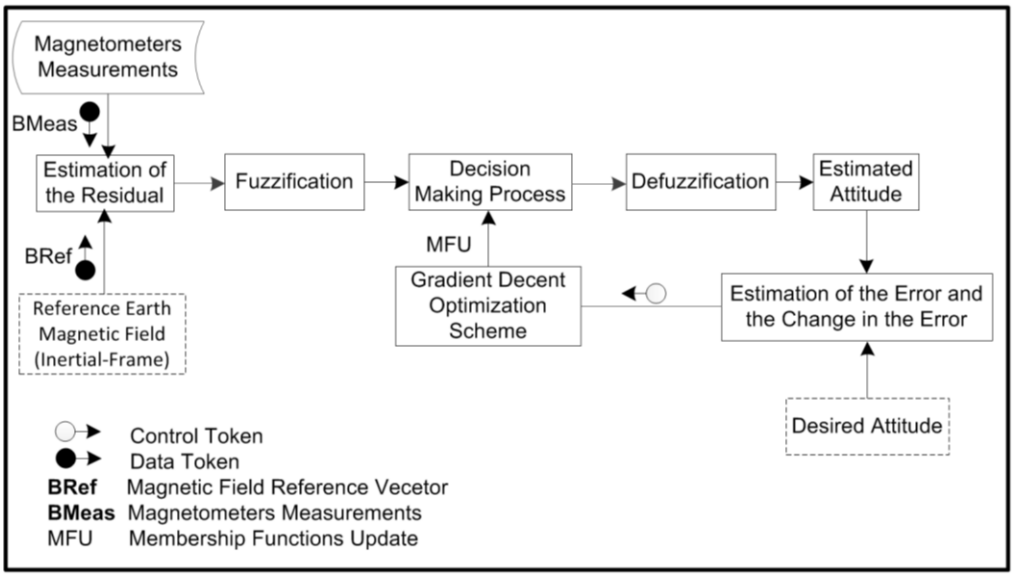

Fig. A.4. Block diagram of the Delta-Fuzzy algorithm software implementation.

Appendix B

DVD Content

There is one DVD uploaded on MSpace of the University of Manitoba's institutional repository. The DVD includes all the reference and measurement data, source code, and Matlab libraries used for the simulations of the attitude determination algorithms and different controllers. The content of the appended DVD is explained below.

- **Lib:** This folder contains the reference and measurement data used during the simulations. Also, the desired attitude profile is included.
- **FracCalcLib:** This folder provides the fractional calculus library needed to implement the FPID.
- **SimulinkLib:** The Simulink models used for the implementation of an IPID and a FPID proportional integral derivative controller are available in this repertoire.
- **AD_Algorithms:** This folder contains three subfolders for deterministic and stochastic algorithms described in this thesis, as well as the Delta-Fuzzy algorithm.
- **TestCases:** The different test cases considered to evaluate the performance of the algorithms studied in this thesis are available in this folder.

- **IGRF2005:** IGRF script used to generate the Earth magnetic field.
- **Output:** All the results of the different test cases are stored here. The results are saved under the extension **.fig* and **.png*.

Appendix C

Colophon

This thesis is typeset in MS office 2010. The body is written in 12 point Times New Roman with figure and table captions displayed in 10 point Arial.

The figures published in this thesis are created in Microsoft Visio 2010 Professional and generated using Matlab version 2010b and saved as a *Portable Network Graphics* (PNG) file.

All the work was performed using a Mac OS X version 10.6.8 and Windows 7 Professional running as dual boots in a 2×2.4 GHz Quad-Core Intel Xeon processors with 12 GB of 1066 MHz DDR3 memory.